2017

The Electrochemical Behavior of Molybdenum and Tungsten Tri-Nuclear Metal Clusters with Ethanoate Ligands

Edward Nelson Kennedy
Wright State University

THE ELECTROCHEMICAL BEHAVIOR OF MOLYBDENUM AND TUNGSTEN TRI-NUCLEAR METAL CLUSTERS WITH ETHANOATE LIGANDS

A dissertation submitted in partial fulfillment of the
requirements for the degree of
Doctor of Philosophy

By

EDWARD NELSON KENNEDY
M.S. Wright State University, 2009
B.A., Wright State University, 1995
A.A., A.S., Clark State Community College, 1993

2017
Wright State University

WRIGHT STATE UNIVERSITY

GRADUATE SCHOOL

June 1, 2017

I HEREBY RECOMMEND THAT THE DISSERTATION PREPARED UNDER MY SUPERVISION BY Edward Nelson Kennedy ENTITLED "The Electrochemical Behavior Of Molybdenum And Tungsten Tri-Nuclear Metal Clusters With Ethanoate Ligands" BE ACCEPTED IN PARTIAL FULFILLMENT OF THE REQUIREMENTS FOR THE DEGREE OF Doctor of Philosophy

Committee on Final Examination

_____
William R. Heineman, Ph.D

_____
Vladimir Katovic, Ph.D.
Dissertation Director

_____
Suzanne Lunsford, Ph.D.

_____
Jay Johnson, Ph.D.
Co- Director

_____
Doyle Watts, Ph.D.

_____
Don Cipollini, Ph.D.
Director, Environmental Sciences
Ph.D. Program

_____
Christopher C. Barton, Ph.D.

_____
Robert E. W. Fyffe, Ph.D.
Vice President for Research and
Dean of the Graduate School

ABSTRACT

Kennedy, Edward Nelson. Ph.D., Department of Environmental Sciences, Wright State University, 2017. The Electrochemical Behavior Of Molybdenum And Tungsten Tri-Nuclear Metal Clusters With Ethanoate Ligands.

The goal of this research was to study the electrochemical behavior of tri-nuclear clusters of molybdenum and tungsten. In addition, the feasibility of using these clusters as catalysts for the purpose of oxidizing ethanol was investigated. Four tri-nuclear cluster compounds were studied: hexa-μ2-acetatotriaquadi-μ3-oxotrimolybdenum (IV, IV, IV) trifluoromethanesulfonate $[Mo_3O_2(O_2CCH_3)_6(H_2O)_3](CF_3SO_3)_2$, hexa-μ2-acetatotriaquadi-μ3-oxodimolybdenum (IV, IV) tungsten (IV) trifluoromethanesulfonate $[Mo_2WO_2(O_2CCH_3)_6(H_2O)_3](CF_3SO_3)_2$, hexa-μ2-acetatotriaquadi-μ3-oxomolybdenum (IV) ditungsten (IV, IV) trifluoromethanesulfonate $[MoW_2O_2(O_2CCH_3)_6(H_2O)_3](CF_3SO_3)_2$, and hexa-μ2-acetatotriaquadi-μ3-oxotritungsten (IV, IV, IV) trifluoromethanesulfonate $[W_3O_2(O_2CCH_3)_6(H_2O)_3](CF_3SO_3)_2$.

Data was gathered from experimental results with cyclic voltammetry for the four tri-nuclear clusters. Initially, an ionic liquid, $EMIBF_4$ (1-ethyl-3-methylimidazolium tetrafluoroborate), was used as the solvent. Subsequent solvents for use with these clusters were investigated, including ACN (acetonitrile) and NMF (N-methylformamide).

The secondary solvent system settled on was the DMSO-TBAHFP solvent system. Each tri-nuclear cluster displayed a reversible redox reaction and one or more irreversible reduction reactions. The redox peak potentials were found to be Ep,a: -0.44V and Ep,c: -0.42V for Mo_3, Ep,a: -0.32V and Ep,c: -0.43V for Mo_2W, Ep,a: -0.31 V and Ep,c: -0.44 V for MoW_2, and Ep,a: -0.42 and Ep,c: -0.46 for the W_3 tri-nuclear cluster. The irreversible reduction reactions for each tri-nuclear cluster were observed at Ep,c(2): -0.74 for Mo_3, Ep,c(2): -1.15 for Mo_2W, Ep,c(2): -1.14 for MoW_2, and Ep,c(2): -0.84 for the W_3 tri-nuclear cluster. The diffusion coefficients in DMSO were determined to be $D_{Mo_3} = 9.105E^{-06}$ cm^2s^{-1}, $D_{Mo_2W} = 1.743E^{-05}$ cm^2s^{-1}, $D_{MoW_2} = 1.764E^{-05}$ cm^2s^{-1}, and $D_{W_3} = 1.991E^{-05}$ cm^2s^{-1}.

Exploring the electrocatalytic capability of these compounds was another effort made, by attempting to electroplate the compounds on platinum electrodes. Although some types of deposition events did appear to occur, it is unlikely they were of the intact tri-nuclear clusters. Thus far, the ethanol molecule has been partially oxidized, but breaking the carbon-carbon bond in the molecule proved to be a challenge that was not achieved.

Table of Contents

List of Figures

List of Equations

List of Tables

Keywords

Current

Cyclic Voltammetry (CV)

Cyclic Voltammogram

Diffusion Coefficient

Dimer

EDS

EDX

Electroanalytical Chemistry

Electrochemical Cell

Electrochemical Window

Electrochemistry

Electrode, Auxiliary

Electrode, Reference

Electrode, Working

Electrodeposition (used interchangeably with Electrolysis and Electroplating)

Electrolysis (used interchangeably with Electrodeposition and Electroplating)

Electrolysis/Electroplating/Electrodeposition

Ethylmethylimidazolium tetrafluoroborate (1-ethyl-3-methylimidazolium or $EMIBF_4$)

Functional groups

Heteronuclear

Homonuclear

Hydrophilic

Hygroscopic

Metal clusters

Metal-metal bond

Molybdenum

Oxidation

Polynuclear

Potential

Reduction

Scanning Electron Microscopy -

Sparging

Trimer

Tungsten (W)

Voltammetry

Voltammogram

XPS

Xray diffraction

Abbreviations

$BMIBF_4$ - 1-butyl-3-methylimidazolium tetrafluoroborate

CF3SO3 - Chemical formula for trifluoromethanesulfonic acid. Also known as triflic acid.

CV - Cyclic voltammetry

D - Diffusion coefficient

Dimers - Di-Nuclear Clusters

DMSO - Dimethyl sulfoxide

E - Potential (Voltage)

$EMIBF_4$ - 1-ethyl-3-methylimidazolium tetrafluoroborate

Ep,a - Peak anodic potential

Ep,c - Peak cathodic potential

Ep,c(2) - Second peak cathodic potential

IL - Ionic liquid

Ip,a - Peak anodic current

Ip,c - Peak cathodic current

IR - Infra-red

Mo_2W - Refers to the dimolybdenum-tungsten tri-nuclear cluster

$[Mo_2WO_2(O_2CCH_3)_6(H_2O)_3](CF_3SO_3)_2$

Mo_3 - Refers to the molybdenum tri-nuclear cluster

$[Mo_3O_2(O_2CCH_3)_6(H_2O)_3](CF_3SO_3)_2$

MoW_2 - Refers to the molybdenum-ditungsten tri-nuclear cluster

$[MoW_2O_2(O_2CCH_3)_6(H_2O)_3](CF_3SO_3)_2$

nm - Nanometer

Ox, ox - Oxidized form

Pt - Platinum

Red, red - Reduced form

RTIL - Room temperature ionic liquid

SEM - Scanning Electron Microscope

TBAHFP - Tetrabutylammonium hexafluorophosphate

Trimers - Tri-Nuclear Clusters

UV-Vis - Ultra Violet - Visible

W_3 - Refers to the tungsten tri-nuclear cluster $[W_3O_2(O_2CCH_3)_6(H_2O)_3](CF_3SO_3)_2$

Acknowledgments

The author would like to thank the following individuals for their involvement, whether direct or indirect, with this project.

My mother Polly, grandmother Ida and wife Lori for their unwavering love and belief in me. Dr. Don Cipollini and Dr. Steven Higgins for the incredibly generous support afforded to me, and for their thoughtful guidance through the program. It is very much appreciated. The members of my committee, each of whom uniquely contributed to my efforts: Dr. William R. Heineman, the Distinguished Research Professor in the Department of Chemistry at the University of Cincinnati. His book "Laboratory Techniques in Electroanalytical Chemistry" was of particular value to me. Dr. Doyle Watts and Dr. Christopher Barton, both of the Earth & Environmental Sciences Department. Their feedback and encouragement gave me the hope I needed. Dr. Suzanne Lunsford, who assisted me with the written revisions of my dissertation in addition to helping in completing my research tasks and with real-world problem solving. Dr. Jay Johnson, my co-advisor. Dr. Katovic for taking me on as his first Ph.D. student. Mr. Michael Hall for forging the platinum electrodes for my electrodeposition efforts, repairing equipment important to my research, and providing a great many things that were necessary for this project. Drs. May and Paul for helping me improve my laboratory techniques and assisting in many ways. My fellow E.S. students for their friendship and encouragement. Ms. Kim Napier and Ms. Cathy Kempf for handling the many formal aspects I asked of them.

Dedication

I would like to dedicate this dissertation to my mother Polly, and to my grandmother Ida. They always believed in me and they made it possible for me to pursue my path. Ida passed away on December the 24th, 1999. Polly passed away March the 31st 2014. They are deeply missed every day.

VITA

The author was born in Springfield Ohio on July 2, 1961. He graduated from public high school in 1979. He attended Clark State Community College and graduated with Associates degrees in Science and in the Arts. He graduated from Wright State University in 1995 with an undergraduate degree in Anthropology, and a minor in Health Sciences. In 2007, he returned to Wright State University and completed his Master's degree in Chemistry. He then began his PhD in 2012.

Equipment Inventory

Type of Instrument	Company	Model
UV spectrophotometer	Varian-Corey	50 Bio dual-beam
Karl Fisher Titrator	Denver Instruments	Model 260
Potentiostat/CV	PAR/EG&G	Model 173
Universal Programmer	PAR/EG&G	Model 175
Electrometer	PAR/EG&G	Model 178
Noise filter	PAR/EG&G	Model 178/41
Measures electric charge	PAR/EG&G	Model 179 Digital Coulometer
Mass Spectrometer	Agilent Technologies	Model 7820A
FT-IR Spectrometer	Nicolet	Model 6700
Multimeter	Keithley	Model169
Potentiostat/Galvanostat CV	Pine instruments	2186
Data collection and processor	eDAQ e-Corder Pty Ltd.	Model 201
Supplies potential and current	HP Harrison DC Power Supply	Model 6204B
Measures current & potential	Tenma Multimeter	72-7765
Measures current & potential	Fluke Multimeter	8024A
Scanning Electron Microscope	SEM	FEI Quanta SEM / electron energy dispersion scope
Laptop computer	IBM Thinkpad running Microsoft XP Professional Version 2002 Service Pack 3 with an Intel(R) Pentium(R) III Mobile CPU @ 1133 MHz. 724 MHz	

1. INTRODUCTION

1. Introduction

The following research project was an expansion of the past work of the Dr. Katovic et al., research group, and their work with ionic liquids and metallic tri-nuclear clusters (transition metals). Using an ionic liquid, the tri-nuclear clusters were to be utilized to deposit upon working electrodes - such as Pt - to enhance electrocatalytic activity. Past researchers from 2006-2014 (Antolini and Perez, 2013, Courtois, 2013, Gyenge, 2008, Idriss, 2004, Lai et al., 2010, Li et al., 2014, Li and Adzic, 2013, Masa et al., 2013, Roquero et al., 2007, Schwarzacher, 2006, Yang et al., 2013) have found that transition metals deposited onto electrode surfaces have displayed promising results due to increased catalytic activity.

This electrode "augmentation" approach has led to efforts to oxidize ethanol using these electrode systems and has been met with some degree of success, as shown by the work of Li et al (1996), and other groups (Li et al., 2014, Ota and Ishihara, 2013, Roquero et al., 2007, Xu, 2013). Improving electrode functionality has been a major route to this goal and approaches vary widely(Abbott and McKenzie, 2006, Endres et al., 2008, Endres, 2001, Patel, 1990, Schwarzacher, 2006, Suryanto et al., 2012, Yang et al., 2013).

This research includes the electrodeposition effort with molybdenum and tungsten-based tri-nuclear clusters onto Pt electrodes using first, an ionic liquid ($EMIBF_4$), and later with a polar aprotic solvent (DMSO/TBAHFP).

1.1 Synthesis of Metal-Cluster Catalysts

1.1.1 Synthesizing di-nuclear clusters

The first phase involves the synthesis of "di-nuclear" clusters (dimers) of molybdenum (Mo) and tungsten (W). The two metal atoms are bonded directly to each other (Mo_2 and MoW) with a quadruple bond between the metal atoms. The dimers are only intermediates however; they are necessary starting material for the synthesis of the following compounds that are the real analytes of interest.

1.1.2 Synthesizing tri-nuclear clusters

Tri-nuclear clusters are synthesized from the di-nuclear clusters. The trimers contain three inter-connected metal atoms at the core, of either molybdenum (Mo_3), tungsten (W_3), or 1:2 ratios of each metal (Mo_2W, or MoW_2). Three of the tri-nuclear clusters (Mo_3, MoW_2, and MoW_2) can be synthesized from just the two types of di-nuclear clusters mentioned above (Mo_2 and MoW). However, the W_3 trimer synthesis does not involve the use of a dimer (requiring tungsten hexacarbonyl instead). The flowchart in Figure 1.1 briefly represents the synthesis.

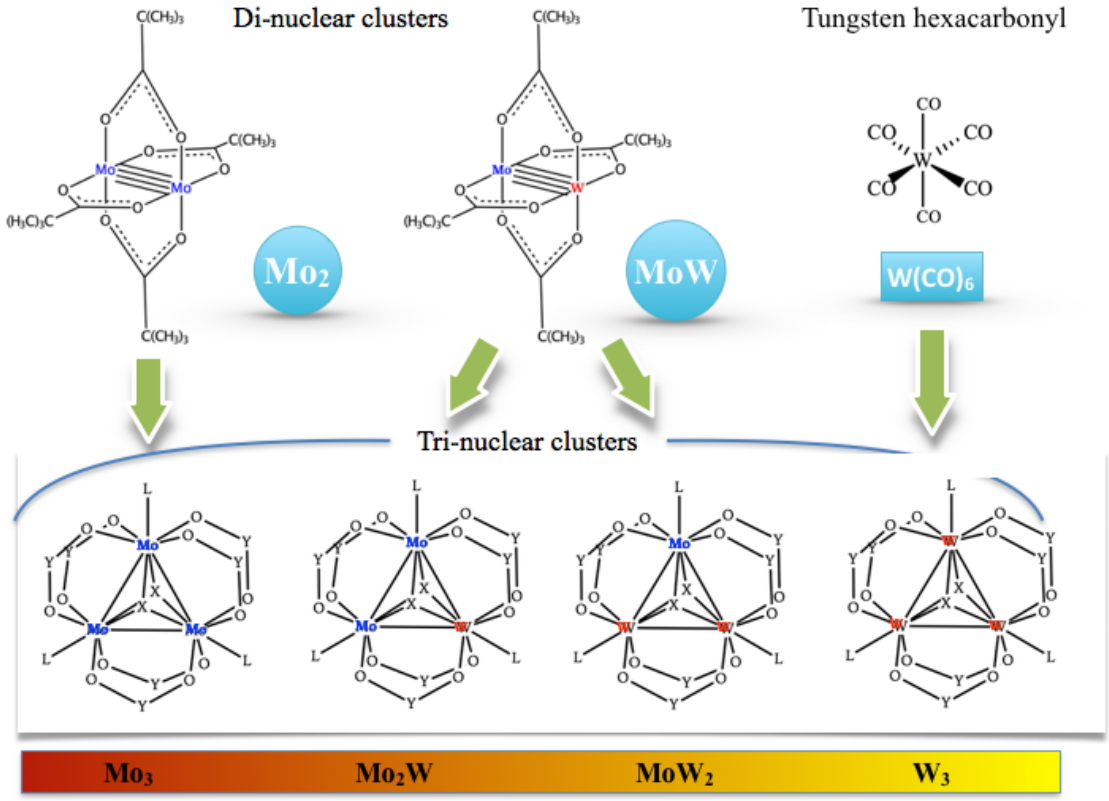

Figure 1.1. Flowchart depicting the synthesis path of the tri-nuclear clusters.

1.2 Purifying the solvents

Dimethyl sulfoxide and 1-ethyl-3-methylimidazolium tetrafluoroborate ($EMImBF_4$), were purified by a method put forth by Earle (2007) and used as a solvents/transport medium for the tri-nuclear clusters (Earle et al., 2007). This is elaborated on in the Experimental section of chapter 2.

1.3 Characterizing the clusters in a DMSO-based solvent system

The electrochemical behavior of these tri-nuclear compounds was studied in the DMSO/TBAHFP solvent system by cyclic voltammetry to obtain values pertaining to various electrochemical parameters which had yet to be reported.

1.4 Electrodeposition of clusters and oxidation of ethanol

Ethanol is considered to be an ideal biomass-acquired fuel (Roquero et al., 2007), except for the high overpotential required to break its carbon-carbon bond. By depositing each of four tri-nuclear clusters of varying composition onto Pt electrodes, using the ionic liquid EMIBF4 as the transport medium, it is our hypothesis that this method of electrode augmentation will achieve this goal of oxidizing ethanol at the desired carbon-carbon bond (Katovic, 1975, Suzuki, 1994, Ubadigbo, 2009, Wanamaker, 1998).

Electrodeposition of the four tungsten- and molybdenum - based trimers onto a Pt (Pt) electrode was attempted. A scanning electron microscope was used to obtain "before" images to compare with "after" images, should the deposition occur. Cyclic voltammetry (CV) was the electrochemical technique utilized to determine first if electrodeposition had occurred, and if so, the new electrode-system would be utilized to attempt the oxidization of the carbon-carbon bond of ethanol.

CV was the electrochemical method used to determine the redox potential and reversible/ irreversible behavior of the materials electrodeposited on the bare Pt electrode surface. This technique involved scanning the potential backwards and forwards on the

working electrode, where the resulting graph plotted current versus potential (Kissinger and Heineman, 1983, Van Benschoten et al., 1983).

A compact overview in the form of a flowchart depicts the research design, as shown in Figure 1.2. . However, due to unsuccessful electrodeposition of the tri-nuclear clusters, a new approach was required to understand the properties of these materials in more detail. Figure 1.3. illustrates the revised scheme of research.

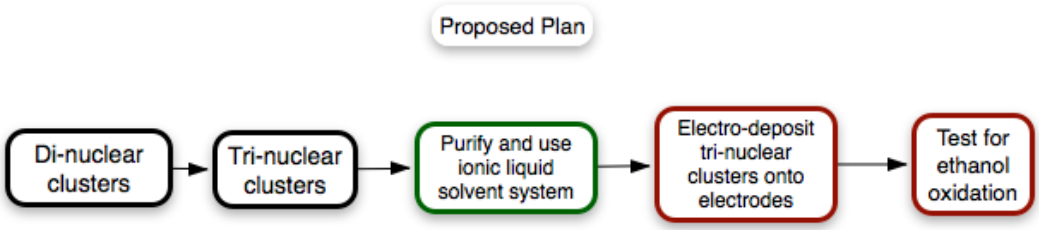

Figure 1.2. . A summary flowchart for the synthesis, processes, and goal of this research. The catalysts and their solvent are first synthesized and/or purified, followed by the process of attempting to deposit the catalysts onto Pt electrodes. Finally, the catalytic ability of the electrode complexes would be used to attempt oxidation of the carbon-carbon bond of ethanol.

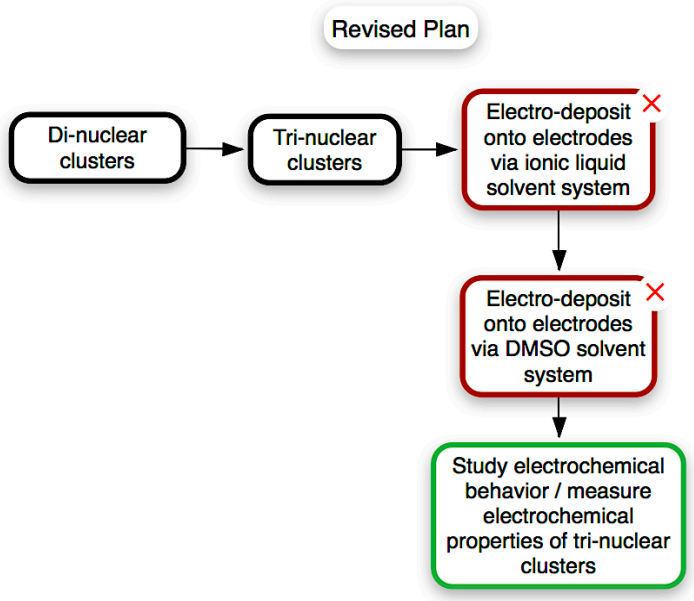

Figure 1.3. The revised scheme devised to understand the properties of these materials, after electrodeposition was not detected.

1.5 Previous work from Dr. Vladimir Katovic

The history of tri-nuclear clusters began with the discovery of homonuclear metal-metal bonded compounds. Prior related-work to this research by the advisor of this student included the study of niobium (IV) polynuclear species and of tantalum (IV) polynuclear species formation. The metals formed tri-nuclear octahedral complexes. Ligand substitutions were explored and the composition and properties of these substances were discussed with regard to infra-red (IR), thermal (TGA), and NMR evidence (Katovic, 1970).

The lead researcher then included the study of dimeric (two metal atoms at the center) complexes containing strong heteronuclear metal-metal bonds. They contained bonds of order 3.5 and 4.0 - bonds unheard of in any branch of chemistry until the

discovery of these compounds in the mid 1960's (Cotton and Bratton, 1965, Cotton, 1969, Cotton, 1975). This new discovery is elaborated in more depth in the Introduction, with a diagram of the general structure. These "dimers", or "dinuclear clusters", contained molybdenum *and* tungsten in the same compound and these were the metals used in this project (Katovic, 1975).

Continued work with these types of compounds included the determination of structure by x-ray diffraction and IR (Katovic and McCarley, 1978), and of bond distance (Katovic and McCarley, 1978), their catalytic properties toward small molecules, and the effects on ligand substitutions (Bursten et al., 1986, Paul et al., 1994).

1.6 Previous work from the Katovic research group

1.6.1 Analysis of past electrodeposition attempts by the Katovic group

Electrodeposition attempts with clusters of this type were made by previous members of this research group (Davis, 2012, Frock, 2012, Harris, 2008, Ubadigbo, 2009, Woods, 2010). The results were somewhat inconclusive and are examined below in the following section.

1.6.2 SEM Imaging

Although before and after images of the electrodes were supplied in previous work, one cannot capture a true "before and after" image of the same area. The nature of the sampling method employed by the SEM precludes the ability to sample the same area of an electrode, as the sample tray that must be used to hold the sample is very small (a few mm^2), necessitating the sacrificing of a piece of the foil electrode tiny enough to fit into the tray. To view the same area of the electrode before and after, the electrode would have to remain intact through the imaging, but that was not possible.

Although the platinum-foil electrode seen in Figure 1.4 displayed a visible change, the accumulation of material on the surface of the foil electrode could belong to decomposition products of the solvent and/or the metal clusters themselves. The extremely (and uncharacteristically) long duration of the electroplating sessions, where current was sent through the cell for lengthy durations - 51 hours in one case, ((Frock, 2012)) and 120 hours in another (Ubadigbo, 2009), may be supportive of that outcome. In contrast, electroplating copper from copper sulfate onto a platinum electrode was accomplished in about 30 seconds. Therefore this project has found that the long electroplating sessions by Ubadigbo, 2009; are not producing the desired metal clusters on the Pt foil but instead producing decomposition products.

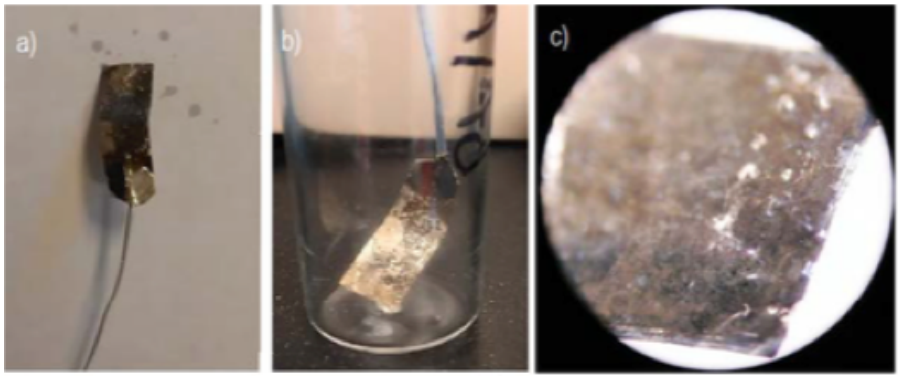

Figure 1.4. Image of modified Pt electrode after electrodeposition attempt (Ibid.).

1.6.3 Energy Dispersion x-ray diffraction (EDAX) and UV

In one thesis (Frock, 2012), electrode composition was measured with Energy Dispersion x-ray diffraction scans of the platinum electrode after electrochemical deposition was attempted with the Mo_3 trimer, $[Mo_3O_2(O_2CCH_3)_6(H_2O)(CF_3SO_2H)_2$. The results, taken from the student's thesis are shown in Figure 1.5.

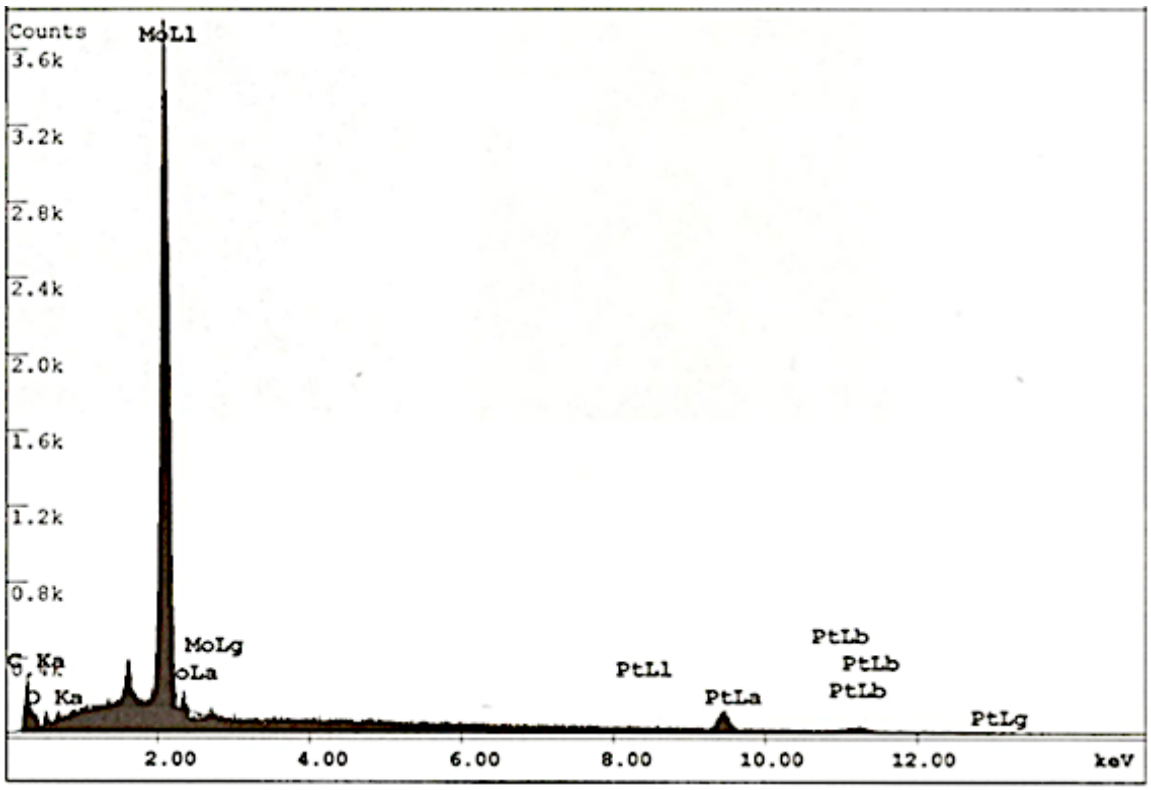

Figure 1.5. Results from energy dispersion spectroscopy (EDS) showing a change in the metal composition of the pure platinum foil electrode. Taken from Frock (2012).

Frock et al., results show that after the attempt to deposit the clusters, the percent composition of the platinum electrode changed from 100% platinum to 88.01% platinum with 1.59% molybdenum. Oxygen was also measured at 1.26%, and carbon at 9.13% (Ibid.). However, as before, this can be accounted for as decomposition products from the clusters and/or the solvent. The following UV-Vis evidence may be supportive of that conclusion.

The student also had attempted to deposit a chromium-molybdenum tri-nuclear cluster $[Cr_2Mo(u2\text{-}CH_3COO)_6(u3\text{-}O)(H_2O)_3][CF_3SO_3]$ onto a platinum electrode. However, no deposition appeared to occur based on the EDAX results in Figure 1.6. In other words, there was no change in the % composition of the electrode thus a follow-up UV-Vis examination was carried out. The UV-Vis of the electrolyzed solution failed to show the characteristic absorption peaks of chromium-molybdenum tri-nuclear cluster in Figure 1.7., which were present before the electrodeposition attempt as seen in Figure 1.8. It was postulated by the researcher that the clusters likely disintegrated (Ibid.).

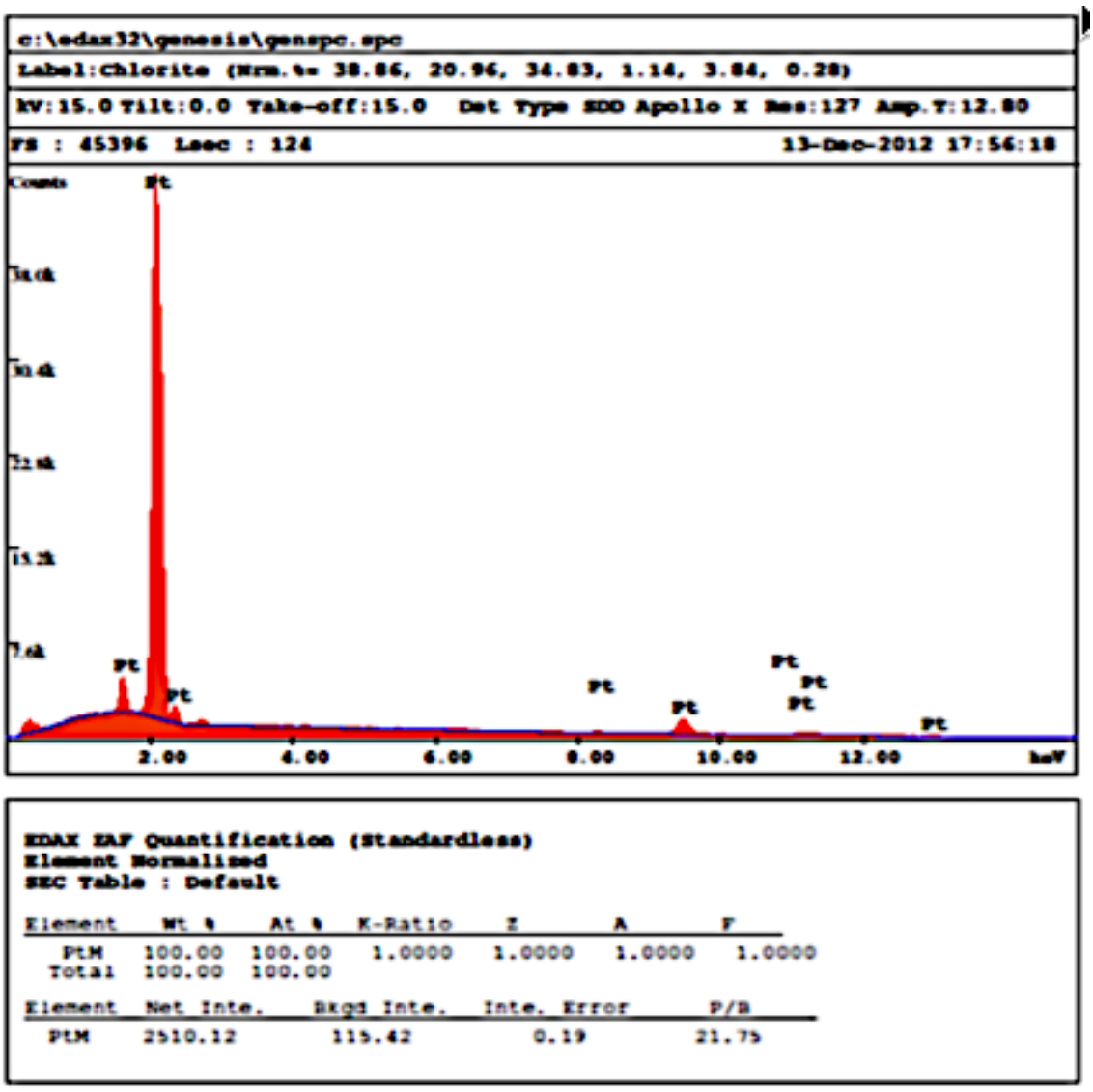

Figure 1.6. Data from Energy Dispersion x-ray diffraction scans for platinum electrode after electrochemical deposition attempt with [Cr2Mo(u2-CH3COO)6(u3-O)(H2O)3][CF3SO3] (Ibid.) Taken from Frock (2012).

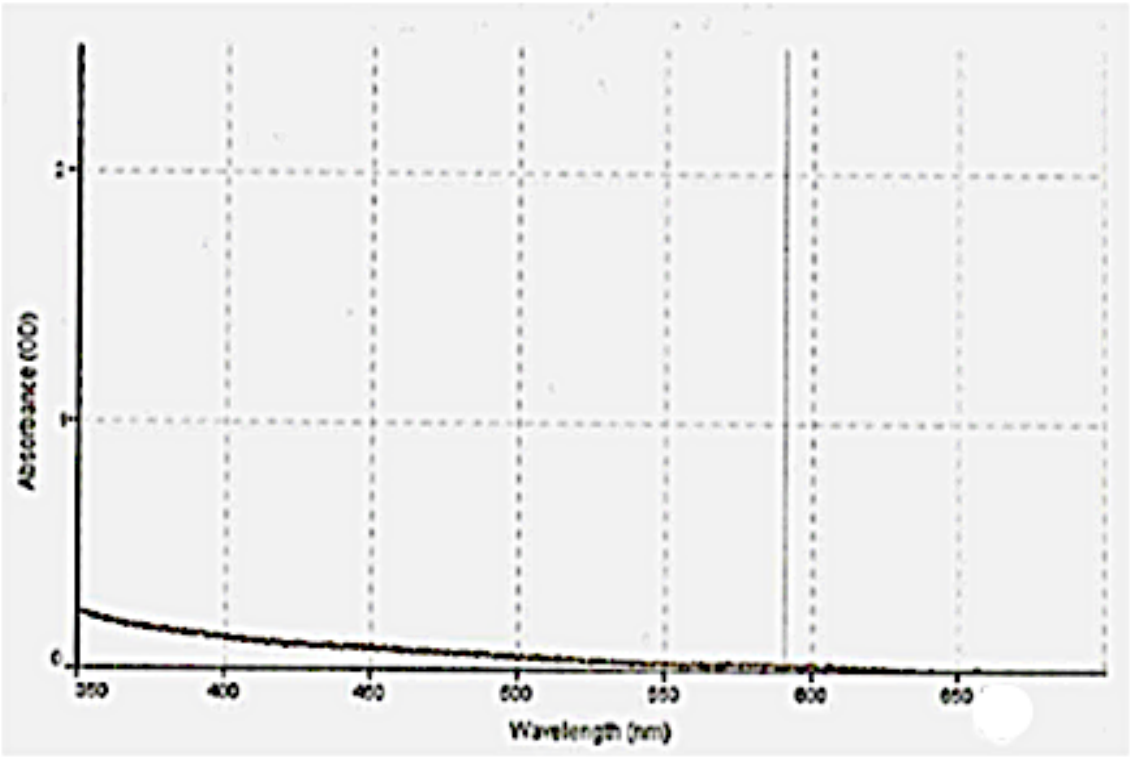

Figure 1.7. A UV-Vis absorption spectrum of [Cr2Mo(u2-CH3COO)6(u3-O)(H2O)3][CF3SO3] in $EMIBF_4$. Previously-observed peaks are absent (Frock, 2012).

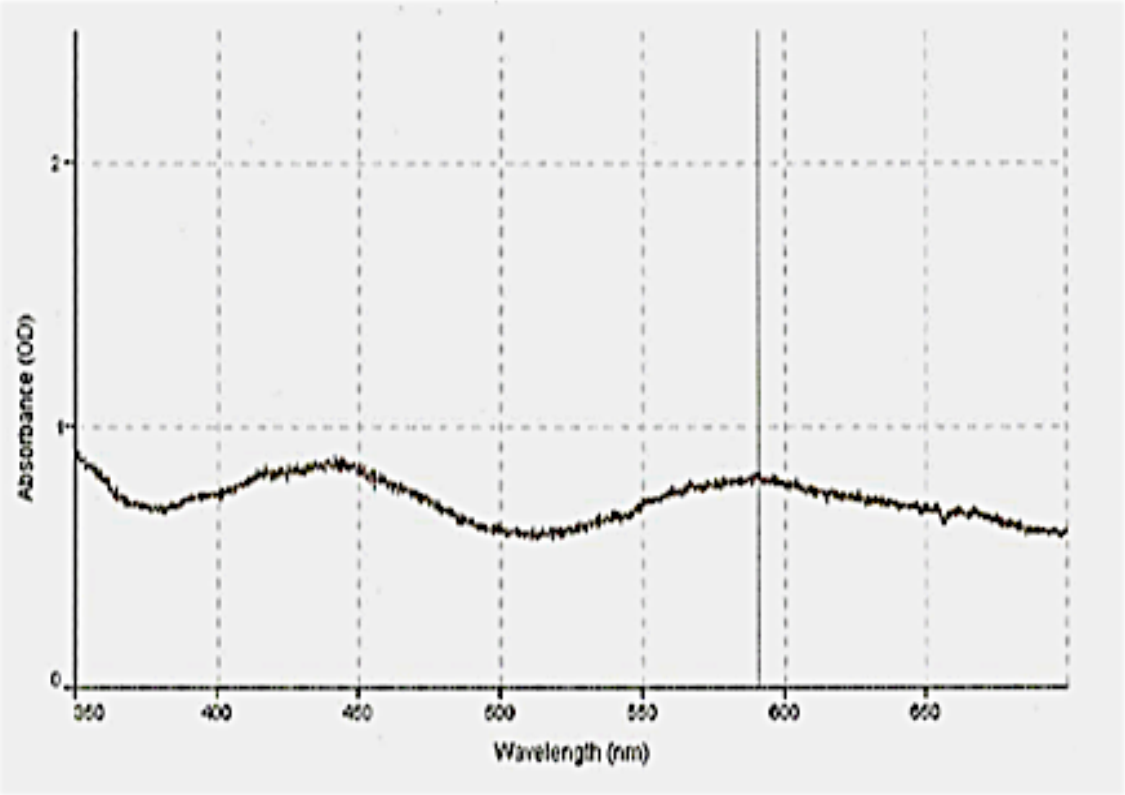

Figure 1.8. A UV-Vis absorption spectrum of [Cr2Mo(u2-CH3COO)6(u3-O)(H2O)3][CF3SO3] in $EMIBF_4$ before electrodeposition attempt.

This research project was based upon past work by Frock et al,. regarding the electrodeposition of tri-nuclear clusters in ionic liquids. However this research project has established that the successful electrodeposition of tri-nuclear clusters on bare Pt in various ionic liquids such as $EMIBF_4$ was not successful. Also, other solvents such as DMSO were studied to determine any changes in the electrodeposition of the tri-nuclear clusters which were found unsuccessful in modifying the electrode surfaces as well. Therefore this project has found the tri-nuclear clusters did not electrodeposit intact onto the Pt electrode surface. Past researchers such as Ardon et al., had successful electrodeposition with Mo and W, which were simple structures without steric hindrance and not clusters. Thus, it could be postulated that the tri-nuclear clusters /ligand cage discouraged or prevented deposition onto the Pt electrode surface of the intact structure due to steric hindrance(Ardon et al., 1982).

An interest in tri-nuclear clusters as described above is due to the fact they can oxidize small alcohols. Therefore, the tri-nuclear clusters possibly have the electrocatalytic ability to break the carbon -carbon bond in ethanol without the aspect of fouling the electrode surface. This novel quest to realize ethanol's full potential as a renewable fuel is as timely as ever. The task of oxidizing the carbon-carbon bond of ethanol - the last remaining bond to break - has been currently achieved by two groups. In 2009, at the Department of Energy's Brookhaven National Laboratory in New York, this goal was achieved with the use of platinum-rhodium clusters on a surface of tin dioxide. This electrocatalyst can split the carbon-carbon bond and oxidize ethanol to carbon dioxide within fuel cells (Available at: https://www.bnl.gov/newsroom/news.php?a=110898). The article was written by Kendra

Snyder for the Brookhaven National Laboratory's Newsroom Media & Communications Office.

More recently, Ozlem Sahin et al., (2015) published "The Effect of iridium Addition to platinum on the Alcohol Electro-oxidation Activity", in which the authors achieve the same goal - this time with iridium and platinum. Both of these metals have the distinction of being the most precious and expensive metals on earth. However, rhodium is more expensive than platinum. Therefore, the search for more abundant, less costly metals for this purpose is a current endeavor thus Mo and W were our metals of choice in this project.

1.7 Introduction to Metal Clusters

Until the early 1960s, the chemistry of the transition metals was based entirely on the conceptual framework established by Alfred Werner (1866-1919), a Swiss chemist. Briefly, this model is built around the concept of a single metal ion such as surrounded by a set of ligand donors (an ion or molecule attached to a metal atom through coordinate bonding). The framework centers on the characteristics of the individual metal ion, the interaction of the metal ion with the ligand group, and the geometrical and chemical characteristics of this ligand set (Cotton, 2005). Complexes containing oxidized transition metals were also viewed as conforming to this same model. Although great progress in the area of transition metals followed, it still equated to continuous, evolutionary advancement (Telser, 1984).

In 1964, a discovery was made that opened up an entirely new domain of chemistry - the discovery of "multi-center" chemistry with direct metal-to-metal bonds. This discovery was so significant, that it is thought of as a *dis*continuous *revolutionary* step. It constituted an innovation not just in a branch of chemistry, but to the entire science of chemistry (Cotton, 2005). The adoption of X-ray diffraction was conducive to this work on metal –to metal bonds {Chisholm, 1977, #64076}.

Accompanying this discovery, there were a number of notable unexpected observations of metal clusters. The first was that metal clusters could form that contained direct metal-metal bonds. The second was the bond order - the number of bonds between the two metal atoms. The maximum number of bonds known to exist between atoms until that time was three. These compounds displayed a quadruple bond - four bonds between the metal atoms (see Figure 1.9). Of course, as bond order increases, bond length between the atoms comprising the bond decreases, and this was no exception. What *was* perhaps unexpected was that the 4^{th}-order bond created a bond length between the two metals that was even shorter than the pure metallic bond found between these atoms in bulk metals. This was found to relate to yet another unexpected observation: the 4^{th}- order delta-bond comprising the d_{xy} orbital of each of the two metal atoms was in an eclipsed configuration thus not staggered as expected. If the orbitals were staggered however, there would not be a sufficient degree of overlap to form this bond.

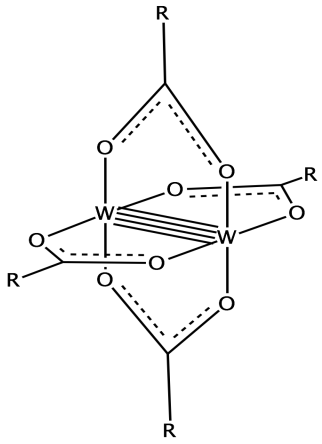

Figure 1.9. A ditungsten tetraalkyl di-nuclear cluster.

And so the period 1963-1965 heralded in "multicenter chemistry", a new, "non-Wernerian" model of transition metal chemistry (Ibid.). Subsequently, the di-nuclear clusters lead to tri-nuclear clusters and other polynuclear metal clusters. Di-nuclear clusters provide the building blocks for the syntheses of tri-nuclear clusters (see Figure 1.10**)** and other polynuclear cluster compounds which have important catalytic ramifications (Chisholm, 1977). There are now more than 4000 compounds, and elements in all of the groups 5 to 10 are represented (Telser, 1984).

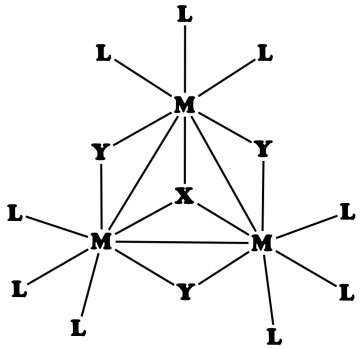

Figure 1.10. A tri-nuclear cluster with generic notation (M=Metal), referred to as an M3X13, meaning three metals and 13 ligands.

1.7.1 The Constellation of Clusters

The clusters differ in several ways based upon identity, form, number of transition metal elements per cluster unit, composition of cluster and configuration that are described below in more detail.

1. The identity of the transition metal(s) themselves

- Nearly all of the transition metals such as Pt, Sn, and Ru - (Xu, 2013), V, Cr, Co, Ir, Fe, Mo, Ni, Tc, Os, Re, Rh, W (Cotton, 2005)

2. The form they are designed to take

- Cluster or non-cluster forms
- Planar, one-layer, two-layer(Xu, 2013)
- Linked to oxides such as ZrO_2, Al_2O_3, SiO_2, TiO_2, and SnO_2 (Kim et al., 2009)
- Linking together di-metal units through axial linkers, equatorial linkers, and by making extended metal atom chains (Cotton, 2005)

3. If clusters are being used, they can differ by:

- The number of transition metal elements per cluster unit
  - One (Li et al., 2014)
  - Two (Roquero et al., 2007, Xu, 2013)
  - Three or more(Katovic, 1970, Patel, 1990)

4. The composition of the clusters

- All one type of transition metal, or mixtures in varying ratios
  - C:Pt (1:1), Pt:Mo (1:1), (1:4), (4:1)(Roquero et al., 2007)
  - Mo_3, Mo_2W, MoW_2, W_3

- Other elements or groups may be present or absent (Patel, 1990)

5. Different configurations, or connectivity within the clusters

- Metal complexes are numerous in both identity and configuration - the latter meaning the attachment of direct bonds between the metal atoms. Even if the elemental selection is the same, the configuration of the catalytic complex can and often does differ (Bino and Gibson, 1980).

The Mo_3 timer was the only tri-nuclear cluster that was fully-synthesized successfully by Kennedy in 2017. Previously synthesized tri-nuclear clusters by Katovic et al., were available and used in an attempt to electrodeposit onto the Pt electrode after verifying the compounds with spectroscopy by Kennedy.

1.7.2 Efficacy of molybdenum and tungsten as catalysts

Previous work has demonstrated the efficacy of using molybdenum and tungsten (along with platinum and in some cases carbon) to oxidize methanol and to partially oxidize ethanol(Kim et al., 2009, Li et al., 2014, Roquero et al., 2007). Roquero (2007) found that Pt-Mo and Pt-W catalysts oxidized methanol better than platinum catalysts alone. The higher performance was attributed to a lowering of the oxidation onset potential compared to platinum-carbon electrodes. Kawamura et al (1987) also investigated the oxidation methanol by testing tungsten-based double carbides (a carbide is a binary compound containing carbon and one other element), where powdered tungsten was doped with either V (vanadium), Cr (chromium), Mn (manganese), Ni (nickel), or Mo (molybdenum). They found that only Mo was able to promote methanol

oxidation activity. Moreover, it was discovered that the most active catalyst for methanol oxidation was found to be (W, Mo)C with the atomic ratio for Mo/(W + Mo) = 0.2 (Kawamura et al., 1987). Roquero (2007) also found ratios of molybdenum and tungsten that performed better than others. Platinum electrodes containing 4:1 ratios of Pt to Mo and 4:1 ratios of Pt to W were found to be optimum for catalytic performance in the oxidation of methanol.

1.7.3 Application of molybdenum and tungsten to electrodes

Work with molybdenum and tungsten has shown positive results towards enhancing catalytic capabilities of carbon and platinum electrode systems (Ibid., Tseung and Chen, 1997, Jiang et al., 2007, Roquero et al., 2007, Kim et al., 2009). Roquero et al. (2007) used molybdenum, tungsten, and platinum based electrodes, as well as carbon-supported platinum-molybdenum and platinum-tungsten catalysts for methanol oxidation in direct alcohol fuel cells. With small amounts of Mo or W, the authors report increased catalytic activity towards oxidation of methanol compared to a catalyst containing only platinum. The authors state the higher performance observed is due to a decrease in the oxidation electrical potential of methanol (Roquero et al., 2007).

The catalysts for this research, whether molybdenum, tungsten, or combinations of these, all share direct metal-metal bonds. Figure 1.11 shows a few of these different configurations.

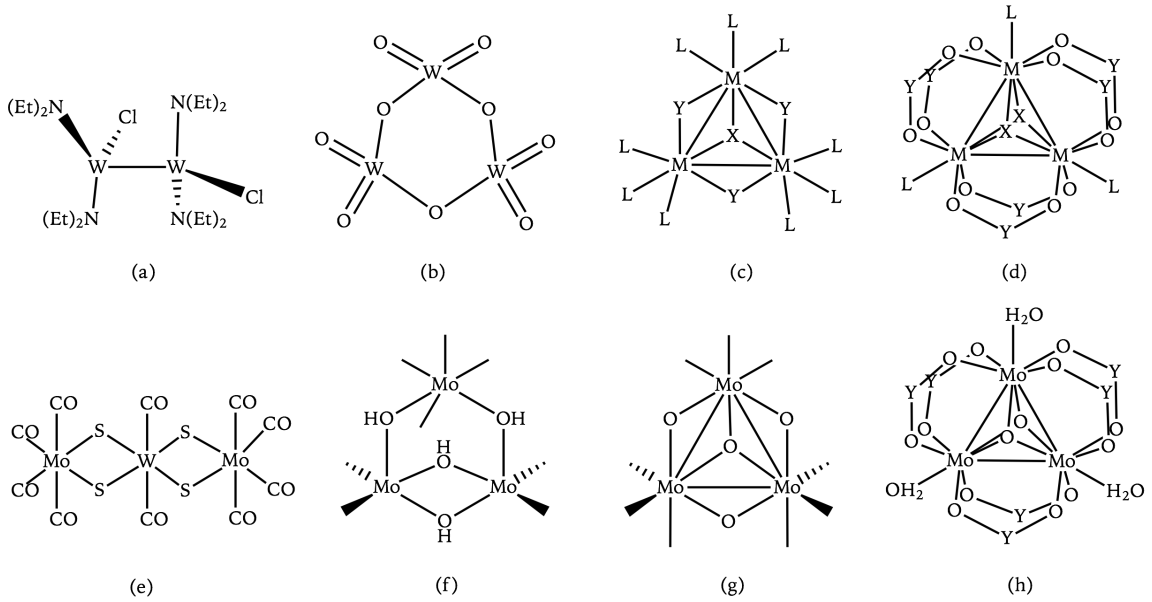

Figure 1.11. A di-nuclear tungsten cluster with a direct metal-metal bond (a), a tungsten tri-nuclear cluster without metal-metal bonds and a different arrangement (b)(Kim et al., 2009), a generalized tri-nuclear cluster with metal-metal bonds and 1 "capping atom [x]" (c), a generalized tri-nuclear cluster with 2 "capping atoms [x]" (d), a mixed tri-nuclear cluster of molybdenum and tungsten with no direct metal-metal bonding (e), a molybdenum tri-nuclear cluster without direct metal-metal bonding (f), a molybdenum tri-nuclear cluster with direct metal-metal bonding and 1 capping atom [O] (g), and one of our tri-nuclear clusters; a molybdenum tri-nuclear clusters with direct metal-metal bonding and 2 capping oxygens, with Y = acetate groups (h). Images were created in ChemDoodle software, v 6.0.1.

1.7.4 Characterization

In addition to color, tri-nuclear clusters can be characterized by the following techniques: UV-Vis (Ryan, 1982), IR (Li et al., 2014), X-ray diffraction (Cotton and Bratton, 1965, Lawton, 1964, Stephenson et al., 1964), proton NMR (Zhuang et al., 1998), cyclic voltammetry, and other methods.

1.7.5 The four tri-nuclear clusters

Substitution of one or more tungsten atoms for molybdenum atoms at the base of the tri-nuclear cluster gives rise to the four clusters used in this research. Huang et. al., (1994) has determined that the crystal structure is the same for each of the trimers. Figure 1.12 shows the four clusters used in this research (Huang et al., 1994).

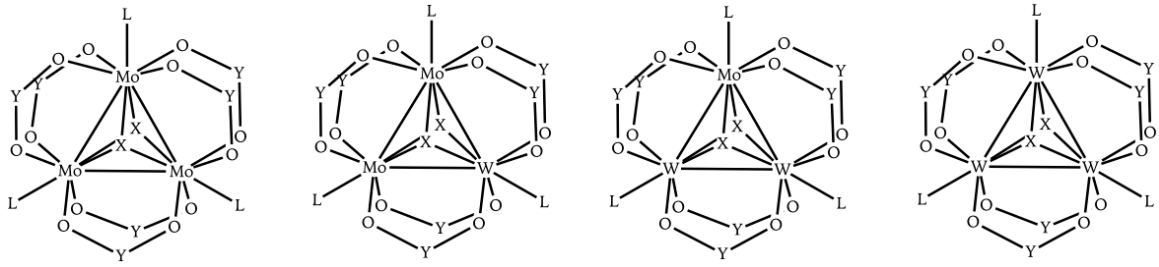

Figure 1.12. Moving from left to right, the Mo_3, Mo_2W, MoW_2, and W_3 trimers. The upper and lower μ-3 capping ligands (labeled *x*) are both oxygens, and the carbons and oxygens shown are symmetrically repeated around the molecule. The above images were created with ChemDoodle version 6.0.1.

1.8 More on electrodeposition

The purpose behind electrodeposition is to modify a metal's surface properties. The electrodeposition process adheres one metal onto the surface of another. It is used to obtain the desired electrical and corrosion resistance, to diminish friction & wear, to enhance heat tolerance, sometimes for decoration, and for additional purposes. In this case, we wish to modify the surface of the platinum working electrode by depositing

metal clusters on its surface to enhance its catalytic capabilities. Platinum has been the traditional catalyst for the oxidation of ethanol since the 1960's. It is regarded as the most effective single-metal type catalyst for electro-oxidizing the class of organic molecules to which ethanol belongs (Lai et al., 2010).

There are various factors which influence electrodeposition. They include: the viscosity of the ionic liquid (Suryanto et al., 2012), the nature of the anions or cations in the solution, solution concentration, the presence of impurities, and the physical & chemical nature of substrate surface (Gunasekara, 2015). In this instance, that surface is the platinum electrode.

1.9 Introduction: ionic liquids

One of the solvents used in this research is the ionic liquid 1-ethyl-3-methylimidazolium tetrafluoroborate, or $EMIBF_4$. The history of ionic liquids goes back over one hundred years and is rooted in traditional high-temperature molten salts (ionic compounds that melt, but only at high temperatures). A historical definition of an ionic liquid is a salt having a melting temperature below the boiling point of water. But the high temperatures involved made working with molten salts difficult. The quest for useful molten salts with lower melting temperatures was one of the driving forces that led to the discovery of ionic compounds that were liquid at <100ºC in the 1960's (Endres et al., 2008, Welton and Wasserscheid, 2002). Some use this criterion to distinguish ionic liquids from molten salts, but another valid distinction is that ionic liquids contain organic cations rather than the inorganic ones expected in a salt. This is particularly the

case with room-temperature ionic liquids (RTILs), which are water and air stable salts that are liquid at room temperature, and are being developed for green chemistry applications (Kennedy, 2009).

The motivation for using molten salts in the first place (when water and other molecular solvents are more convenient) is the great stability of their salts – thermally, chemically, and electrochemically. They concurrently possess the qualities of non-volatility and thermal stability, which confers upon them a very wide liquid range. Furthermore, because they are typically derived from minerals that are naturally occurring, they are available in large quantities. Their very high electrical conductivity (from the high concentration of ions) and wide electrochemical windows make them premier solvents for many electrochemical processes (Ibid.). Ionic compounds are typically solids and require very high temperatures before melting. Sodium chloride is a fine example of these physical properties. The positive and negative charges are expressed by single atoms. Like magnetic ball bearings, they can directly border their oppositely-charged neighbor, clump together, and agglomerate into a 3-dimensional structure known as a lattice. Because each charged atom can get very close to an oppositely-charged atom, they can stack and form a solid. By contrast, the charges in ionic liquids originate within relatively large molecules, often highly-branched. Though oppositely-charged, and therefore attracted to each other, they cannot get close enough to each other to pack themselves into a symmetrical solid structure. An analogy would be trying to load a pickup truck with thin, highly-branched limbs verses stacking uniformly shaped logs into the truck bed. Unable to tightly stack, the ionic molecules slide past each other as a viscous fluid. The two examples are depicted below in Figure 1.13.

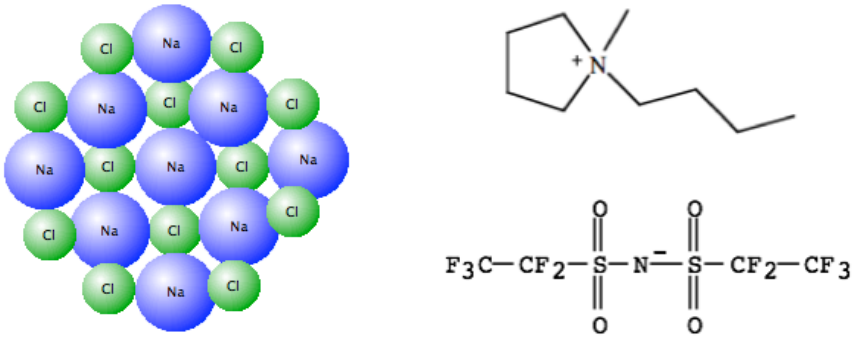

Figure 1.13. The solid ionic compound NaCl on the left, and the ionic liquid 1-butyl-1-methyl-pyrrolidinium BETI (BMPyrrBETI) on the right. Images were made in MarvinSketch version 15.10.26.0 and ChemDoodle version 6.0.1.

The energy contained in a solid ionic compound lattice is known as its lattice energy, and it has a direct bearing on its melting point, and thus, its state (solid vs. liquid).

The strength of the bond between the ions of opposite charge in an ionic compound depends on both the charges on the ions and on the distance between the ion's centers when they pack to form a solid. (http://chemed.chem.purdue.edu/genchem/topicreview/bp/ch7/lattice.html) In quantitative form, the force of attraction between oppositely charged particles is directly proportional to the product of the charge magnitudes of the two particles (q_1 and q_2) and inversely proportional to the square of the distance between the objects (r^2) as seen in Equation 1.1.

Equation 1.1.

$$F = \frac{q_1 \bullet q_2}{r^2}$$

In ionic liquids, these charges are delocalized, and this leads to a reduction in lattice energy (Endres et al., 2008). The thermal stability of the ionic liquid is also based upon the stability of the R-X anion type. The size, shape, and composition of the ions making up the ionic liquids affect the melting point by influencing the crystal packing ability and lattice energy of the ionic liquid (Welton and Wasserscheid, 2002). The equation for calculating this energy is known as the Born-Landé equation and is shown below in Equation 1.2:

Equation 1.2**.**

$$E_c = \frac{N_A M z^+ z^- e^2}{4\pi\varepsilon_0 r}\left(1 - \frac{1}{n}\right)$$

where N_A = Avagadro constant, M = the Madelung constant, which is unitless, Ec = Energy, coulombic, Z+ and Z- = the modulus* of the magnitude of positive and negative charges respectively, e = elementary charge in coulombs, ε_0 = the permittivity of a vacuum = 8.854 x 10^{-12} F m^{-1}, and r = internuclear distance between the ions (units = m), n = the Born exponent.

*The modulus of a real number is its positive value. For example, if Z+ = Mg^{2+} then Z+ = 2(+) and if Z- =O^{2-} then Z- = 2(+) also.

Low melting points are preferred when the charges on the ions are +/-1 and when the size of the anions are large (this ensures that r is large), which will also reduce the overall charge density.

1.9.1 Why use ionic liquids for electrochemical applications instead of aqueous or organic solvents?

One desirable feature of aqueous solutions has been their high conductivity from the fact that electrolytes and metallic salts are very soluble in such a medium. As a result, the electroplating industry has historically (well over 100 years) relied on aqueous solutions exclusively (Abbott and McKenzie, 2006). According to Endres et al. (2008), aqueous solutions have several key advantages:

- Cost
- Non-flammable
- High solubility of electrolytes
- High conductivities resulting in low ohmic losses
- High solubility of metal salts
- High rates of mass transfer (due to low viscosity)

However, aqueous solutions also possess limitations such as:

- Limited potential windows
- Necessity for complexing agents such as cyanide
- All water must eventually be returned to the water course

These limitations preclude aqueous solutions from being used to deposit several technically important materials such as Ti (titanium), Al (aluminum), and W (tungsten), which are abundant and excellent for corrosion resistance. These metals are resistant to work with (refractory), and it is this limitation that has been the main driving force for non-aqueous electrolytes.(Endres et al., 2008). Welton and Wasserscheid (2002) state that

the limited electrochemical windows of aqueous solutions make them unsuitable for the electrodeposition of less noble elements. Specifically, with light, refractory, and rare earth metals, they state that water fails as a solvent because hydrogen evolves long before deposition of the metal can occur. However, the wide electrochemical windows exhibited by ionic liquids in addition to good solubilities of most metal salts make them ideal solvents for electrodeposition (Welton and Wasserscheid, 2002), including the electrodeposition of nanocrystalline metals (Suryanto et al., 2012).

Yet ionic liquids have a number of advantages over both water and non-aqueous solvents that make them well-suited for electrochemical work. Like aqueous solvents, they solvate metal salts very well and exhibit high conductivity, compared to non-aqueous solvents. But in addition, they possess wide potential windows, and avoidance of water- and metal/water chemistry. In addition, ionic liquids are a fitting medium for electrodeposition as they are liquid at a range of temperatures and display low vapor pressures. In fact, deposition of resistant metals like tungsten is credited as being the main driving force of ionic liquid electrolytes, and indeed, electrodeposition was the first application studied in this newer medium (Abbott and McKenzie, 2006).

Organic solvents are one of several alternative electrolytes that can overcome the limitations of - and substitute for - aqueous solvents. But even though organic solvents may have wider electrochemical potential windows than aqueous electrolytes, their applications at industrial scales are the major issues due to handling, toxicity, and volatility issues (Suryanto et al., 2012).

Ionic liquids (ILs) are becoming progressively important as electrolytes for the electrodeposition of metals and may be able to circumvent these limitations. In addition

to the properties mentioned above, ILs offer advantages over organic solvents such as large electrochemical potential windows, simplicity of handling due to their non-volatility and inflammability, are non-combustible, easy to recycle, and possess tunable physicochemical properties. In addition to their high thermal and electrochemical stability, they lack reactivity in various electrochemical or industrial applications seen with organic solvents (Patel, 1990, Seddon, 2003) and they are greener replacements of traditional volatile organic solvents (VOS), or conventional organic solvents (COS).

These factors have lead to the study of ionic liquids as novel and much safer electrolyte materials for electrochemical devices (Ohno, 2005, Patel, 1990) and energy storing devices. The latter include lithium batteries for cell phones (Xu, 2006), batteries for vehicles, fuel cells, solar cells, and supercapacitors (Patel, 1990).

1.9.2 Challenges

One of the barriers to the widespread adoption of ionic liquids at industrial scales is the cost. Another is poor mass transport due to the relatively high viscosity of ionic liquids compared to molecular solvents (Suryanto et al., 2012). The electrochemical window is the range of voltages over which the solvent is electrochemically inert and reflects the electrochemical stability of the solvent (Welton and Wasserscheid, 2002), and no less a problem is the sensitivity of ionic liquids to impurities as it impacts their electrochemical windows. The effect can be profound. Welton (2002) references Schröder et al (2000) as a demonstration of this effect. Water is considered to be an impurity, and a mere 3% water by weight was observed by Schröder et al (2000) to

contract the electrochemical window of $BMImBF_4$ from 4.10 V to 1.95 V - a quite disproportional drop to only 47.56% of its original range (Ibid., Schröder et al., 2000) #65154}. Halides are considered another impurity.

Residual halides left over from synthesis can likewise shorten the electrochemical window. For example, during the synthesis of the ionic liquid used in this study, chloride is introduced very early on. Halide ions such as Cl^-, Br^-, and I^- are oxidized more easily than anions containing fluorine. Therefore, the window would be compromised on the anodic side (Welton and Wasserscheid, 2002).

1.9.3 Why use this ionic liquid ($EMIBF_4$)?

The Katovic research group has been studying ionic liquids based upon the various advantages found by other research groups such as Abbott et al as discussed below. Cations based upon imidazolium have been chosen due to their better fluidity and higher conductivity. Due to its high conductivity, 1-butyl-3-methylimidazolium ($EMIBF_4$) is the most preferred cation in particular (Abbott and McKenzie, 2006). Among ions used in ionic liquids, the tetrafluoroborate (BF_4^-) and ethanoate ($C_2H_3O_2^-$) anions are favored for their contribution to air- and water-stable ionic liquids. (Wilkes and Zaworotko, 1992). The $EMIBF_4$ molecule is shown in Figure 1.14.

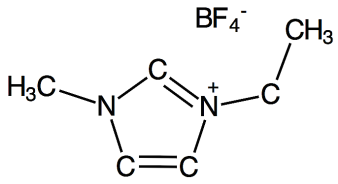

Figure 1.14. The ionic liquid $EMIBF_4$ (1-ethyl-3-methylimidazolium tetrafluoroborate).

The decomposition potential window of 1-ethyl-3-methylimidazolium tetrafluoroborate has reported values of 4.10 - 4.6 V, with most in the range of 4.4 V - 4.6 V (Dyar, 2001, Fuller, 1997, Katayama, 2001, Nakagawa, 2003, Nishida, 2003, Ohno, 2005, Ubadigbo, 2009, Welton and Wasserscheid, 2002).

1.10 The Alternate Solvent System-DMSO

1.10.1 Criteria for Solvent Selection

DMSO was the novel solvent for tri-nuclear clusters attempted by Kennedy due to the unsuccessful electrodeposition of these tri-nuclear clusters onto the Pt electrode. A solvent containing a dissolved electrolyte constitutes a solvent system. There are several criteria to consider when choosing a solvent system. As noted by Kissinger and Heineman (1996), a viable solvent system must meet several general requirements:

1. Chemical inertness
2. Electrochemical inertness

3. Electrical conductivity
4. Good solvent power
5. Convenient liquid range

One such solvent system consists of the electrolyte TBAHFP (tetrabutylammonium hexafluorophosphate), also abbreviated as $TBAPF_6$ (or NBu_4PF_6), in the solvent acetonitrile. TBAHFP is often mentioned as an excellent electrolyte for electrochemical use (Kissinger and Heineman, 1996) When studying the electrochemical behavior of an analyte, one would want as few variables competing for the signals being analyzed as possible. In other words, it would not be desirable to have a solvent system that participates in the process electrochemically (nor chemically for that matter). It is desirable to use a system that stays in the "background" and does not interfere with the electrochemical response(s) of the analyte of interest.

The ACN-TBAHFP solvent system displays viability across a wide potential range of up to 6.3 V (Ibid.) - unfortunately, acetonitrile would not fully dissolve the catalysts, so another solvent had to be chosen. One liability with the use of $EMIBF_4$ was its high viscosity. Because the viscosity of most ionic liquids is relatively high compared to molecular solvents, mass transport is poor (Suryanto et al., 2012) and this can negatively affect the electrochemical signal. $EMIBF_4$ has viscosity ratings ranging from 34cP to 66.5cP at the *same* temperature of 25 °C (Eike et al., 2003, Seddon et al., 2000, Zhang et al., 2006, Zhang et al., 2006). $EMIBF_4$ does, however, possess a high conductivity rating (14 mS/cm) (Welton and Wasserscheid, 2002) as is characteristic of these types of solvents. Nevertheless, deposition of tri-nuclear clusters on the electrode did not occur.

Additionally, previous work in this lab regarding the electrodeposition of tri-nuclear clusters led one researcher to conclude that the anions and cations of the ionic liquid were adsorbed onto the cathode, which may have limited the metal ions available from the tri-nuclear cluster to reduce at the cathode. Therefore, the researcher noted that ionic liquids can act not only as solvent molecules, but as electroactive reagents as well (Ubadigbo, 2009).

A new approach was taken to employ a solvent system that was much less viscous (1.948 cP (Xu et al., 2012) vs. 34-66.5cp at 25ºC), less toxic, and less expensive. The solvent was replaced with dimethyl sulfoxide (DMSO). Although less conductive than $EMIBF_4$, the new solvent system possessed several advantages. In addition, newly ordered electrodes and electrochemical cells were used.

DMSO easily solvated both the catalysts and the electrolyte, and also has a fairly wide potential window (though not as wide as the acetonitrile/TBAHFP system) of 2 to 4.5 V (Ibid.). This is because DMSO is difficult to reduce and is reasonably resistant to oxidation by electrolysis. DMSO also possesses a high dielectric constant of 46.7 (Tsierkezos and Philippopoulos, 2009), vs. 12.8 for $EMIBF_4$ (Wakai et al., 2005), is much less expensive (see Table 1.1), and is not directly toxic. DMSO, a universal solvent, possesses other favorable advantages such as good oxygen diffusion ability, high conductivity (2.11 mS/cm when containing Li+ salts), and especially, remarkable stability against superoxides.(Laoire et al., 2010, Xu et al., 2012). DMSO can, however, transport other substances through the skin, which can be potentially harmful.

A quick look at the Sigma-Aldrich website (10/2016) for similar amounts of $EMIBF_4$ and DMSO revealed a large variation in price. It is especially evident when the two are compared as a percentage of cost per mL.

Table 1.1 Cost comparison between the two solvents used - DMSO and $EMIBF_4$.

Solvent	mass (g)	Vol (mL)	Total cost	Cost / mL	% cost/mL relative to other solvent
DMSO*	/	100	32.00	0.32	1.76
$EMIBF_4$**	50	38.64	701.00	18.14	5669.34

*DMSO (Sigma-Aldrich [Cat # D4540 ≥99.5% CAS #: 67-68-5])

**$EMIBF_4$ (Sigma-Aldrich [for electrochemistry, ≥99.0% (HPLC) Cat.# 00768 CAS #: 143314-16-3]). $EMIBF_4$ is sold by mass instead of volume.

It is not surprising that DMSO is considered to be among the better choices of solvent for electrochemistry (Kissinger and Heineman, 1996).

1.10.2 The Effect of Water on $EMIBF_4$ and DMSO

1.10.2.1 Hygroscopic character of ionic liquids

One of the drawbacks to the use of ionic liquids was their highly hygroscopic nature (Welton and Wasserscheid, 2002). Water is considered an impurity in ionic liquids - one which affects both chemical and physical properties. Impurities in ionic liquids can have a poisoning effect on reactions that are catalyzed by transition metals

(Olivier-Bourbigou et al., 2010). Freire et al., (2007) studied the mutual solubilities of water and imidazolium-based ILs. They found that these mutual solubilities were dependent first upon the anion, and then to a lesser extent, the alkyl side chain length. They ranked several of the most common anions in order of hydrophobicity, which in the following example, increases from left to right: $[BF_4]^- < [CH_3(C_2H_4O)_2SO_4]^- < [C(CN)_3]^- < [PF_6]^- < [N(SO_2CF_3)_2]$ (Freire et al., 2007). Dancevic (2003) similarly reported that short alkyl chain possessing ionic liquids were more hygroscopic (Dancevic, 2003).

The ionic liquid used in this study contain the least hydrophobic anion reported on by (Freire et al., 2007), as well as the two shortest of alkyl chains and is therefore very hygroscopic.

As noted above, the presence of water in ionic liquids can considerably compromise the range of the solvent's breakdown limits. This has been observed by Schröder et. al. (2000), and reported on by Welton (2002). The addition of water reduced both the anodic and cathodic limits of several ionic liquids, including 1-butyl-3-methylimidazolium tetrafluoroborate ($BMIBF_4$) - a very similar ionic liquid to that used in this research. The authors reported > 50% reduction in the electrochemical window of dried $BMIBF_4$ from 4.10 V to 1.95 V, with the addition of 3% water by weight (Dyar, 1999, Schröder et al., 2000, Ubadigbo, 2009, Welton and Wasserscheid, 2002).

Water not only displays its own electrochemistry, it can also interact with components of the ionic liquid - more so with the anion - yielding electroactive products that further complicate the voltammogram.

1.10.2.2 Hygroscopic character of DMSO

DMSO is not nearly as hygroscopic as $EMIBF_4$. In fact, as Heineman and Kissinger note, water does not seem to hurt the performance of DMSO. The authors reveal that DMSO is not nearly as water-sensitive as ionic liquids, and in fact commercially available DMSO displayed identical behavior to DMSO that had been purified. Moreover, intentionally adding a substantial amount of water had no effect (Kissinger and Heineman, 1996).

1.10.3 Electrochemical window of $EMIBF_4$ and DMSO

The electrochemical window of $EMIBF_4$ has been observed to be between 4.1V - 4.5V when dried to around 50ppm (Dyar, 1999, Ubadigbo, 2009, Welton and Wasserscheid, 2002). Water severely compromises this window. The electrochemical window of DMSO has been reported to be approximately 2.7 V, with the anodic range limited to about +0.9V at a stationary platinum electrode, a cathodic range of -1.8 V vs. SCE, with TEAP as supporting electrolyte (Adams, 1969). Although narrower than the electrochemical window of $EMIBF_4$, the behavior of DMSO is not affected by the presence of water. Not all investigators find the electrochemical window of DMSO to be as narrow however. Xu et al., reports the electrochemical window of DMSO to be between 2.7 V - 4.5 V (Xu et al., 2012).

The electrochemical window of a solvent is also referred to as its breakdown limit. It represents the range within which the solvent is stable enough to display redox processes of dissolved species provided those processes occur within a narrower potential

range than the solvent's reduction-oxidation limits. It is therefore evident that one chooses a solvent with a wider breakdown limit / electrochemical window than the species of interest.

1.11 Ethanol oxidation by catalysis

As a fuel, ethanol has several advantages:

- It is renewable.
- It can be produced from biomass.
- Compared to methanol, ethanol is less toxic.
- The specific energy density of ethanol is high (8.0 kWh/kg, or 29.7 MJ/Kg)
- It is liquid, which makes it easy to store and transport.

These advantages make the use of ethanol in direct ethanol fuel cells (DEFCs) promising as a green energy source(Asiri and Anderson, 2015).

In fact, according to Roquero et al (2007), ethanol can be considered as an ideal biomass-obtained fuel. The caveat to that statement, however, is that a high voltage at the anode is needed to scission the carbon-carbon bond. Cleaving the carbon-carbon bond is important because only then can ethanol be considered totally oxidized, and only then will it yield the full quantity of electrons (12) and supply the maximum current. It is - as Courtois (2013) notes - in fact, inevitable, as a quick look at the products show. It is the breaking of ethanol's carbon-carbon bond that is the primary goal of this research. The reaction is shown below in Equation 1.3:

Equation 1.3

$$C_2H_5OH + 3H_2O \rightarrow 2CO_2 + 12H^+ + 12e^-$$
$$3O_2 + 12H^+ + 12e^- \rightarrow 6H_2O$$
$$C_2H_5OH + 3O_2 \rightarrow 2CO_2 + 3H_2O$$

Equation 1.3. The oxidation of ethanol by oxygen into carbon dioxide, and water.

The electrode system we will employ is a platinum electrode with tri-nuclear clusters of molybdenum and tungsten combinations electrodeposited onto the surface. Lai et al., notes that platinum is considered the best monometallic catalyst for the electro-oxidation of small organic molecules and that research on the ethanol electro-oxidation reaction has traditionally focused on platinum electrodes (Lai et al., 2010).

However, because the electro-oxidation reaction of ethanol on platinum is slow and inefficient, it has hindered the commercialization of DEFCs. Platinum *is* active as the anode electrocatalyst in *hydrogen* fuel cells but is much less active for ethanol oxidation(Asiri and Anderson, 2015). Another problem is that platinum catalysts are susceptible to CO poisoning - a byproduct of oxidizing ethanol (Courtois, 2013). Nor is CO the only undesirable byproduct - the difficulty in breaking the C-C bond leads to a high concentration of partial oxidation products, such as CH_3CHO (ethanal) and CH_3COOH (ethanoic acid) at the surface of platinum catalysts. In the direct ethanol fuel cell, this causes a significant drop in efficiency (Ibid.). Thus, augmenting the electrode with the addition of other metals is being pursued.

The application of molybdenum and tungsten to electrodes has shown increased catalytic activity toward the oxidation of methanol compared to catalysts containing only platinum (Kim et al., 2009, Roquero et al., 2007). Roquero et al even states that such

catalysts are sufficient for liquid-fuel alcohol fuel cell systems, noting that oxidation potentials are lower than those observed with platinum (only) catalysts (2007). These conclusions were also reached by Kim et al., (2007).

1.12 Literature Review

As noted, there are a myriad of iterations and conformations of tri-nuclear clusters that have been synthesized. While similar compounds have been investigated, the research focused on different areas than those investigated in this research, such as the kinetics of ligand substitution, characterization by NMR and UV, or categorizing by crystallography, but not electrochemically (Ardon et al., 1982, Bino et al., 1981, Bino and Gibson, 1980, Bursten, 1982, Chisholm, 1977, Cotton et al., 1983, Cotton et al., 1984, Cotton et al., 1985, Cotton and Feng, 1991, Cotton and Kühn, 1996, Hibble and Fawcett, 1995, Katovic, 1975, Lawton, 1964, Nakata et al., 1991, Patel, 1990, Roquero et al., 2007, Santure, 1985, Suzuki, 1994, Wang et al., 1986).

1.12.1 Comparison to Huang (1994)

A 1994 paper titled "Electrochemical Study of Trinuclear Metal Complexes" by Huang et al., was easily the most relevant study to this dissertation work (Huang et al., 1994). The researchers studied three of the four trimers that were used in this research, namely $[Mo_3O_2(O_2CCH_3)_6(H_2O)_3](CF_3SO_3)_2$ abbreviated here as Mo_3,

$[MoW_2O_2(O_2CCH_3)_6(H_2O)_3](CF_3SO_3)_2$, abbreviated MoW_2, and $[W_3O_2(O_2CCH_3)_6(H_2O)_3](CF_3SO_3)_2$ as W_3. The fourth, $[Mo_2WO_2(O_2CCH_3)_6(H_2O)_3](CF_3SO_3)_2$, or Mo_2W, was mentioned initially, but was not studied.

The Huang et al., paper was novel from the aspect that these tri-nuclear cluster compounds were studied for the first time by electrochemical techniques. They reported on the peak potentials and the reversibility character of the clusters. Below are the similarities and differences of the studies found on tri-nuclear clusters comparing Kennedy to Huang. Huang (1993) employed a 3-electrode system made of a Pt working electrode, a SCE reference electrode, and a Pt counter electrode where Kennedy employed the 3 electrode system but with a Ag/AgCl reference electrode. CV scans by Huang were run at 150 mV/s where Kennedy varied the scan rates (1-1000mV/s). The scan range for Huang was from +1.0V to -1.5V for every compound where Kennedy expanded the scan range from +1.0V to-2.0 V. For Huang, the solvent chosen was dimethyl-formamide (DMF) with the supporting electrolyte Bu_4NClO_4 (tetrabutylammonium perchlorate) and for Kennedy the solvent was DMSO with TBAHFP.

A similar arrangement as described by Huang et al (a 3-electrode system) was used in our study. Three types of platinum working electrodes were used in all - a 1.6 mm diameter platinum disk electrode, a 3mm diameter platinum disk electrode, and platinum foil working electrodes. A Ag/AgCl reference electrode was used rather than SCE used by Huang et al., and a platinum wire served as the counter electrode (for both groups). Scan rates of 150 mV/s could not be performed on our equipment, so scans at 100 mV/s

and 200 mV/s were used to compare to results from Huang et al (all scan rates available to us were in fact used (1, 5, 10, 20, 50, 100, 200, 500, and 1000 mV/s)). A wider scan *range* was used, up to the solvent breakdown limits (~ +1.5V to -2.0V), encompassing the range used by Huang et al., of +1.0V to -1.5V.

The first solvent used was an ionic liquid, 1-ethyl-3-methylimidazolium, or $EMIBF_4$. It was later abandoned in favor of dimethyl sulfoxide (DMSO). Tetrabutylammonium hexafluorophosphate, or TBAHFP, served as the electrolyte. In addition, to studying the published parameters (such as Ep,a and Ep,c of the redox couple, and Ep,c-1 of the reduction wave), additional values were obtained experimentally, $E_{½}$, ΔE, Ip,a, Ip,c, Ip,c/Ip,a, and D, the diffusion coefficient. In addition, electrodeposition was attempted with all four of the tri-nuclear clusters onto platinum electrode and reported. Diffusion coefficients were found experimentally for each cluster in the latter solvent system.

2. EXPERIMENTAL

Diagrams, molecules, and reaction schemes were created with ChemDoodle, version 6.0.0 © iChemLabs, LLC 2007-2015. Flowcharts were created with Scapple version 1.2, © Literature and Latte, 2005-2015. Peak current and baseline-fitting was performed using eL-Chem Viewer, open-source software.

2. EXPERIMENTAL

2.1 Material Synthesis and Purification

2.1.1 Metal Cluster Synthesis

2.1.1.1 Syntheses of di-nuclear clusters

2.1.1.1.1 The molybdenum dimer (Mo_2)

Synthesis begins with the production of a molybdenum di-nuclear cluster, or "dimer" for short. This di-nuclear cluster, abbreviated as Mo_2, is an intermediate product in the synthesis of the desired tri-nuclear clusters. The reagents used for this synthesis are: molybdenumhexacarbonyl ($Mo(CO)_6$), trimethylacetic acid, also known as pivalic acid, ($(CH_3)_3CCOOH$), and ortho-chlorobenzene ($C_6H_4Cl_2$). The first two reagents are solids, necessitating use of the third (o-chlorobenzene) as a solvent. Equation 2.1 gives the chemical equation for the synthesis of the molybdenum dimer.

Equation 2.1 $2\ Mo(CO)_{6(s)} + 4\ (CH_3)CCO_2H_{(s)} \longrightarrow Mo_2(O_2CC(CH_3)_3)_{4(s)} + 12\ CO_{(g)} + 2H_{2(g)}$

A 100 mL Schlenk reaction flask (see Figure 2.1) was used in this synthesis, to which was added a thin glass dowel and magnetic stir-bar. Each of these components were cleaned and allowed to dry in an oven for ≥4 hours.

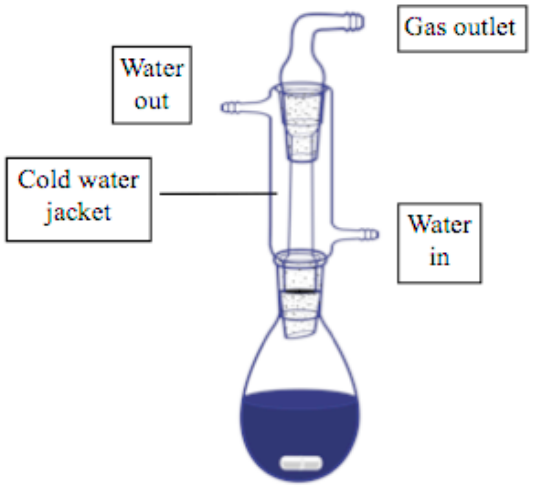

Figure 2.1. The Schlenk reaction flask.

The dimers are both air- and water-sensitive (Chisholm, 1977, Katovic, 1975), so the ortho-chlorobenzene was first dried at ~ 180 ºC under high vacuum for > 2 days. It was then tested for moisture with the Karl Fisher method, and found to contain 102.6 ppm of water. To further reduce water, molecular sieves (3Å, Sigma Aldrich) were applied to the solvent. The sieves were first dried by holding them at 350 ºC for 3.5 hours in a muffle oven. Once dried, two techniques for applying the sieves were explored to determine which was more effective at removing the remaining water from the ortho-chlorobenzene.

The first method was to send the o-chlorobenzene through a column containing the activated sieves. The 2nd method was to add ~ 64 mL of 3Å activated molecular sieves to ~120 mL of the solvent and allow to soak overnight. Samples were once again tested for

water using the Karl Fisher method. Samples of the solvent from method 1 were found to have decreased in H_2O content from 102.6 ppm before drying to 27.0 ppm after drying, whereas method 2 took the H_2O content down to 3.6 ppm. As reported by Breck (1956), this method is capable of lowering water content to single-digit ppm levels (D. W. Breck, 1956).

2.1.1.1.2 Schlenk method

Because the molybdenum dimer is both air and moisture-sensitive, the Schlenk method (Shriver, 1986) was used (a method that uses a system of specialized glassware, inert gas(es), and a vacuum system that isolates the reagents and products and helps to control their environment).

The components of the Schlenk setup used in this research included:

- A glove box (and/or a glove bag) to provide an inert atmosphere for working
- Nitrogen gas (as the source of inert gas)
- Vacuum pumps (for multiple uses - purging glasswares of air and moisture, providing dynamic control of the environment inside the reaction vessel during syntheses, etc.)
- Cannulas (very long needles of varying gauges of diameter) for transferring liquids without exposing them to the atmosphere
- An assortment of specialized glassware to dry the materials used in the synthesis, and to protect the materials from oxidizing once synthesized.

Figure 2.2 depicts the Schlenk method setup used to synthesize the dimer in this lab.

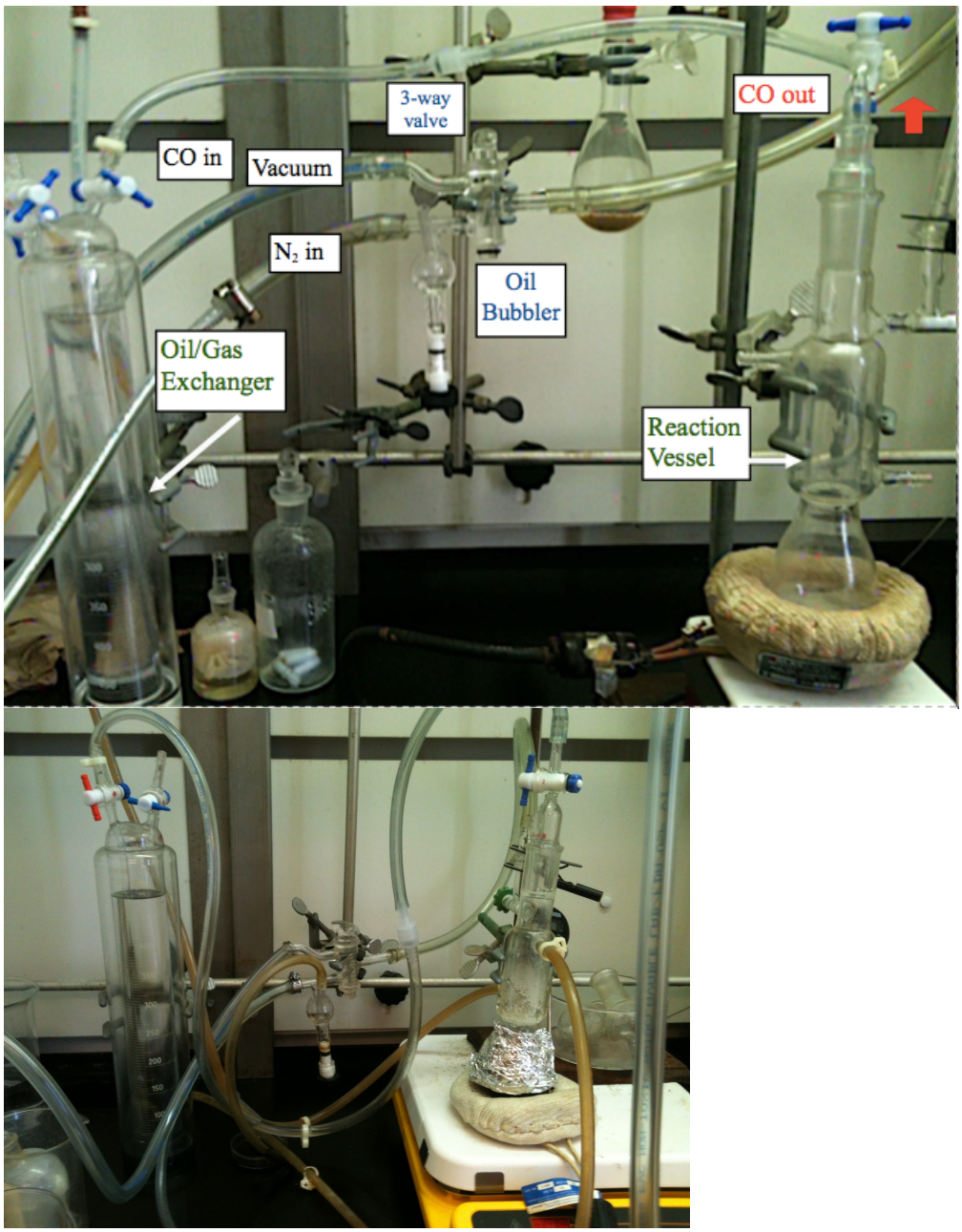

Figure 2.2. Schlenk method apparatus. Above: The oil/gas exchanger, the oil ”bubbler", the 3-way valve, and the reaction vessel on the hot/stir plate. Below: synthesis underway.

The reaction vessel and attached lines are first purged of air by use of a vacuum, and then filled with inert gas (nitrogen). This procedure is repeated several times. Unfortunately, the reaction progress is not conducive to visual observation, as the mixture quickly takes on an opaque black tint and does not change its appearance throughout the synthesis while all reagents are in contact with each other. Therefore, to monitor the progress of the reaction as well as its end-point, an oil displacement vessel (Figure 2.3) was connected to the reaction vessel. This is useful, because in addition to the solid dimer product we want, two gases are also produced. By recording the volume of oil displaced by the gaseous products, the theoretical product yield of the reaction can be calculated. Generally speaking, the end-point can also be determined in this manner, as the oil will no longer displace.

Figure 2.3. Oil displacement vessel.

In practice, a number of factors contributed to the appearance that the reaction has reached its end-point, when it in fact had not. For example, this synthesis leads to

deposition of the material on the walls of the reaction flask, and leads to an obstruction at its neck. This also has the effect of blocking the escape of the gaseous products CO and H_2. No further gaseous products can make it through to displace the oil. This can not only make it appear that the reaction has stopped (if monitoring by the volume of oil displaced), but can also lead to a dangerous situation where gases continue to build up below the obstruction, which can lead to an explosion.

Traditionally, the corrective method involved removing the top from the condenser (under positive pressure by an inert gas) and clearing the blockage with and instrument such as a glass dowel. The disadvantage to this technique is that the reaction would need to be monitored almost continuously - as the condensate can accumulate rapidly - yet the reaction can take many hours or days. The author used a cleaned, dried glass dowel that could operate inside the closed condenser by inserting it before starting the reaction, and leaving it in during the synthesis as depicted in Figure 2.4 The glass dowel makes a random stirring motion with both rotating and revolving components thanks to the action of the magnetic stir-bar. This method was useful for keeping the neck of the condenser free of blockages by essentially self-cleaning, and does not require monitoring.

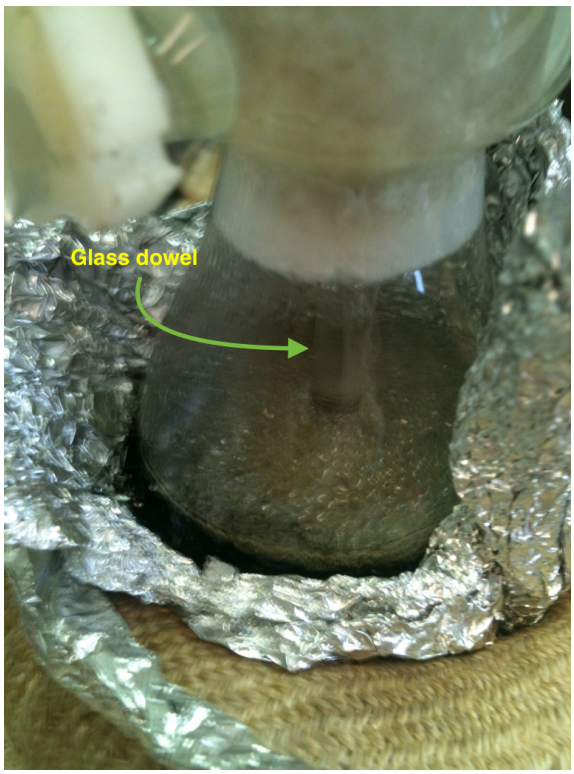

Figure 2.4 A glass dowel helps to keep the neck of the condenser free of obstruction.

Once the reaction reached completion, the solid molybdenum dimer was transferred to a Schlenk filter flask (Figure 2.5). This was also done in a controlled fashion with Schlenk glassware, nitrogen gas, and vacuum to prevent oxidation of the newly-synthesized dimer.

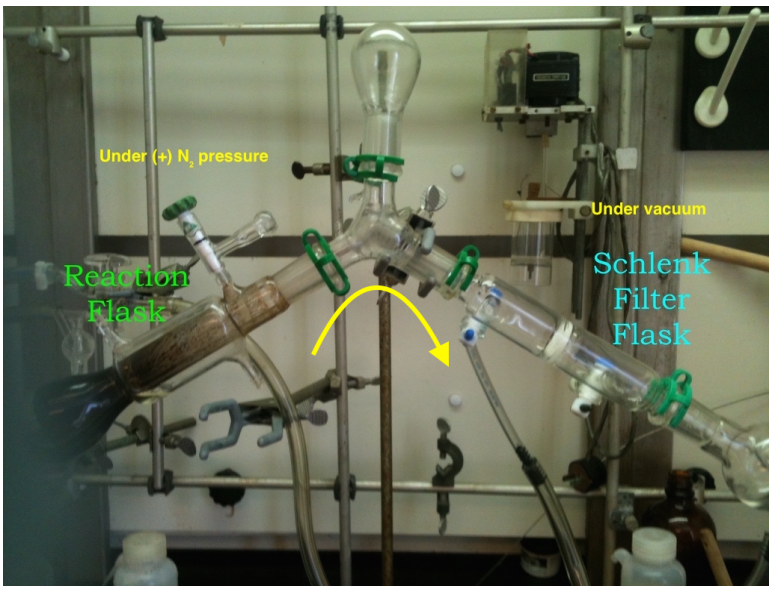

Figure 2.5. A Schlenk filter flask connected to vacuum and inert gas. The assembly can be tilted, so that the contents of the reaction flask can be transferred into the filter flask without exposure to air.

After the crystals have been transferred to the glass filter flask, they were then washed with cyclohexane that had been dried over activated 4Å molecular sieves. The wash was also carried out using the Schlenk technique, as shown in Figure 2.6* below.

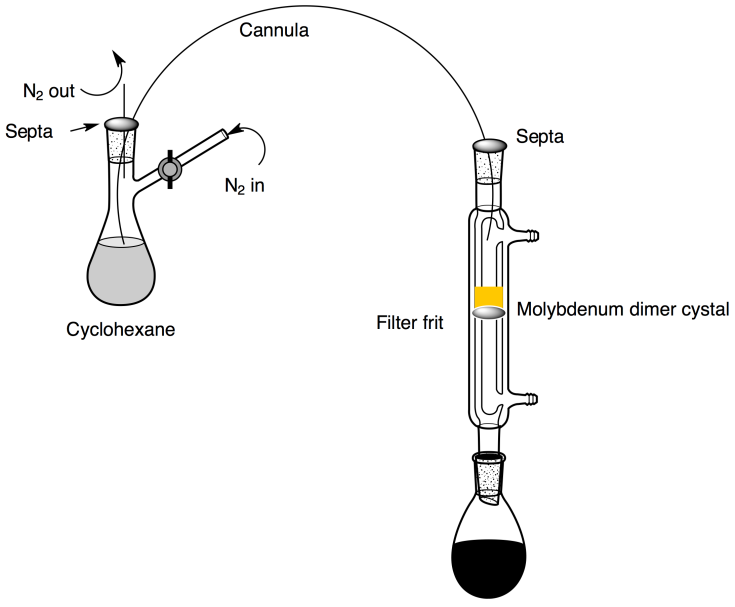

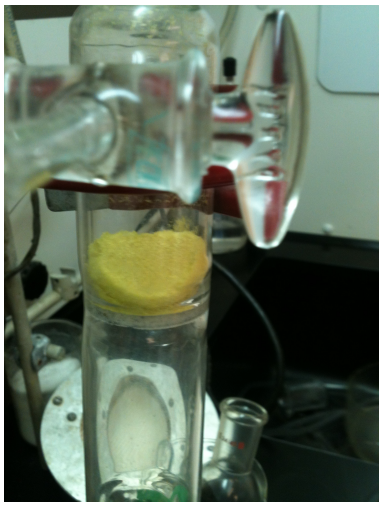

Figure 2.6. Washing the dimer crystals with cyclohexane. Diagram was created with ChemDoodle, version 6.0.1.

The molecular structure is shown in Figure 2.7.

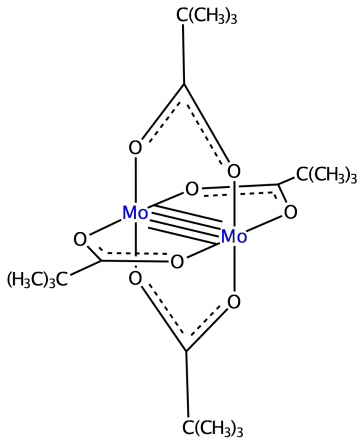

Figure 2.7. The structure of the $Mo_2(O_2CC(CH_3)_3)_4$ dimer. Note the quadruple bond between the two molybdenum atoms.

After washing, the Mo_2 dimer was stored inside a small bottle filled with argon, which was placed inside a larger bottle, also filled with argon. These containers were then stored in a degassed desiccator containing Drierite® desiccant, along with phosphorous pentoxide as an added measure to maintain a dry environment.

2.1.1.1.3 Synthesis of MoW dimer

The synthesis of the other dimer was very similar to the previous synthesis, except that a mixture of molybdenum (Mo) and tungsten (W) was used, as molybdenum hexacarbonyl $Mo(CO)_6$ and tungsten carbonyl $W(CO)_6$. This synthesis leads to a mixture of the two dimers, but it is worth noting that previous work has shown that the largest concentration of both dimers results from supplying a 1:3 ratio of **Mo**$(CO)_6$ to **W**$(CO)_6$

(Suzuki, 1994). The product cools to form yellow, needles-like crystals. As with the molybdenum dimer, this heteronuclear dimer is very air sensitive. It has been observed that on exposure to air, the crystals turn black within just a few minutes(Ubadigbo, 2009). The solution contains a mixture of the 2 dimers - $(Mo_2(O_2CC(CH_3)_3)_4$ and $MoW(O_2CC(CH_3)_3)_4$, so the product can be selectively-oxidized when iodine in benzene is added(Cotton, 1969, Suzuki, 1994). After the compound (brown) was run through a Schlenk filter, it is washed again with benzene and reduced with zinc in acetonitrile to yield a sample of the $MoW(O_2CC(CH_3)_3)_4$ dimer (Katovic, 1975). However, the compound could not be kept from oxidizing and it's synthesis was halted.

{Zhang et al., 2006, #48299}2.1.1.2 Syntheses of the tri-nuclear molybdenum cluster

The synthesis protocols for the four trimers were taken from previously-published methods (Cotton et al., 1984, Katovic, 1975, Paul et al., 1994, Wang et al., 1986). Using the molybdenum dimer [$(Mo_2(O_2CC(Me)_3)_4$], synthesized in the previous section, ($n:figure:quadbondmo), the molybdenum trimer was then synthesized as one of the desired trimer products used in this research. To a 100 mL Schlenk reaction flask, 1.20 g of the molybdenum dimer, $Mo_2(O_2CC(Me)_3)_4$, or dimolybdenum tetraacettate, was combined with 1.21 g of sodium molybdate $(Na_2MoO_4)•2H_2O$, 70 mL of dried acetic acid, 7 mL of acetic anhydride, and 1 mL of triethylamine. A cleaned and dried glass dowel and magnetic stir bar were also added. Synthesis was performed under N_2 and vacuum.

Once the reaction was complete, the solution (now burgundy wine colored with a purple hue) was diluted with 200 mL dH_2O per Suzuki (1994) and Wanamaker (1998) (Suzuki, 1994, Wanamaker, 1998) and filtered to remove any unreacted solid reagents.

Dowex® ion exchange resin (50WX2 hydrogen form) was added to an ion exchange column, which had been previously cleaned and dried. To prime the Dowex resin, 40 mL of 1N HCl was applied, and the filtrate was added to the column.

Ion exchange was accomplished with the addition of 1.0 M triflic acid (CF_3SO_3H). The eluents formed bands (Figure 2.8) with distinct hues (steel-blue, dilute rust-colored, purple) which were captured and examined with UV to identify the band containing the trimer product.

Figure 2.8 The Mo_3 trimer in the ion-exchange column with 1.0M trifluoromethanesulfonic acid added.

The clusters' formulas are shown below in Figure 2.9. For less cumbersome notation, the clusters will often be abbreviated by referring to just their metal composition as follows:

Mo_3 represents $[(\mathbf{Mo_3}O_2(O_2CCH_3)_6(H_2O)_3](CF_3SO_3)_2$

Mo_2W represents $[(\mathbf{Mo_2W}O_2(O_2CCH_3)_6(H_2O)_3](CF_3SO_3)_2$

MoW_2 represents $[(\mathbf{MoW_2}O_2(O_2CCH_3)_6(H_2O)_3](CF_3SO_3)_2$

W_3 represents $[(\mathbf{W_3}O_2(O_2CCH_3)_6(H_2O)_3](CF_3SO_3)_2$

Figure 2.9. The four tri-nuclear clusters used in this study.

2.1.2 Ionic Liquid Purification

2.1.2.1 Decolorizing

It is well-established that impurities in ionic liquids compromise their electrochemical window (narrowing it) and each type of impurity should be kept below 50 ppm (Abbott and McKenzie, 2006, Dyar, 2001). It is therefore important to remove these impurities before settling on the final product.

1-ethyl-3-methylimidazolium tetrafluoroborate ($EMIBF_4$) was received from Sigma Aldrich. Before use, it was tested for water by Karl Fischer titration and found to contain 287.5 ppm. The ionic liquid was purified to remove color and any remaining impurities using a method published by Earle (Earle et al., 2007) and scaled to a POR-B, ASTM 70-100µ column by Ace Glass Co. The column was packed with ~2 cm of Celite 545 (Fisher Scientific), followed by ~2 cm of Silica Gel (Fisher Scientific), and finally with ~30 cm of Carbon (C-177 Nuchar S-N) for decolorizing (See Figure 2.10).

Figure 2.10. The column used to purify $EMIBF_4$.

$EMIBF_4$ is fairly viscous at 34 cP (Zhang et al 2006) as opposed to water at 0.894 cP, so acetonitrile was used to reduce the viscosity. Acetonitrile was dried over activated 3Å molecular sieves (Sigma-Aldrich) for 4 days, then tested with a Coulometric Karl Fisher Titrator (Model 260), and was found to contain 19.6 ppm water. Pretreated was performed by sending approximately 123 mL of the dried acetonitrile though the column. Next, a 1:3 ratio of $EMIBF_4$ and acetonitrile was combined and stirred for several hours. This solution was sent through the column, followed by one more addition of ~123 mL of dried acetonitrile.

The mixture went from a clear but slightly yellow tint before being sent though the column to clear and colorless afterward as seen in Figures 2.11 and 2.12.

Figure 2.11. New $EMIBF_4$ purchased from Aldrich, before treatment to remove impurities.

Figure 2.12. The same ionic liquid after running through the column.

The acetonitrile was then separated from the ionic liquid by use of a condenser equipped with vacuum and a cold trap, which contained liquid N_2 as depicted in Figure 2.13.

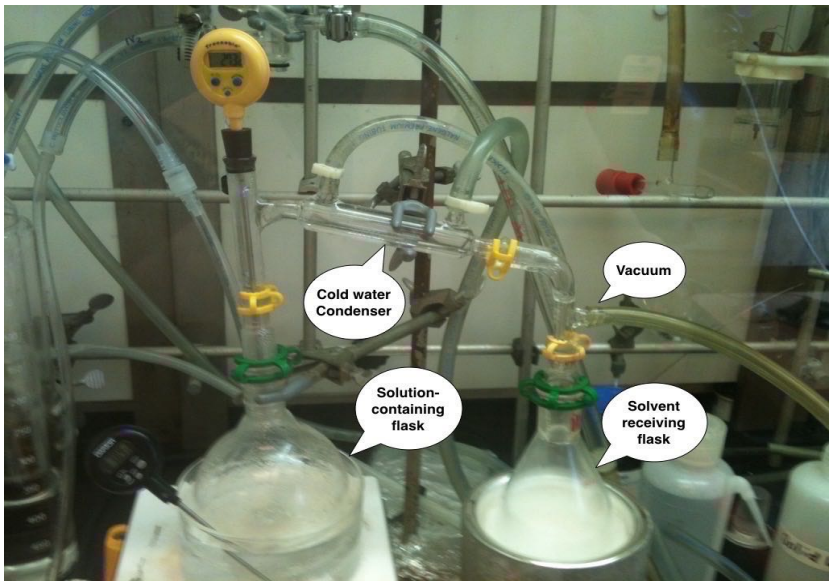

Figure 2.13. The relatively low boiling point of acetonitrile is used to separate the solution by the use of the condenser. Heat is applied to the flask containing the solution on the left. As acetonitrile has a lower boiling point (81 - 82 °C) than water, it will enter the vapor phase before the water residing in the solution. To draw the solvent vapor into the receiving flask on the right, a vacuum is applied to the receiving end and the flask itself rests in a cold bath of liquid N_2 and ethanol. The solvent then collects in the receiving flask, once again in the liquid phase.

The condenser was initially drawn upon by the house vacuum. After it could pull no more solvent off, the remaining solution was subjected to a "low" vacuum of 10^{-1} torr and finally to a "high" vacuum of 10^{-5} torr. During each step, the solution was heated to just below the boiling point of the solvent to further facilitate water removal. Water content of the remaining ionic liquid was then checked with a Karl-Fischer titrator and found to be 142.0 ppm. The ionic liquid was then verified with a Thermo Scientific Nicolet 6700 FT-IR. Scientific Nicolet 6700 FT-IR.

2.1.2.2 Selecting and Preparing the alternate solvent

The ACN-TBAHFP solvent system displays viability across a wide potential range of up to 6.3 V (Kissinger and Heineman, 1996) - unfortunately, acetonitrile would not fully dissolve the catalysts, so another solvent had to be chosen. That solvent chosen was DMSO (dimethylsulfoxide).

TBAHFP was ordered from Aldrich and used as received. DMSO was ordered from Aldrich and tested for water content with a Denver Instruments Model 260 Coulometric Karl Fisher titrator before use. After injecting 0.837 g of the solvent, the water content was found to be 293.0 ppm. Activated Aldrich 3Å molecular sieves (Liu et al., 2012, Olivier-Bourbigou et al., 2010) were combined with 100 mL of the solvent in a 100 mL round-bottom flask and allowed to sit for 1.5 days. The sieves were previously baked in a muffle oven for 3 hours at 350 °C. Subsequent water testing with 1.394 g of the dried solvent gave a value of 29.5 ppm, or roughly 10% of the previous value.

2.2 Catalyst Preparation in $EMIBF_4$ & DMSO

2.2.1 Preparation of catalysts in $EMIBF_4$

The four tri-nuclear clusters were combined with the ionic liquid in a dry-box under inert gas (N_2). Approximately 10.3 mg (1.004 mM) of $[Mo_3O_2(O_2CCH_3)_6(H_2O)_3](CF_3SO_3)_2$ was combined with $EMIBF_4$ in clean, dry 50 mL round-bottom flask, containing a dry stir-bar. The trimer was dissolved under heat and vacuum with stirring. Approximately 11. mg (0.9873 mM) of the $[Mo_2WO_2(O_2CCH_3)_6(H_2O)_3](CF_3SO_3)_2$ trimer along with 12. mg of the MoW_2 trimer (0.9983 mM), and 12.9 mg (1.00 mM) of the $[W_3O_2(O_2CCH_3)_6(H_2O)_3](CF_3SO_3)_2$ trimer were dissolved in the same manner. The data are summarized below in Table 2.1.

Table 2.1. Concentrations of each tri-nuclear cluster when dissolved into 10.0mL of the solvent system.

Cluster	C (mM)
Mo_3	1.004
Mo_2W	0.9873
MoW_2	0.9983
W_3	1.000

2.2.3 Preparation of catalysts in DMSO

The four tri-nuclear clusters were dissolved into the solvent system. A 1.08 mM

solution of the tungsten trimer, W_3, was made by dissolving 13.9 mg of the trimer into 10.0 mL of the solvent system. A 1.05 mM solution of the MoW_2 trimer was made by dissolving 12.6 mg of the trimer into 10.0 mL of the solvent system. A 1.00 mM solution of the Mo_2W was made by dissolving 11.1 mg of the trimer into 10.0 mL of the solvent system. A 1.28 mM solution of the molybdenum trimer, Mo_3, was made by dissolving 13.1 mg of the trimer into 10.0 mL of the solvent system. The data are summarized below in Table 2.2.

Table 2.2. Concentrations of each tri-nuclear cluster when dissolved into 10.0mL of the solvent system.

Cluster	C (mM)
Mo_3	1.28
Mo_2W	1.00
MoW_2	1.05
W_3	1.08

The solutions were stirred and gently heated until the solution exhibited a clear, uniform tint as shown in Figure 2.14. The new solutions were then stored in a desiccator containing Drierite® and P_2O_5 until use.

2.3 Parameters measured by voltammetric analysis

According to Adams (1969), cyclic voltammetry is best suited for investigating chemical and electrochemical processes that may transpire in complex electrode

reactions. This tool allows for the study of the current-potential relationship. Cyclic voltammetry also indicates at which potential redox processes occur. In addition, it reveals the "reversibility" of a redox process (whether reversible, irreversible, or "quasi-reversible")(Adams, 1969).

Each trimer catalyst was scanned at rates of 1, 5, 10, 20, 50, 100, 200, 500, 1000 mV/s in both the forward and reverse direction. The plots were carefully measured to obtain the following parameters obtained from the data:

- Ep,a Anodic peak potential
- Ep,c Cathodic peak potential
- E^0 The Formal potential (Ep,f + Ep,r) / 2
- ΔEp The change in potential
- Ip,a Anodic peak current
- Ip,c Cathodic peak current
- Ip,c/Ip,a Ratio of cathodic to anodic peak current
- D Diffusion coefficient

2.4 Electrodes and the Electrochemical Cell

Electrochemical cells and electrodes were ordered from BASi. The 3-electrode cell used was a BASi VC-2 Voltammetry Cell assembly (MF-1052) with platinum counter electrode and deaerating tube supplied. The working electrode used was a BASi platinum 1.6 mm diameter electrode (MF-2013, 99.95% purity), and a BASi silver/silver chloride electrode containing a 3M KCl solution was used as the reference electrode. The

deaerating tube was used allowed argon to flow into the cell. It was used to both to purge the solution of air and to maintain a positive pressure of the inert gas over the solution during the experiment. Figure 2.14 shows the electrodes and electrochemical cell (left) and the assembled electrochemical cell (right).

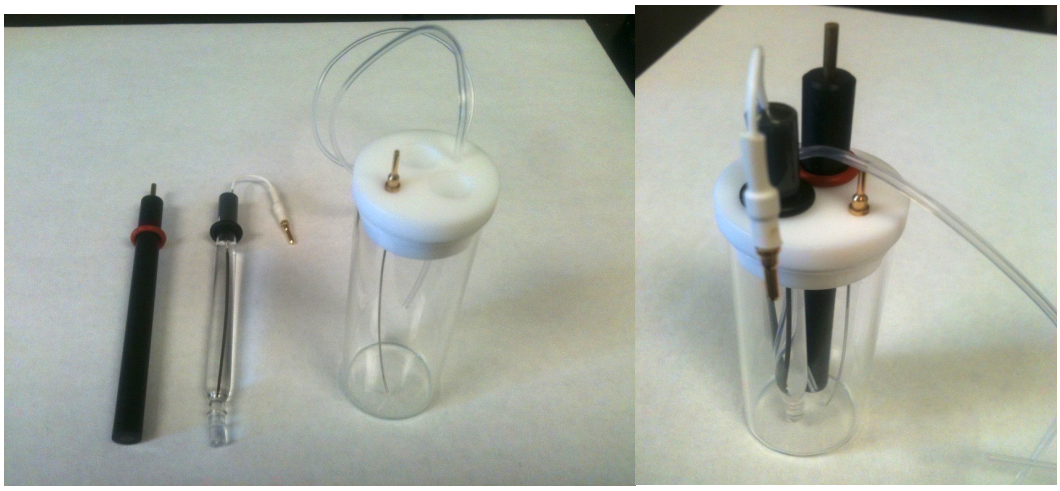

Figure 2.14. Left image: The components of the electrochemical cell used: Platinum disc working electrode (left), Ag|AgCl reference electrode (middle), with the platinum auxiliary electrode in the cell. Right image: the assembled cell.

In addition to the cleaning protocol followed with the previous solvent (Abbott and McKenzie, 2006), diamond polish was also used. Scans were performed at 1, 5, 10, 20, 50, 100, 200, 500, and 1000 mV/s. The scans most often depicted are from 100 and 200 mV/s, as these are the closest to the 150 mV/s scan rate used by Huang et. al. (1995).

2.5 Sample Preparation for UV-Vis Analysis

Small samples of each of the four trimeric compounds were weighed and placed into separate small vials. After the masses were recorded, a measured amount of dH_2O was added to each vial, and the concentration was recorded as shown in Table 2.3 below:

Table 2.3. The masses and concentrations of each tri-nuclear cluster sample used in the study.

Trimer	Mass (g)	Molarity (x 10^{-6})
$[Mo_3O_2(O_2CCH_3)_6(H_2O)_3](CF_3SO_3)_2$	0.0044	4.28
$[Mo_2WO_2(O_2CCH_3)_6(H_2O)_3](CF_3SO_3)_2$	0.0050	4.48
$[MoW_2O_2(O_2CCH_3)_6(H_2O)_3](CF_3SO_3)_2$	0.0020	1.66
$[W_3O_2(O_2CCH_3)_6(H_2O)_3](CF_3SO_3)_2$	0.0022	1.70

UV analysis was performed with a model 50 Bio dual-beam Varian-Corey UV spectrophotometer, shown in Figure 2.15 below.

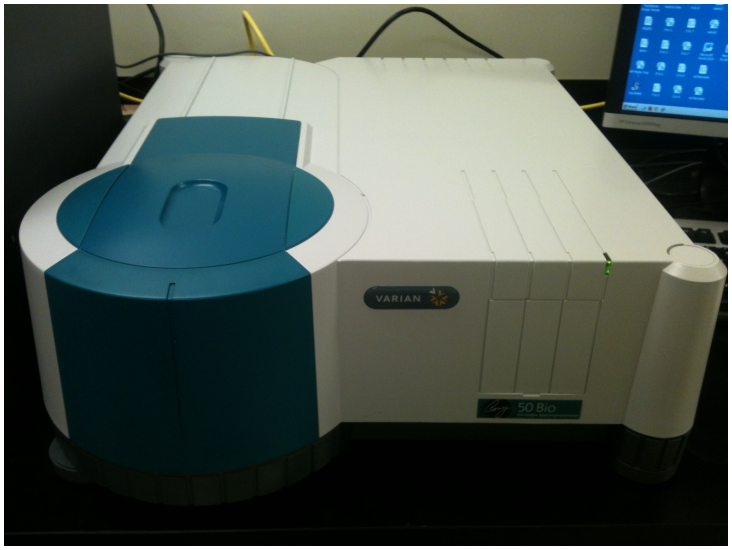

Figure 2.15. The Varian-Corey Bio dual-beam UV spectrophotometer (model 50).

2.6 The Pt foil electrodes for electrodeposition

Platinum foil squares were received from Aldrich, each of four measuring 25mm x 25mm x 0.025mm. Platinum wire was micro-welded to each piece to render the electrode.

Cleaning the electrode surface is the most important step in the practice of electroplating (Ibid.).To ensure a clean-surface conducive to electroplating, the platinum-foil electrodes were first soaked for 30 minutes in an alkaline solution consisting of (by weight) 30% sodium hydroxide (NaOH) and 10% triethylamine (TEA). The electrodes were then rinsed in deionized water, and soaked for ~15 minutes in concentrated nitric acid, and finally rinsed again. This procedure is reported by Abbott (2006) (Ibid.) and is shown in Figure 2.16.

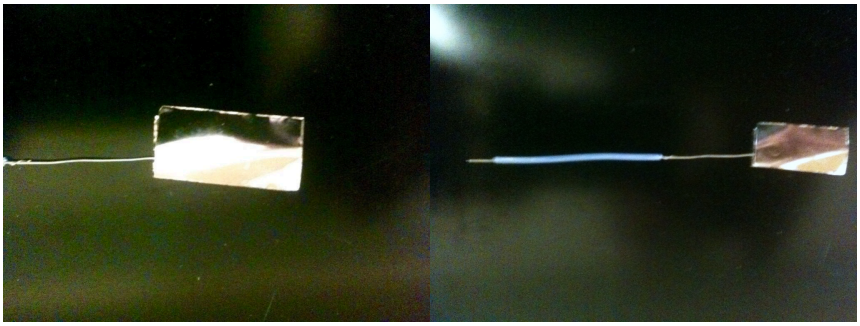

Figure 2.16. The bare Pt-foil electrode above is an example of the type of electrode used.

After cleaning but before use, the electrode was examined with an SEM (Scanning Electron Microscope) coupled to an AMT xr611 camera. These provided a

view of the electrode surface before deposition was attempted. However, because the SEM requires a very small sample (a few mm^2) to be loaded into a proprietary tray, an intact electrode could not be used. Consequently, “before” and “after” images of the same surface sample could not be obtained.

2.7.1 Voltammetric analysis inventory

The solvent system was then scanned by cyclic voltammetry to establish a baseline before the catalysts were added. Scans of the baseline and all subsequent scans were performed with a Princeton Applied Research/EG&G (PARC/EG&G) Model 173 Digital Potentiostat/Galvanostat equipped with a Model 179 Digital Coulometer and linked to a Model 175 Universal Programmer and is shown in Figure 2.17. The system also uses a PARC/EG&G Model 178 electrometer containing a Model 178/41 noise filter.

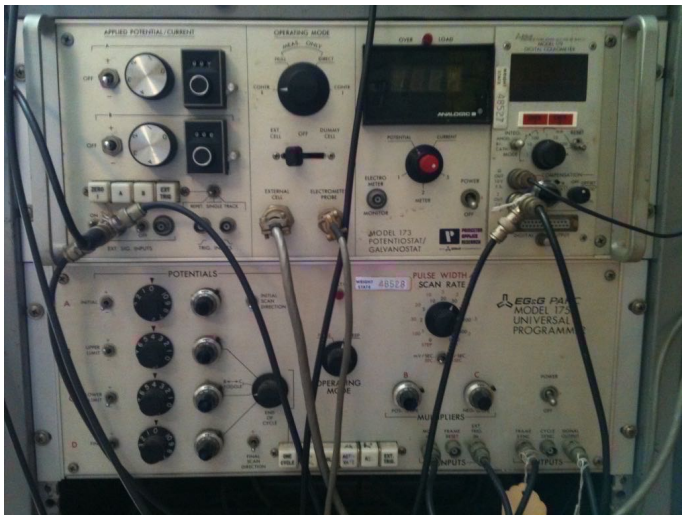

Figure 2.17. The Princeton Applied Research/EG&G model 173 Digital Potentiostat/Galvanostat equipped with model 179 Digital Coulometer linked to a model 175 Universal Programmer.

2.7.2 Data Collection Inventory

Data was collected with an eDAQ Model 201 eCorder running Chart software version Using Chart software v. 5.0 for Macintosh. The eCorder was connected to an IBM Thinkpad running Microsoft XP Professional v. 2002 with Service Pack 3, using an Intel Pentium III Mobile CPU @ 1133 MHz. These components are shown in Figure 2.18.

Figure 2.18. The model 201 eDAQ eCorder data capture device, used with an IBM ThinkPad laptop PC.

The temperature in Celsius was recorded for each of the analytes tested.

2.8 Baselines

As noted by Adams (1969), at its core, the entire problem of quantitative Ip measurement in CV is establishing the correct base line. In order to obtain quantitative data from cyclic voltammetry, measuring true peak currents from the CV is a requirement (Adams, 1969).

To do so, a free open-source software program known as eL-Chem Viewer was used. The software was written in the LabView 2011 Full Development System with the Report Generation Toolkit add-on (National Instruments, Austin, TX, USA, www.ni.com). Figure 2.19 shows the program display once it has selected the baseline of the desired peak.

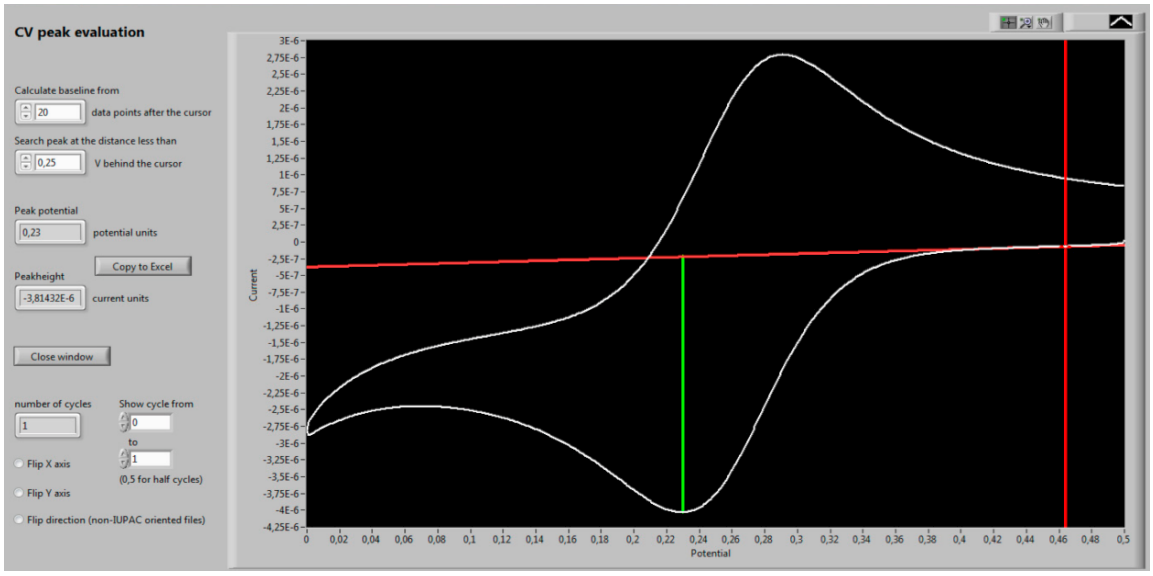

Figure 2.19. The program eL-Chem Viewer aids in establishing the proper baseline, from which peak currents can then be measured. Image taken from the free publication titled "eL-Chem Viewer: A Freeware Package for the Analysis of Electroanalytical Data and Their Post-Acquisition Processing (Giridhar et al., 2014, Hrbac et al., 2014).

2.9 Electrodeposition

2.9.1 Electrodeposition with $EMIBF_4$

The samples were bubbled with argon gas for at ≥ 10 minutes. The potential was held at or in slight excess of the reduction potentials observed. The data was captured with a eDAQ model 201 data collector used in conjunction with an IBM Thinkpad running Microsoft XP Professional Version 2002.

Before initiating, the argon flow was withdrawn from the solution, but kept inside the cell to provide a positive pressure of argon. Small (1-2mm x 1-2mm) magnetic stir bars were used during the process. The potentiostat and eDAQ units were placed on hold in slight excess of the observed reduction peaks, and then again in excess of the lowest observed reduction peak. At the conclusion of each electrolysis run, the CV unit and the data recorder were released from hold, and the reverse (oxidation) scan was observed and recorded. The experimental conditions can be found in Table 2.4 below.

Table 2.4. Electrodeposition parameters for the tri-nuclear clusters in $EMIBF_4$.

Trimer	E (V)*	Duration (m)	Temp (ºC)
Mo_2W	-0.71	20	20.5
	-1.50	25	20.5
MoW_2	-0.70	10	20.5
	-1.76	10	20.5
W_3	-0.49	11	20.5
	-1.69	14	20.5

*E (V) The potential at which the tri-nuclear clusters was held.

2.9.2 Electrodeposition with the DMSO/TBAHFP system

For electrodeposition, platinum-foil electrodes were initially used. When deposition did not appear to occur, a BASi 3mm platinum-disk electrode was used. This electrode offers more surface area for electrodeposition than the platinum-disk electrode used for electrochemical analysis. The trimers were held at the reducing potentials they displayed during cyclic voltammetry. The experimental conditions can be found in Table 2.5 below.

Each trimer was held for durations of 20-71 minutes. If the trimer displayed 2 reduction peaks, electrolysis was attempted at each reduction peak potential as well as in excess of the lowest reduction potential observed. This was done to make it easier to determine which potential was responsible for the deposition rather than just using the lowest potential.

The solution was stirred with a 2mm x 1mm stir-bar while electrolysis was conducted. After holding the potential for the desired duration, the potentiostat and the eDaq data capturing unit were taken off of hold and the catalyst was scanned in the positive direction to investigate the oxidation character of the catalyst by its resulting signature in the voltammogram.

Table 2.5 Duration of electroplating attempts and temperatures for each of the four tri-nuclear clusters.

Trimer	E (V)	Duration (m)	Temp (ºC)	Trimer	E (V)	Duration (m)	Temp (ºC)
Mo_3	-0.69	31	20.9	MoW_2	-0.57	20	21.0
	-1.20	71	20.9		-1.17	20	21.0
Mo_2W	-0.49	20	20.9	W_3	-0.57	20	21.1
	-1.15	21	20.9		-0.87	20	21.1

3. RESULTS AND DISCUSSION

3. RESULTS AND DISCUSSION

3.1 Characterization of catalysts and solvents

3.1.1 Characterization of the tri-nuclear clusters

Previous research with tri-nuclear clusters has lead to the observation of color associations that can be observed with these products (Ardon et al., 1982, Bino and Gibson, 1980, Chisholm, 1977, Cotton et al., 1983, Cotton et al., 1984, Cotton et al., 1985, Cotton et al., 1989, Davis, 2012, Frock, 2012, Harris, 2008, Katovic and McCarley, 1978, Katovic, 1975, Martinez et al., 1987, Ryan, 1982, Stephenson et al., 1964, Ubadigbo, 2009, Wang et al., 1986, Zaitsev et al., 1976, Zhuang et al., 1998). Each of the four trimers displays a different color on the spectrum from red to yellow, with red being associated with molybdenum content, and yellow associated with tungsten content as shown in Table 3.1 and Figure 3.1.

Table 3.1. The characteristic colors of the four tri-nuclear clusters.

Red	Orange-Red	Orange	Yellow
Mo_3	Mo_2W	MoW_2	W_3

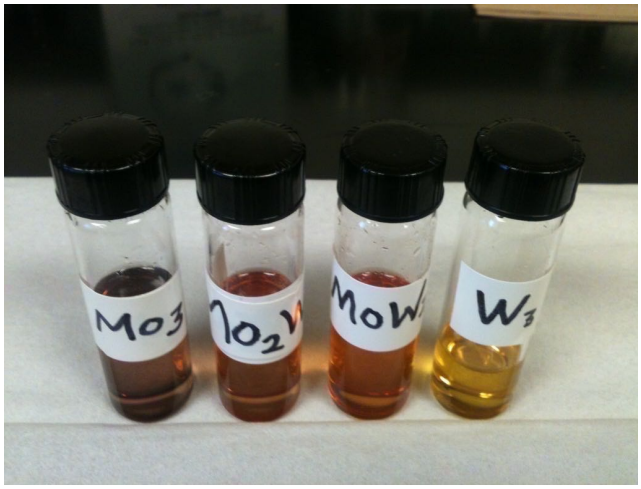

Figure 3.1. The four tri-nuclear clusters after dissolving in the DMSO/TBAHFP solvent system. The Mo_3 tri-nuclear cluster on the far left is a dark, rusty-red hue. Moving from left-to-right the next cluster contains Mo_2W, then MoW_2, and finally W_3. As the compounds contain progressively more tungsten, the hue moves from red toward yellow, with the W_3 tri-nuclear cluster appearing as yellow only.

The UV absorption spectra for the 4 tri-nuclear clusters were plotted in Figure 3.2 with the absorption peaks indicated for each trimer. The scans are color-coded to the tint each trimer exhibits in solution.

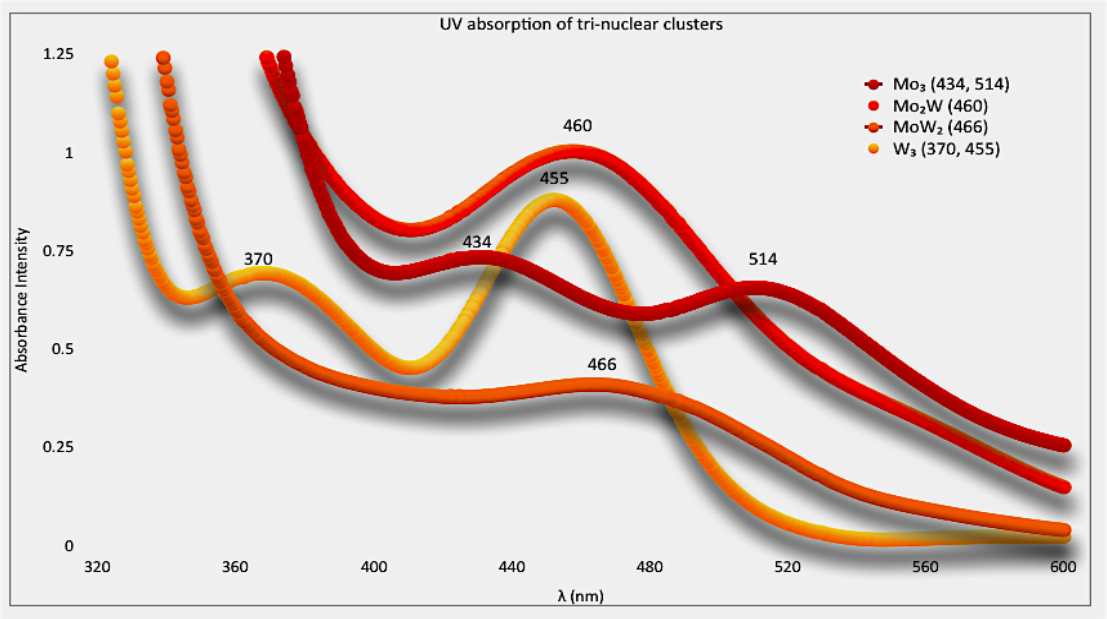

Figure 3.2. UV spectra of the 4 trimers gathered on a Varian-Corey 50 Bio dual-beam UV spectrophotometer. The peaks are labeled to aid in characterizing the spectra with published spectra. The peak values in nm were as follows: Mo_3: two peaks at 434 and 514, Mo_2W: one peak at 460, MoW_2: one peak at 466, and W_3: two peaks at 370 and 455.

Previous studies have used UV-Vis spectra to analyze molybdenum and tungsten trinuclear clusters (Cotton et al., 1984, Patel, 1990, Wang et al., 1986)}. Published literature values of peaks from UV-Vis analysis were reported from several authors such as Wang (1986), Cotton (1984), and Patel (1990). Results from these sources for these clusters were tabulated with experimental values obtained with a Varian-Corey Bio dual-beam UV spectrophotometer. Table 3.2 compares our experimentally obtained absorption peaks to those from the above authors. The values we obtained were in good agreement with the literature values for the

se clusters.

Table 3.2. Absorption wavelength comparison of tri-nuclear cluster compounds of molybdenum and tungsten.

Trimer	Mo_3	Mo_2W	MoW_2	W_3
Wang* (1986)	428, 510	460	400, 480	367, 450
Cotton (1984)	423, 540	-	-	488
Kennedy (2017)	434, 514	460	466	370, 455
Patel (1990)	505	400, 515	-	456

*Values were carefully estimated from plot given. Values were not found directly in text.

3.1.2 IR of Post-Purified $EMIBF_4$

IR (infra-red) spectra have been utilized in the past to analyze the identity and purity of compounds such as $EMIBF_4$. The IR spectra can in effect be compared to a molecule's "fingerprint" because a characteristic "signature" is produced when examined with infra-red light. In fact, results from IR spectroscopy are respected enough as "fingerprinting" that IR spectra are used as evidence in the justice system.

The infra-red light energy imparts vibrational energy to the molecule, which is absorbed in a manner determined by the structure of the molecule. The strength of the bonds within the molecule, and the masses of atoms and groups of atoms dictate the frequencies at which vibration occurs. Groups of atoms within molecules known as "functional groups" - so called because they "function" in reactions the molecule may be involved in - yield valuable identifying features when subject to IR energy. It is because of this relationship between molecular structure, energy, and resulting spectra that allow one to work backwards from the spectra to the structure and identify the substance under investigation. This relationship can be seen in Equation 3.1:

Equation 3.1.

$$E = h\upsilon = \frac{hc}{\lambda}$$

where E = energy, h = Planck's constant (6.6 x 10^{-34} joules-sec), ν = frequency, c = speed of light, and λ = wavelength.

After purifying the $EMIBF_4$ (see section 2.1.2.1 Decolorizing), a sample was analyzed with a Nicolet Model 6700 FT-IR. The spectrum for purified $EMIBF_4$ is seen below in Figure 3.3. The spectrum displays long, sharp peaks near 3151 and 3115 cm^{-1}, a short, sharp peak near1813 cm^{-1}, a very long, sharp peak at 1566 cm^{-1}, and a long, sharp peak near 1142 cm^{-1}. These peaks are expected with 1,3-disubstituted aromatic molecules, to which $EMIBF_4$ belongs.

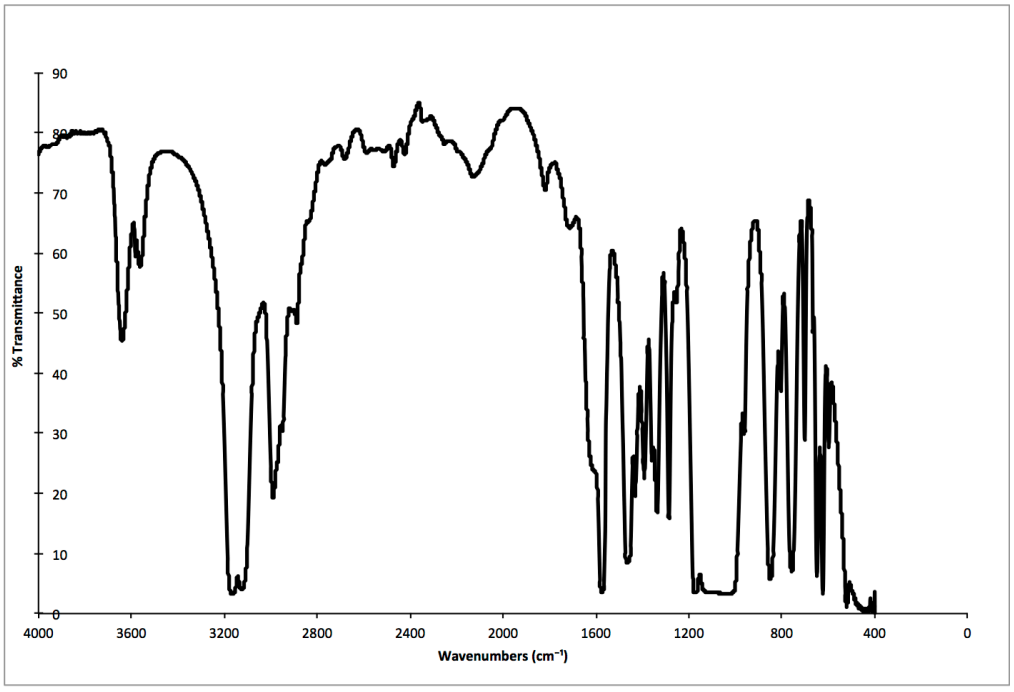

Figure 3.3. IR spectrum of $EMIBF_4$ after purifying with column based on Earle et al. 2007(Earle et al., 2007) $EMIBF_4$ is a 1,3 disubstituted aromatic, and the spectra displays peaks characteristic of such a molecule. The peaks referred to are in the vicinity of 3151 cm^{-1} and 3115 cm^{-1}, 1813 cm^{-1}, 1566 $^{cm-1}$, and 1142 cm^{-1}.

3.1.3 SEM of electrodes

SEM (Scanning Electron Microscopy) provides a detailed, highly magnified image of an object's surface. Reaching down to the nanometer scale, SEM is well suited to surface investigations. It is a commonly used tool for characterizing surface morphology after electrodeposition. SEM was used by Yang et al., (2013) to study the electrodeposition of Cu–Li alloy using the room temperature ionic liquid $BMIBF_4$ (1-butyl-3-methylimidazolium tetrafluoroborate) - an ionic liquid that is very similar to the ionic liquid $EMIBF_4$ used in this study(Yang et al., 2013). Oskam (1999) used SEM to examine the electrochemical deposition of copper onto silicon (Oskam, 1999) and Siek et al., (2013) used SEM to examine silver nanoparticle substrates for neurotransmitter detection (Siek et al., 2013). There are many other examples (Abbott and McKenzie, 2006, Abdel Aal et al., 2009, Abdel Aal et al., 2012, Caballero-Calero et al., 2014, Chen and Chang, 2012, Endres, 2001, Garcia et al., 2013, Ghaziof et al., 2010, Giridhar et al., 2014, Kalska-Szostko, Kim et al., 2013, Le Vot et al., 2012, Nakouzi and Sultan, 2011, Raeissi et al., 2005, Suryanto et al., 2012).

Electrodeposition happens entirely on the surface of the object it is applied to, therefore the SEM was used to acquire an image of the surface of the electrode before electrodeposition was attempted. This was to be contrasted with the same surface after electrodeposition was attempted. The surface of the bare platinum-foil working electrode is shown in Figure 3.4. The magnification increases from left to right.

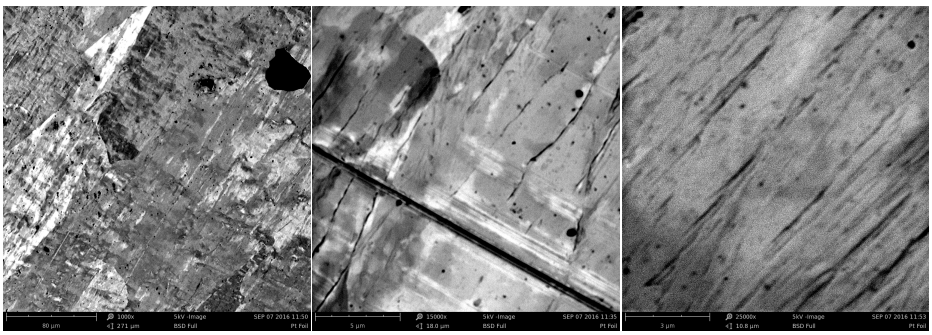

Figure 3.4. SEM microscope images of a platinum-foil electrode before attempting electrodeposition. From left to right: at 1000x, 15,000x, and 25,000x magnifications.

The platinum-foil working electrodes were the first electrodes used to attempt electrodeposition. The set-up of the electrochemical cell remained the same as that referred to in a previous section. If electrodeposition did not occur with foil electrodes, the process was repeated with 3mm diameter platinum-disk electrodes and the distinction noted.

The platinum working electrodes were meant to function after electrodeposition had occurred, and therefore would have had to stay intact. However, as mentioned in section 1.6, the electrode would have to be sacrificed due to the size of the sampling tray and the nature of the sampling technique. When it was observed that electrodeposition was not occurring, SEM was of no continued use, and so was abandoned.

3.2 Solvent Backgrounds

3.2.1 The EMIBF$_4$ solvent-system background

The following plot in Figure 3.5 shows CVs of the ionic liquid solvent system, as yet with no catalyst. This is known as the "background" scan. The background of a solvent system is important because it will indicate if the solvent system contains impurities (or excess oxygen for that matter). There should be no prominent redox activity within the potential window in which the catalysts will be examined. A background scan will therefore show how “clean” the solvent system is before the catalyst is added, since we want the activity we measure to be due to the catalysts - not the solvent system.

In addition, the background scan will show us the “electrochemical window” of the solvent system - also known as the solvent’s “breakdown limits”. It is important to stay within the limits of this “window” as the second name implies. If the potential is exceeded on either the positive or negative side, the solvent in the vicinity of the electrode will begin breaking down forming material that can then coat the electrode and interfere with its functioning. It can do this in two ways relevant to the nature of this research. First, it can cause “pacification” - or desensitization - of the electrode to the signals we hope to measure. Secondly, the return scan may indicate that a deposition has indeed occurred. Effectively however, this is a “decoy” deposit because it is not of the material we are attempting to deposit, but of the solvent we used to facilitate deposition of the catalyst material.

Scans of this ionic liquid gave a cathodic limit of -2.0 V and an anodic limit of +2.42 V for a 4.42 V wide electrochemical window.

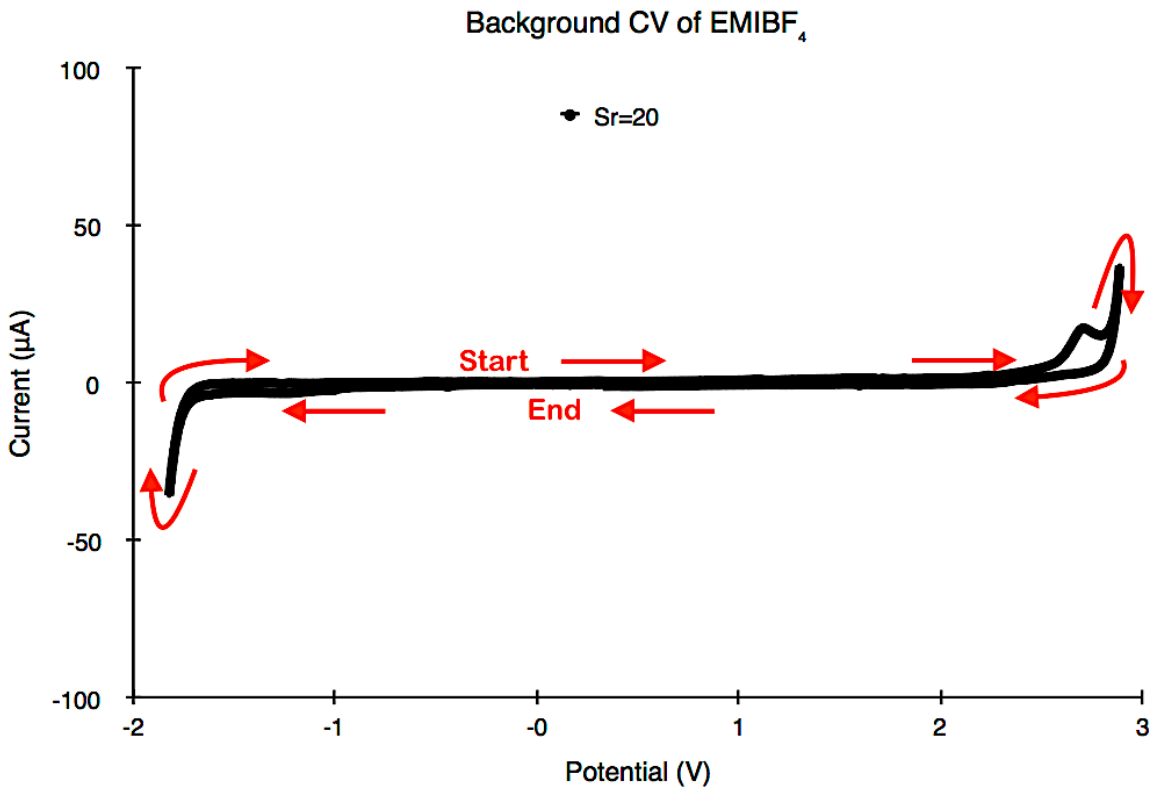

Figure 3.5. Background cyclic voltammogram of the $EMIBF_4$/TBAHFP solvent system.

The electrochemical background window shown in the above Figure 3.5 indicates a satisfactory state for the solvent system, as no redox events are observed. In addition, the limits within which the solvent can operate (at this scan rate and under the conditions of this lab environment) are now known. After the catalysts were added, we had an operational “window” and these potential limits were not exceeded. We could therefore conclude that the redox events were from the catalysts of interest.

3.2.2 The Solvent-System Background

The CVs in Figure 3.6 and Figure 3.7 show the ”background" of the solvent system (DMSO with electrolyte), as yet with no catalyst. The CVs show no existing redox processes. If there had been, peaks would appear, since current would be generated in the y-axis direction.

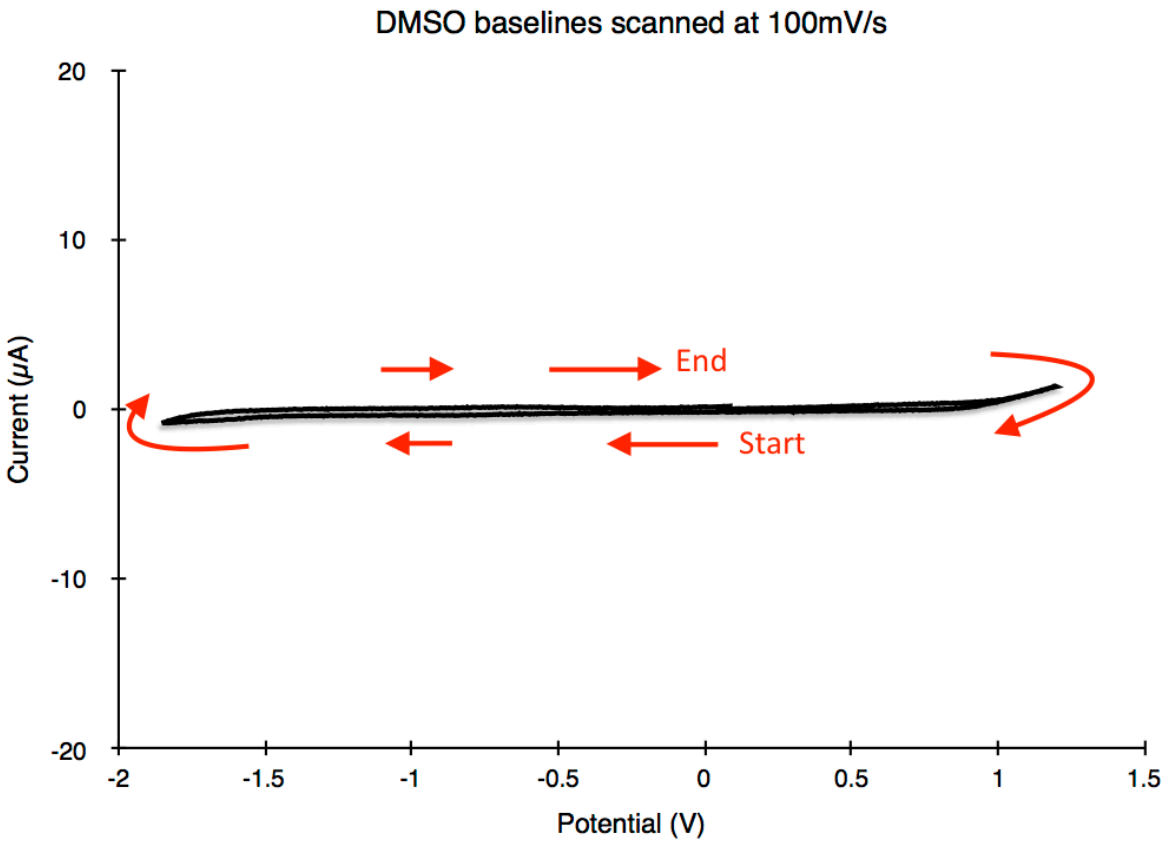

Figure 3.6. Background CVs of the purified solvent system DMSO with 0.1M TBAHFP at a single scan rate of 100 mV/s.

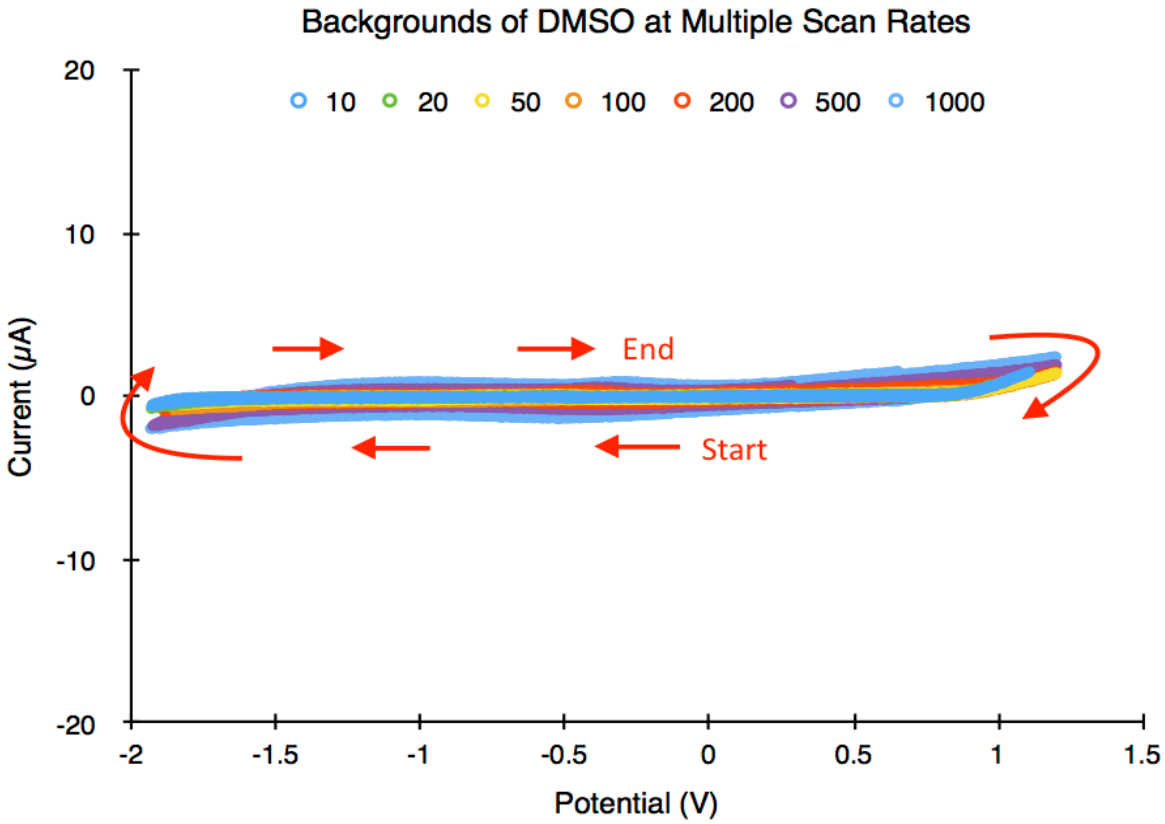

Figure 3.7. Background CVs of the DMSO solvent system at multiple rates of 10, 20, 50, 100, 200, 500, and 1000 mV/s.

3.3 Electrodeposition

In contrast to the rounded peaks seen in CVs during redox processes of species in solution, voltammograms of electrodeposited analytes display a characteristically sharp peak during the opposite sweep. If a material was deposited from a reducing current, the reverse sweep will oxidize the material, resulting in a noticeable current spike. Examples of this behavior can be seen in Figure 3.8 and Figure 3.9. Figure 3.8 shows (red), the oxidation of electrodeposited iron onto polycrystalline Au in an ionic liquid. Peak "c_2" results from the reduction of the iron onto Au, while "a_2" results from the stripping off of the deposit as it becomes oxidized after the system was switched to a positive potential. The mostly flat, black line represents the "background" CV scan of the ionic liquid solvent before the addition of iron analyte. Figure 3.9 shows a bismuth telluride deposit being stripped in a similar manner.

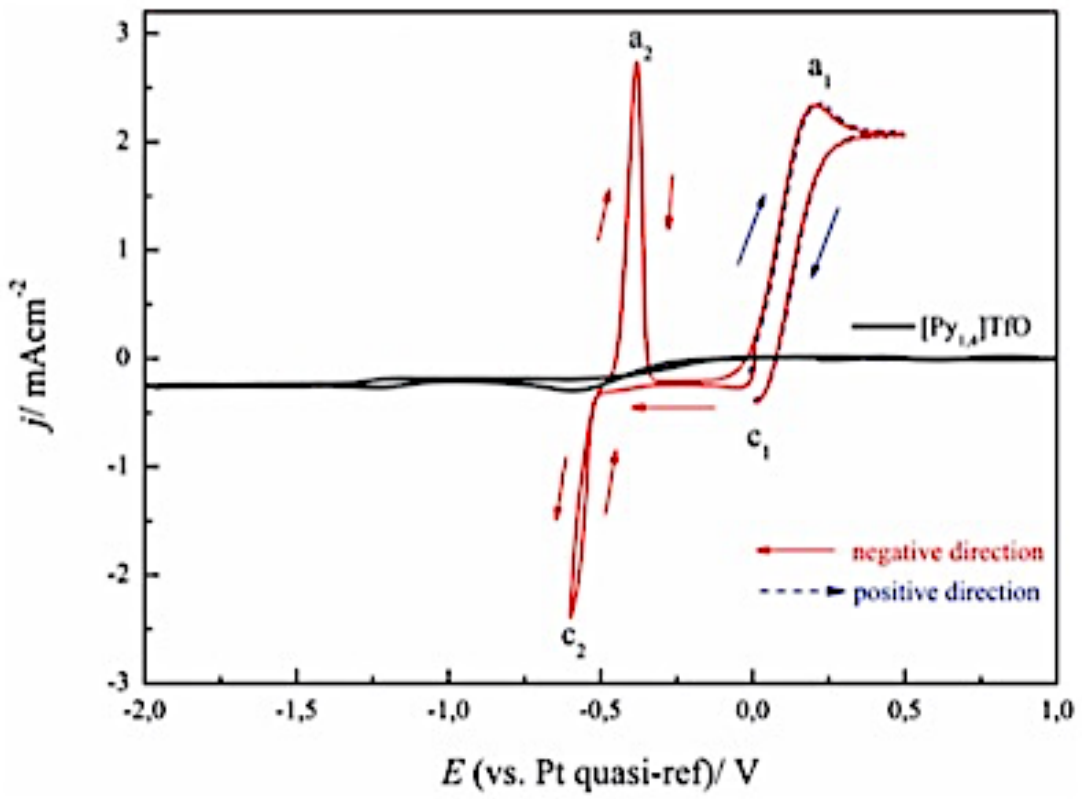

Figure 3.8. Characteristically-sharp peaks resulting from stripping of the iron deposit that occurred during the negative potential sweep. Figure 3.used by premission. Giridhar, P. Weidenfeller, B. El Abedin, S. Z. Endres, F. Phys Chem Chem Phys 2014, 16, 9317-9326.

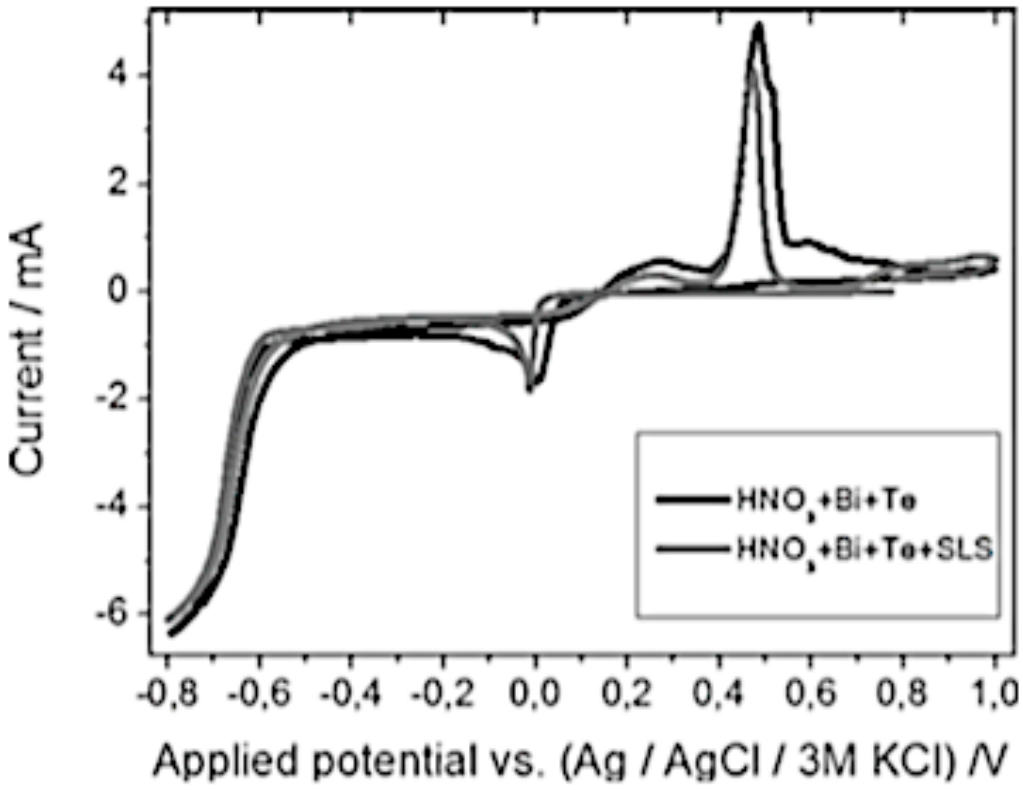

Figure 3.9. CVs of a bismuth telluride electrodeposition being stripped off the electrode. From "Improvement of Bismuth Telluride electrodeposited films by the addition of Sodium Lignosulfonate" (Caballero-Calero et al., 2014) Figure 3.used by premission.

In contrast to Figure 3.8 and Figure 3.9, CVs of redox processes absent the depositing and stripping of deposits lack the sharp peaks characteristic of electrodeposition. For example, Figure 3.10 shows the CV of ferrocene in our DMSO solvent system, run at multiple scan rates. Ferrocene is used as an internal standard for electrochemical measurements (Gagne, 1980). The expected reduction and oxidation events occur, but with relatively smoother and shallower peaks. This is the typical behavior of a system absent of electrodeposition.

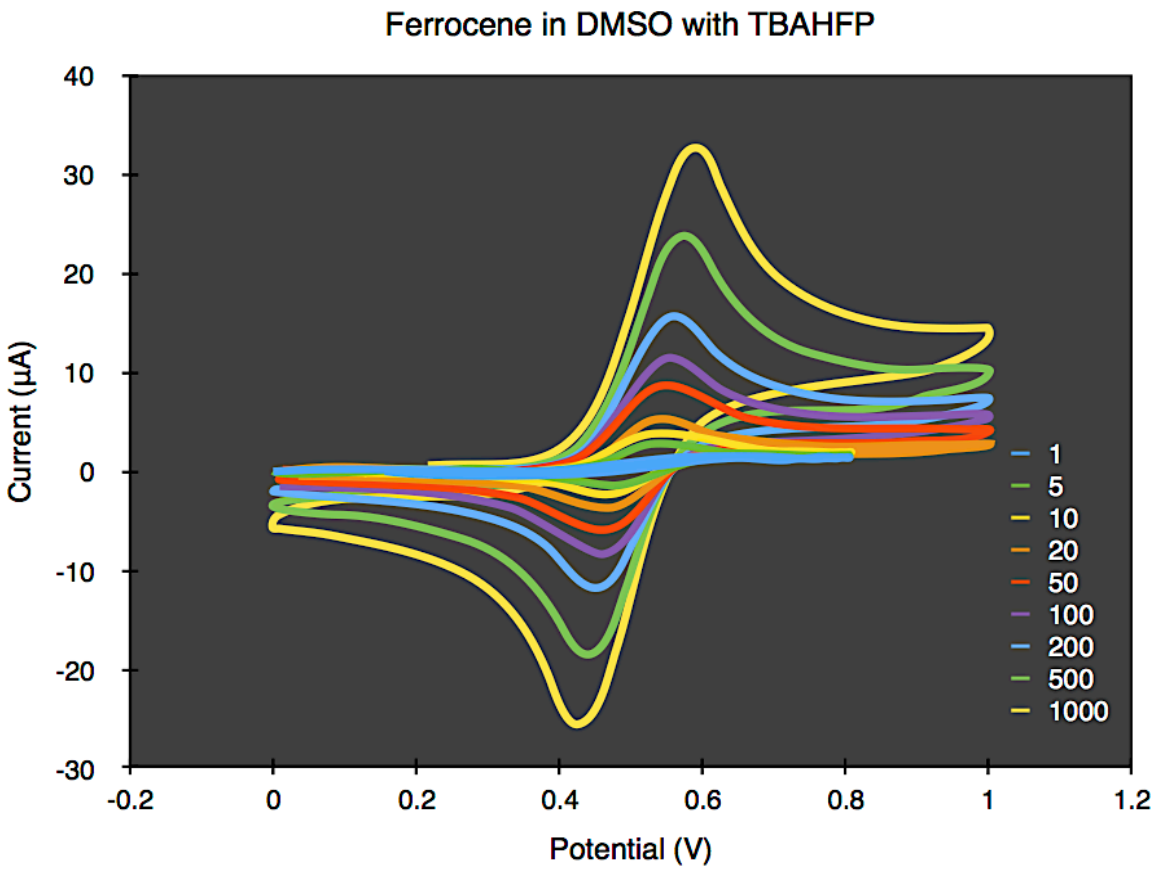

Figure 3.10. CV of ferrocene in the DMSO solvent system, taken at scan rates of 1, 5, 10, 20, 50, 100, 200, 500, and 1000 mV/s scan rates.

3.3.1 Electrodeposition with $EMIBF_4$

All electrodeposition attempts were made after sparging the ionic liquid with argon for a minimum of 10 minutes. The gas delivery tube was then withdrawn from the ionic liquid, but left inside the electrochemical cell to allow the argon flow to maintain a positive pressure throughout the experiment to exclude oxygen from the atmosphere. A small 1mm x 2mm stir bar was used for the duration of the electrodeposition attempts. The temperature for all runs with $EMIBF_4$ was observed to be 20.5°C.

3.3.1.1 Post-Electrodeposition CVs of Mo_2W trimer in $EMIBF_4$

The Mo_2W tri-nuclear cluster was subject to electrodeposition attempts by applying and holding the potential first at -0.71 V for 20 min and later at -1.50 V for 25 min. The potentials at which the trimer was held were in slight-excess of the reduction potentials that had been previously observed. After the system was held at the above times, the potential was reversed. If a deposition had occurred, the CV would depict the sharp types of peaks discussed in the previous section. The voltammograms can be seen below in Figure 3.11 and Figure 3.12.

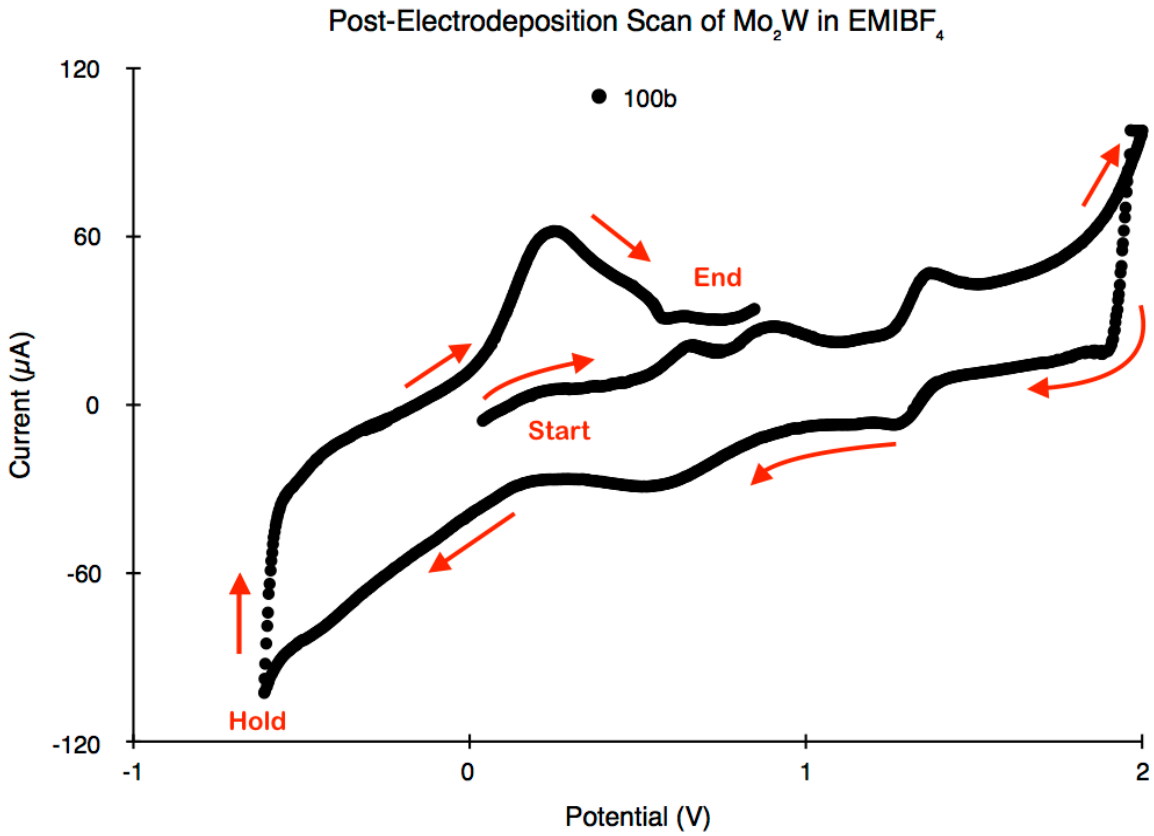

Figure 3.11. CV of Mo_2W in $EMIBF_4$ at a scan rate of 100 mV/s in the positive direction after being held at -0.71 V for 20 min.

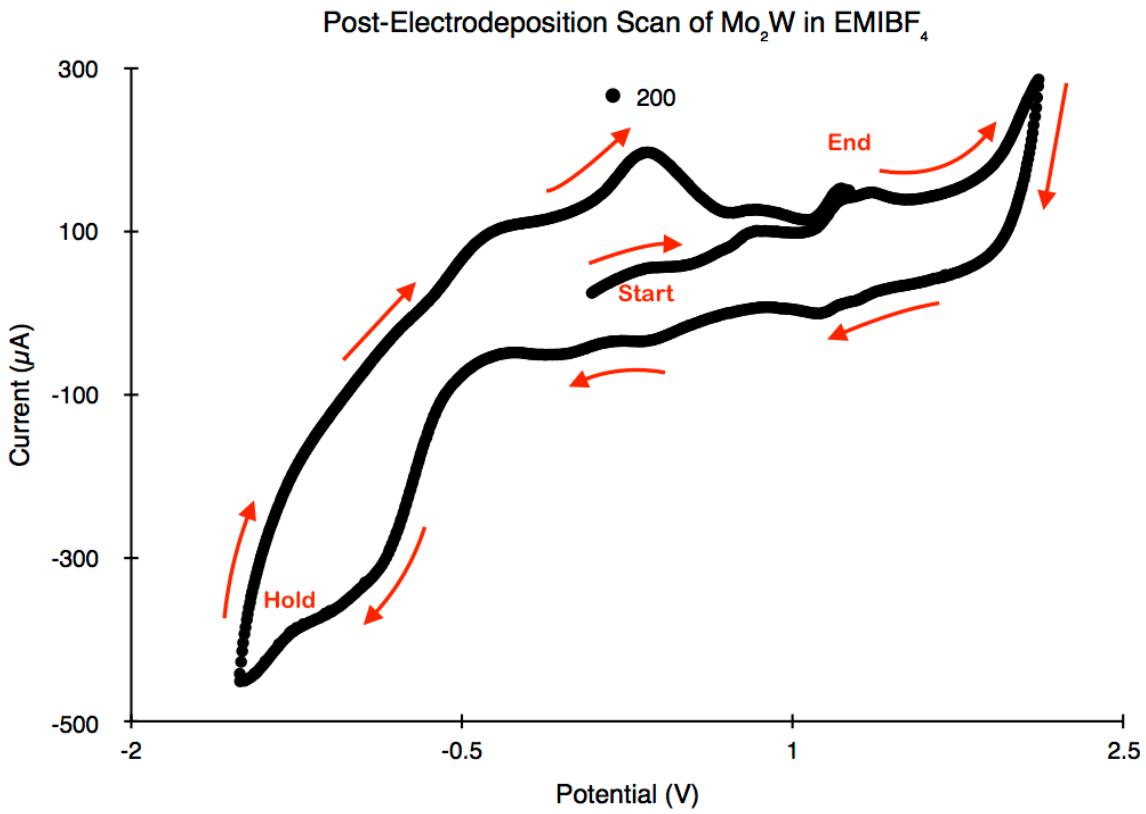

Figure 3.12. CV of Mo_2W in $EMIBF_4$ at a scan rate of 200 mV/s at 20.5ºC, held at -1.50 V for 25 minutes.

As can be seen, there is a conspicuous absence of sharp peaks for this trimer. The CVs suggest that electrodeposition of Mo_2W tri-nuclear clusters did not occur. The remaining tri-nuclear clusters were tested for electrodeposition using first $EMIBF_4$ and then DMSO.

3.3.1.2 Post-Electrodeposition CVs of MoW_2 trimer in $EMIBF_4$

The MoW_2 tri-nuclear cluster was subject to electrodeposition attempts by applying and holding the potential first at -0.70 V for 10 min and then at -1.760 V for 10 min. The temperature for all runs was observed to be 20.5°C. The voltammograms can be seen below in Figure 3.13 and Figure 3.14. The CVs of this trimer are also absent of any peaks characteristic of electrodeposition.

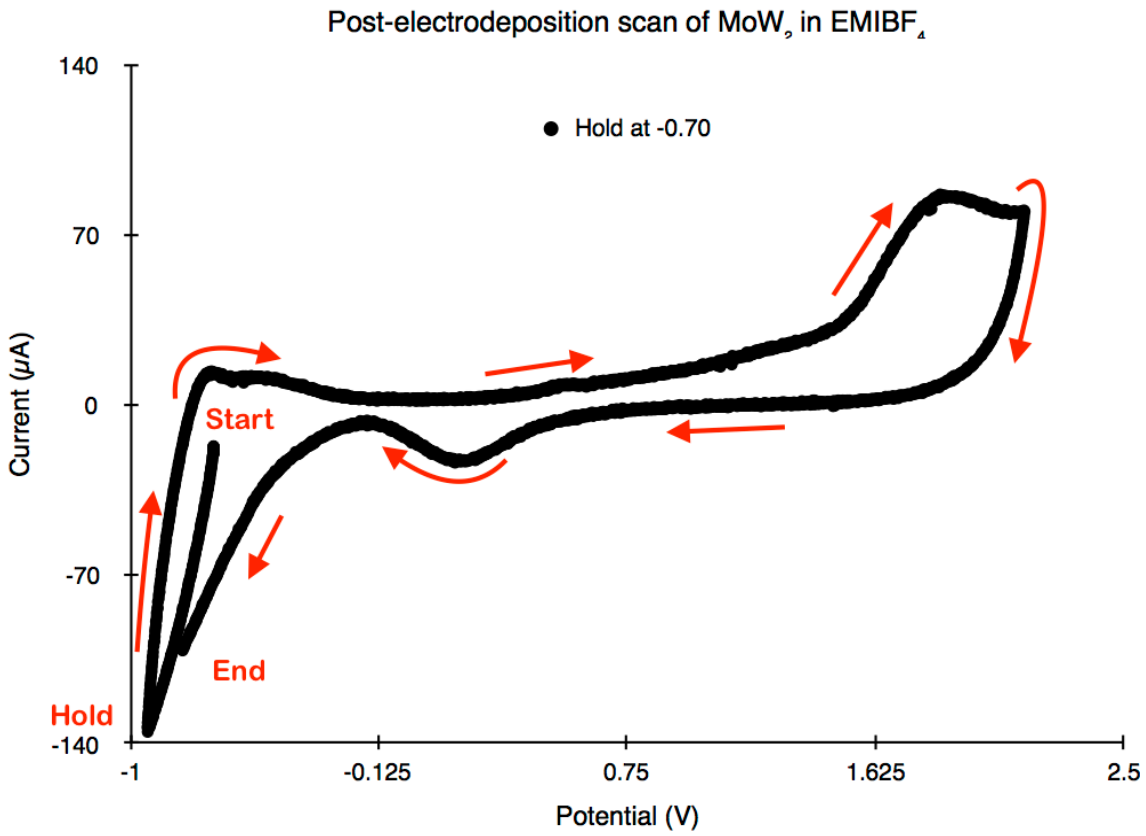

Figure 3.13. CV of MoW_2 in $EMIBF_4$ at a scan rate of 100 mV/s at 20.5ºC after being held at -0.70 V for 10 minutes.

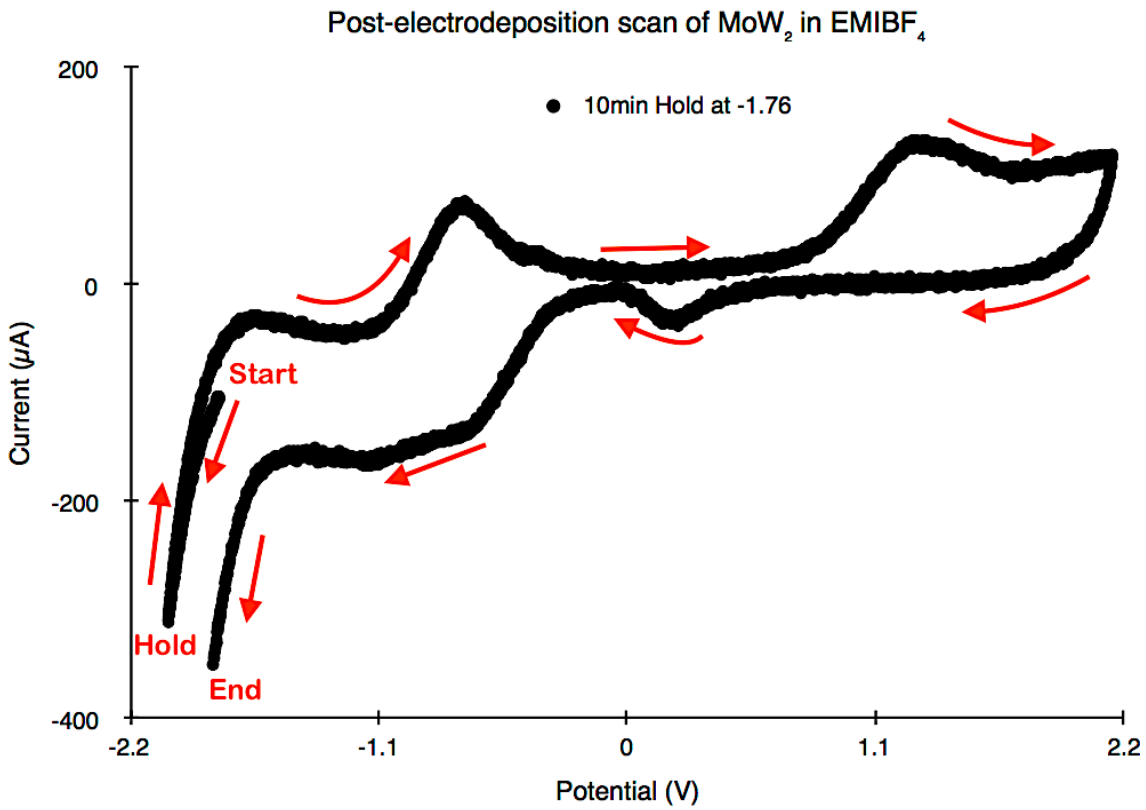

Figure 3.14. The CVs of the MoW_2 trimer in $EMIBF_4$ at 20.5ºC after being held at -1.76 V for 10 minutes at scan rate 100 mV/s.

3.3.1.3 Post-Electrodeposition CVs of W_3 trimer in $EMIBF_4$

Using the same conditions as were present in the previous attempts, the W_3 trimer was held at the reduction potentials of -0.493 V for 11 min, and at -1.69 V for 14 minutes. The temperature for all runs was observed to be 20.5°C. The voltammograms can be seen in Figure 3.15 and Figure 3.16. As before, the data indicate a lack of electrodeposition.

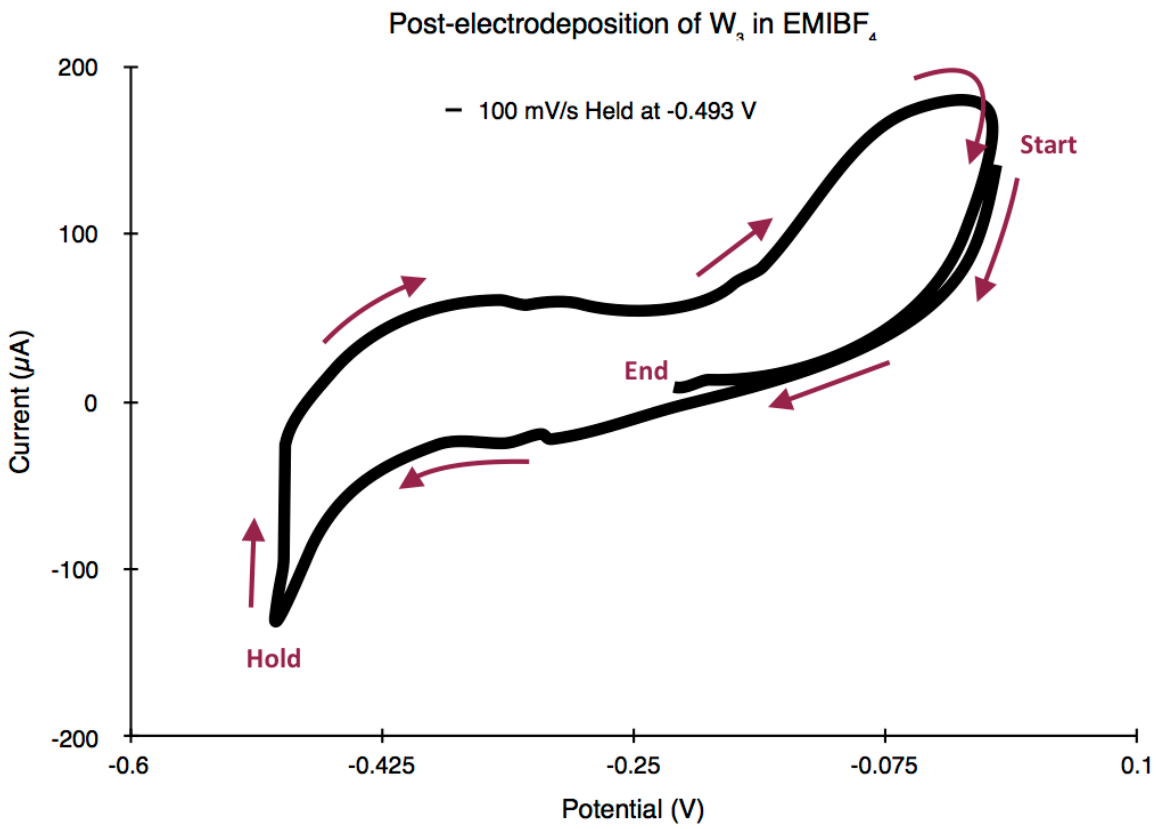

Figure 3.15. The CV of the W_3 trimer in $EMIBF_4$ held at -0.493 V for 11 minutes at 20.5ºC, using a 100mV/s scan rate.

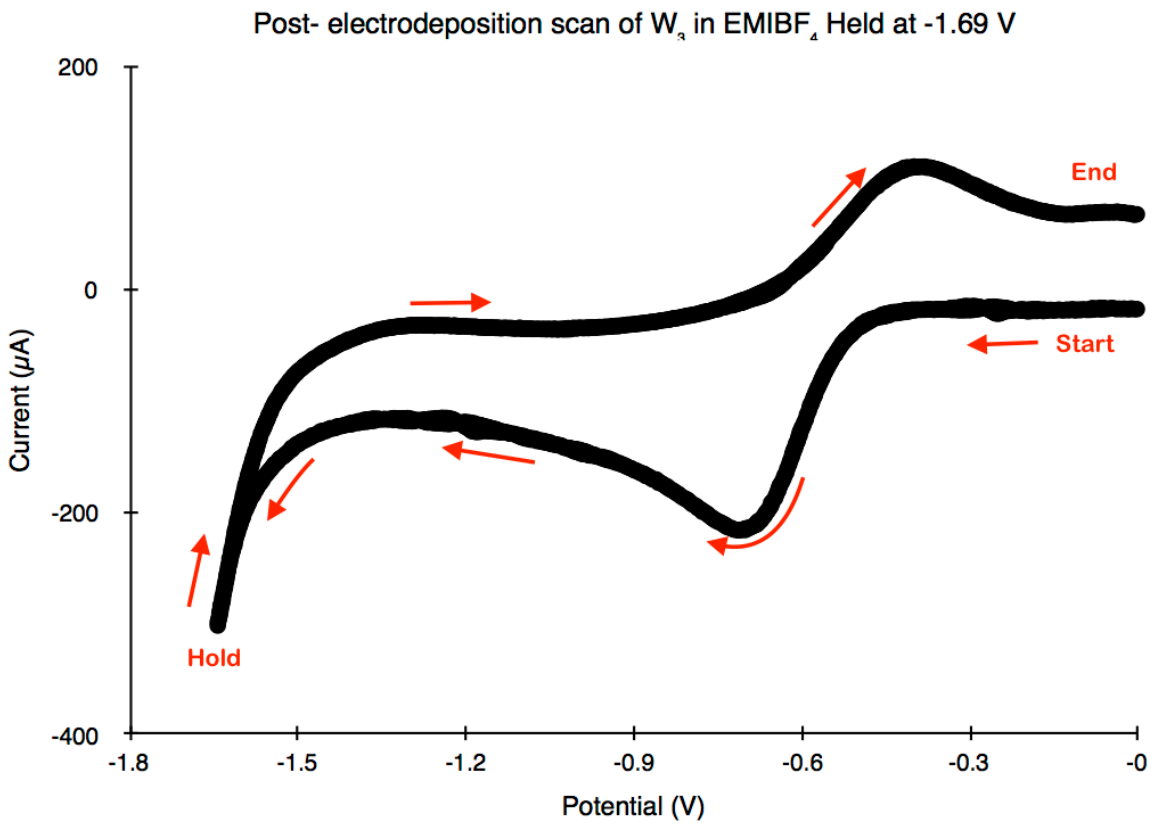

Figure 3.16. The CV of the W_3 trimer in $EMIBF_4$ held at -1.69 V for 14 minutes at 20.5ºC, using a 100mV/s scan rate.

3.3.2 Electrodeposition Attempts in DMSO/TBAHFP

It has been demonstrated that the rate of particle deposition depends on the nature of the particles; namely their size, shape, and charge as well as the operating conditions. Operating conditions include current, density, temperature, pH, and time (Abdel Aal and Hassan, 2009). It has also been shown that temperature influences the deposits in terms of grain size (Liu et al., 2013). Temperature was therefore recorded during this study, but not used as a control variable. Controlling the above factors other than time was beyond the scope of this project however. The experimental conditions for the electrodeposition of all four tri-nuclear clusters were tabulated and can be seen in Table 3.3 below.

Table 3.3. Duration of electroplating attempts and temperatures for each of the four tri-nuclear clusters.

Trimer	E (V)	Duration (m)	Temp (ºC)	Trimer	E (V)	Duration (m)	Temp (ºC)
Mo_3	-0.69	31	20.9	MoW_2	-0.57	20	21.0
	-1.20	71	20.9		-1.17	20	21.0
Mo_2W	-0.49	20	20.9	W_3	-0.57	20	21.1
	-1.15	21	20.9		-0.87	20	21.1

3.3.2.1 The Mo_3 tri-nuclear cluster

As in $EMIBF_4$, electrodeposition of each tri-nuclear cluster was again attempted, but with the new DMSO solvent-system. As with $EMIBF_4$, all electrodeposition attempts were made after sparging the sample with argon for a minimum of 10 minutes. Each attempt was made at a potential that was in slight excess of observed values. Figure 3.17 shows the Mo_3 trimer after electrodeposition was attempted at the reversible redox peak

at -0.69 V for 31 minutes. Figure 3.18 depicts the CV of Mo_3 after being held at -1.20 V, the irreversible reduction peak, for 71 minutes.

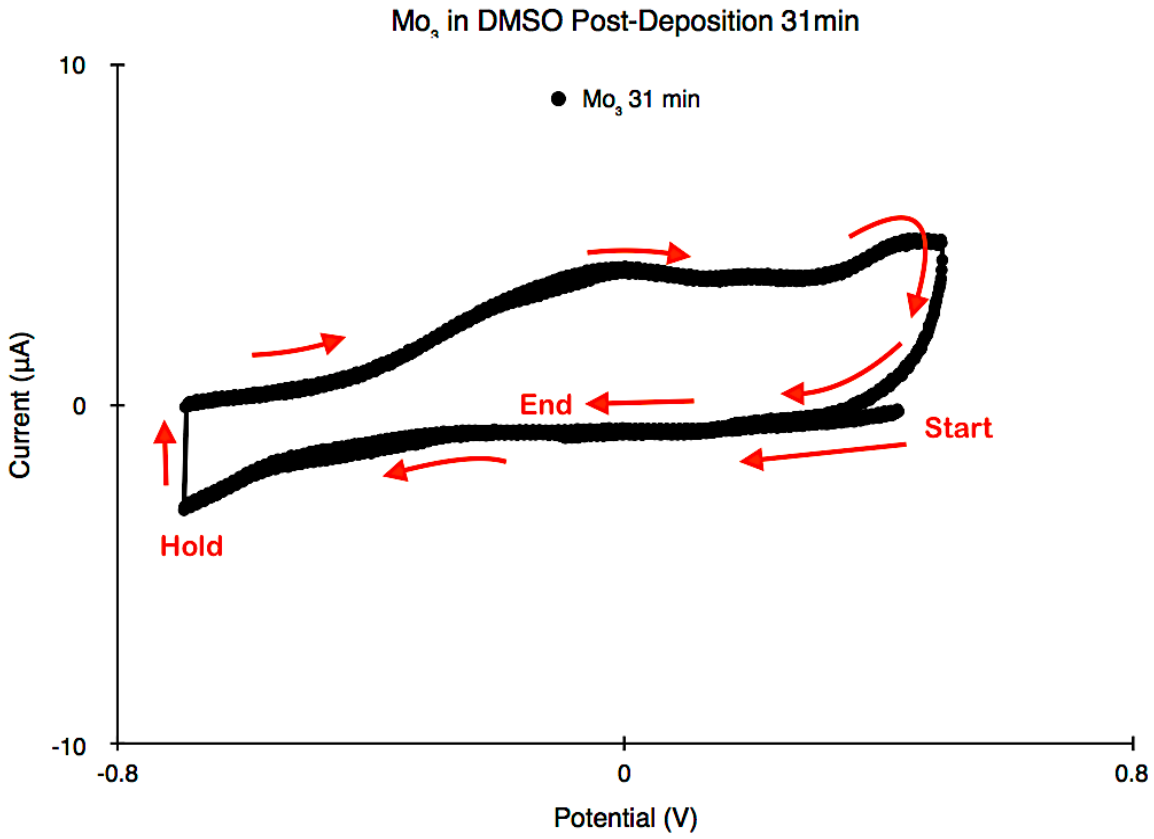

Figure 3.17. CV of Mo_3 in DMSO at a scan rate of 200 mV/s in the negative direction at 21.0ºC, after being held at the reversible redox peak at -0.69 V for 31 min.

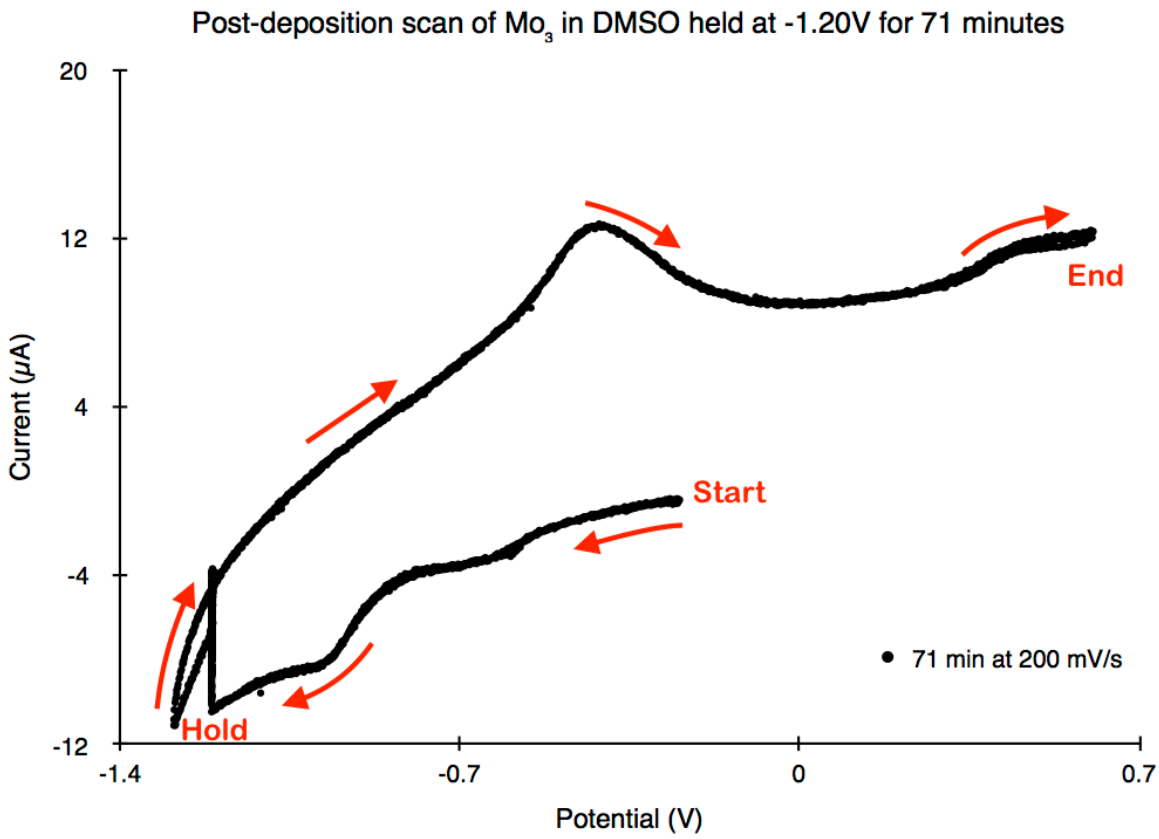

Figure 3.18. CV of Mo_3 in DMSO at a scan rate of 200 mV/s in the negative direction at 21.0ºC after being held at the irreversible reduction peak at -1.20 V for 71 min.

3.3.2.2 The Mo_2W tri-nuclear cluster

The Mo_2W and MoW_2 tri-nuclear clusters were of particular interest because past research has shown that the most active catalyst for methanol oxidation was found to be a combination of Mo and W (Kawamura et al., 1987, Roquero et al., 2007). Electrodeposition was next attempted with the Mo_2W tri-nuclear cluster at 21.0ºC. Figure 3.19 shows the trimer after being held at -0.49 V, which was in slight excess to the reversible redox potential observed. Figure 3.20 shows the Mo_2W trimer after being held at a potential in excess of the irreversible reduction peak observed. As with Mo_3 above, there is a conspicuous lack of sharp features in both voltammograms.

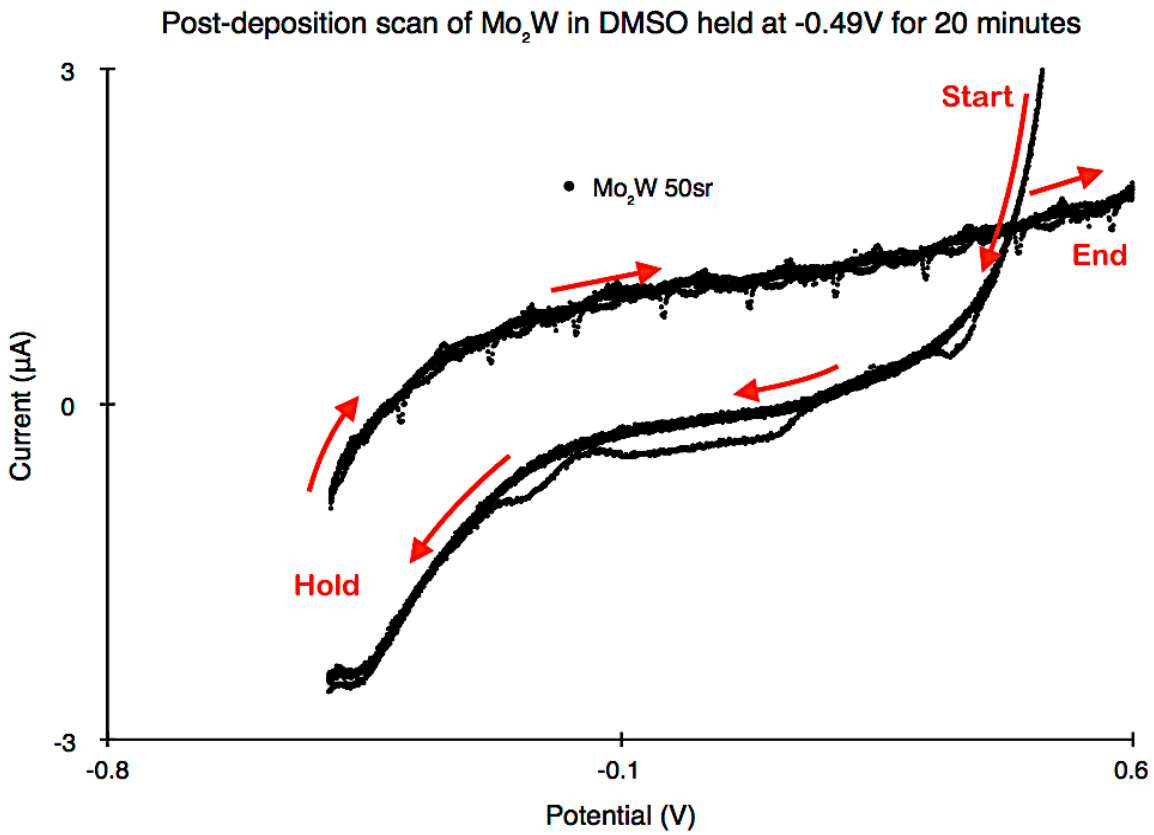

Figure 3.19. CV of Mo_2W in DMSO scanning in the negative direction at a scan rate of 50 mV/s at 21ºC. The CV resulted from beginning at +0.5V, holding 20 minutes at -0.49 V, then reversing direction.

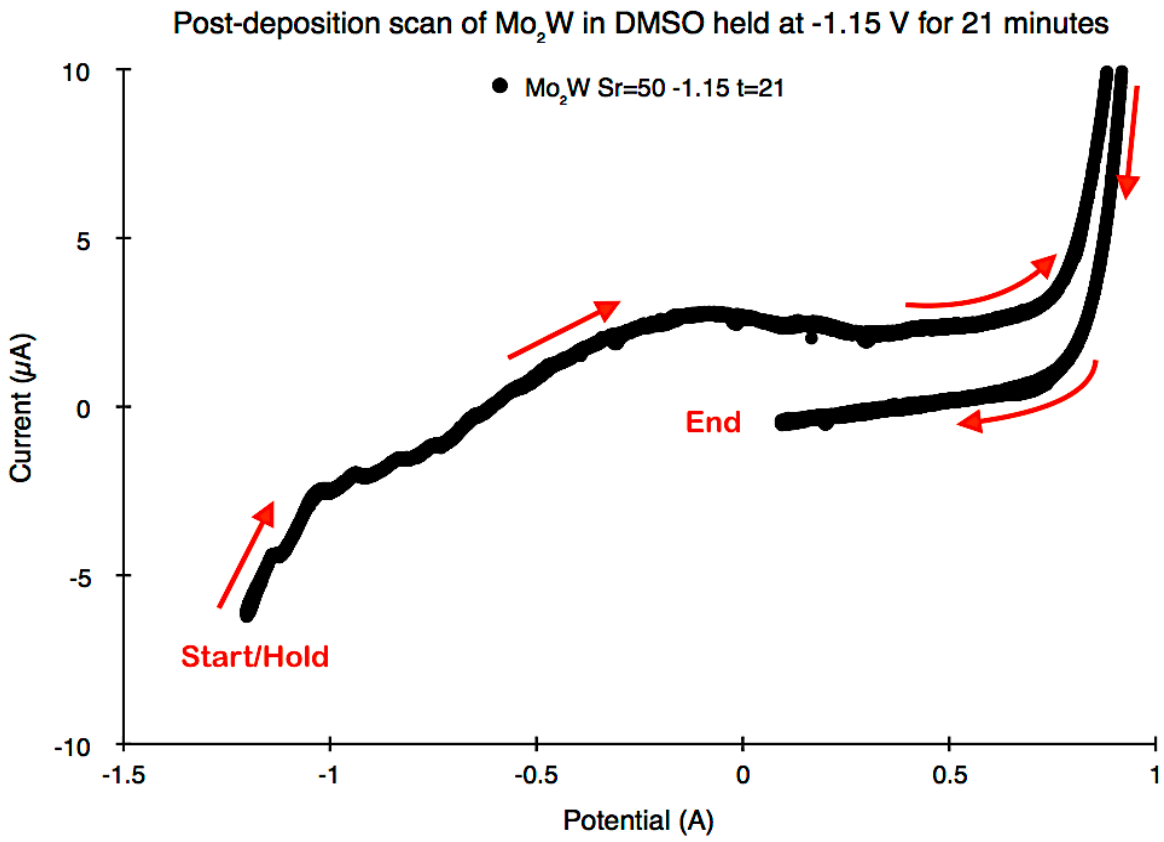

Figure 3.20. CV of the Mo_2W trimer scanned at 50 mV/s immediately after electrodeposition attempts. The trimer was scanned at -1.15 V for 21 minutes at 21.0ºC. The scan was initiated at -1.0 V, held for 21 minutes at -1.15 V, then reversed.

3.3.2.3 The MoW_2 tri-nuclear cluster

The MoW_2 tri-nuclear cluster was the second of two cluster compounds studied possessing the combination of both Mo and W. Figure 3.21 shows the MoW_2 after being held for 20 minutes. Figure 3.22 depicts the same trimer after being held at a potential in slight excess of the irreversible reduction peak observed, -1.17 V for 20 minutes.

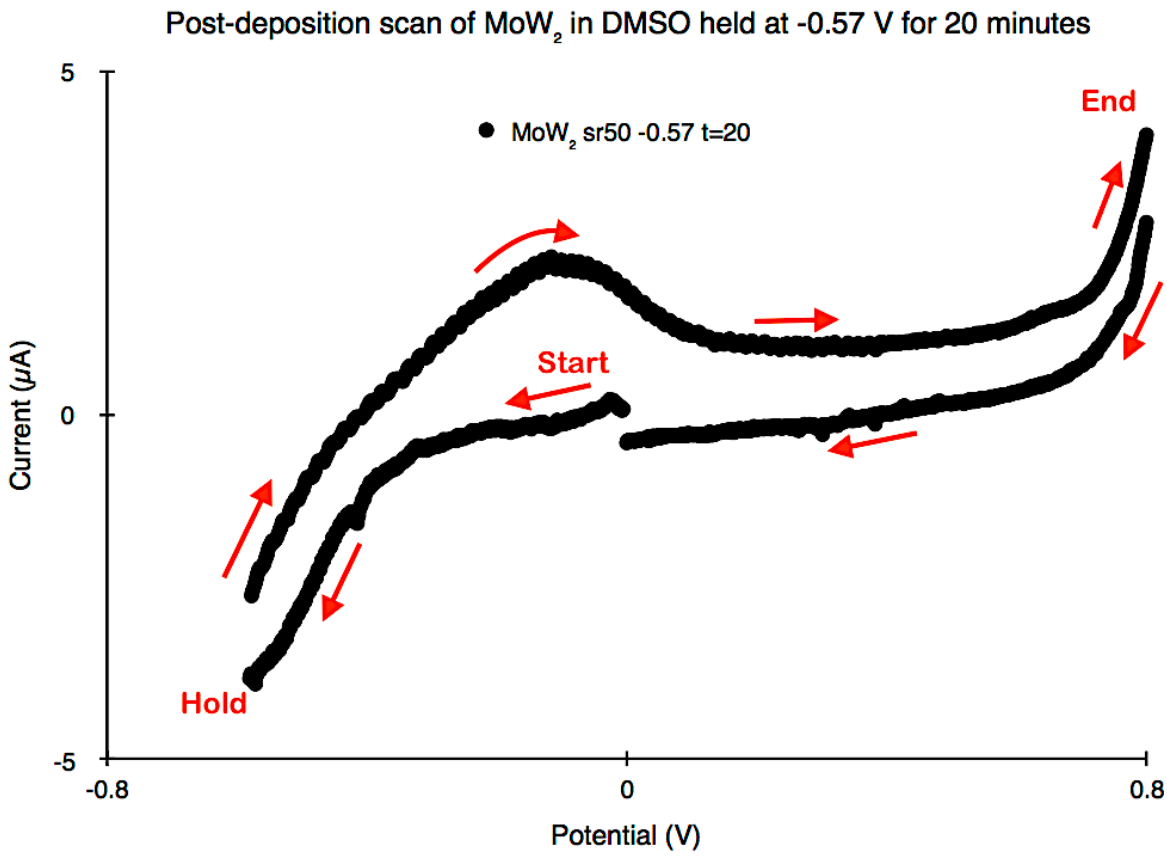

Figure 3.21. The image shows the CV of MoW_2 scanned at 50 mV/s, beginning at 0.0V and scanning in the cathodic direction. It was held at -0.57 V for 20 minutes.

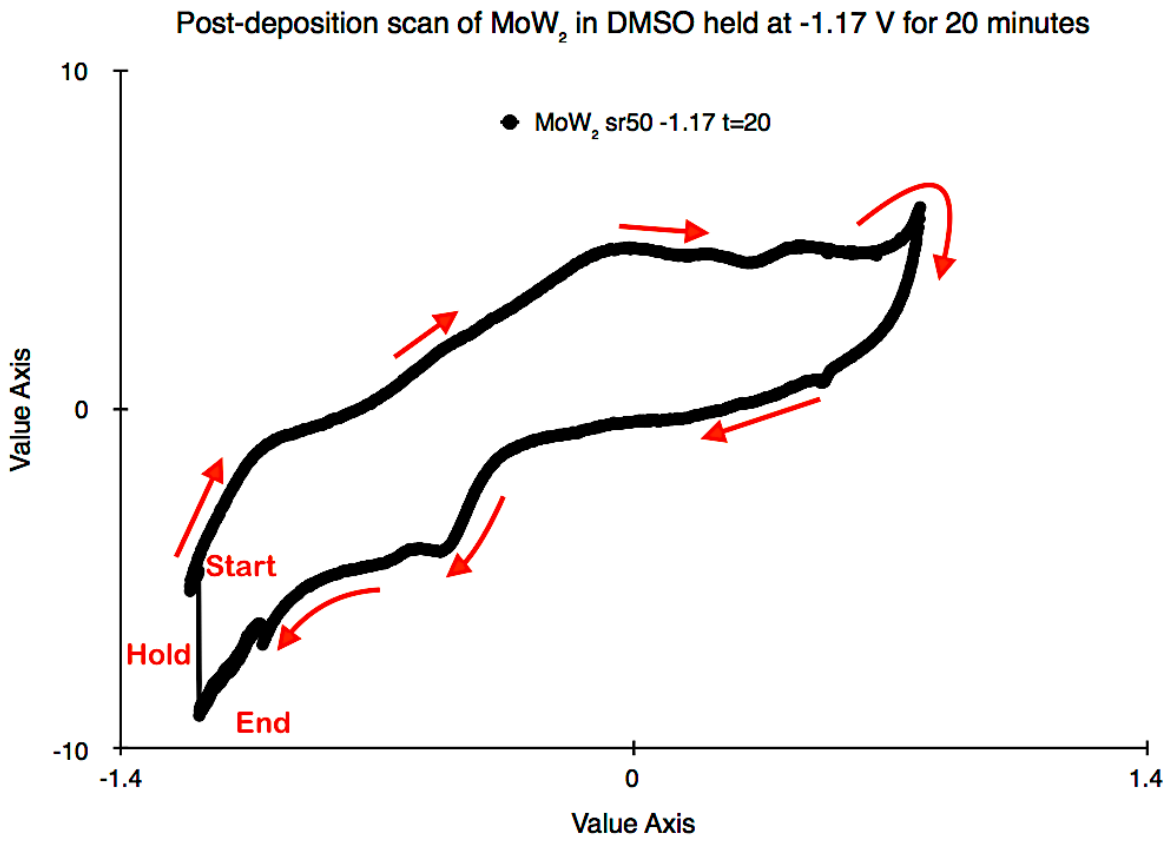

Figure 3.22. CV of MoW_2 in DMSO scanned immediately after attempting electrodeposition at 21.0ºC. Using a scan rate of 50 mV/s, the scan was held at -1.17 V for 20 minutes.

3.3.2.4 The W_3 tri-nuclear cluster

Electrodeposition was then attempted with the W_3 tri-nuclear cluster at a temperature of 21.1ºC. The W_3 trimer was held for 20 minutes in slight excess of the observed redox potential, at -0.57 V. This CV can be seen in Figure 3.23. Electrodeposition was also attempted by holding the potential for 20 minutes at -0.87 V, the irreversible reduction potential, and can be seen in Figure 3.24.

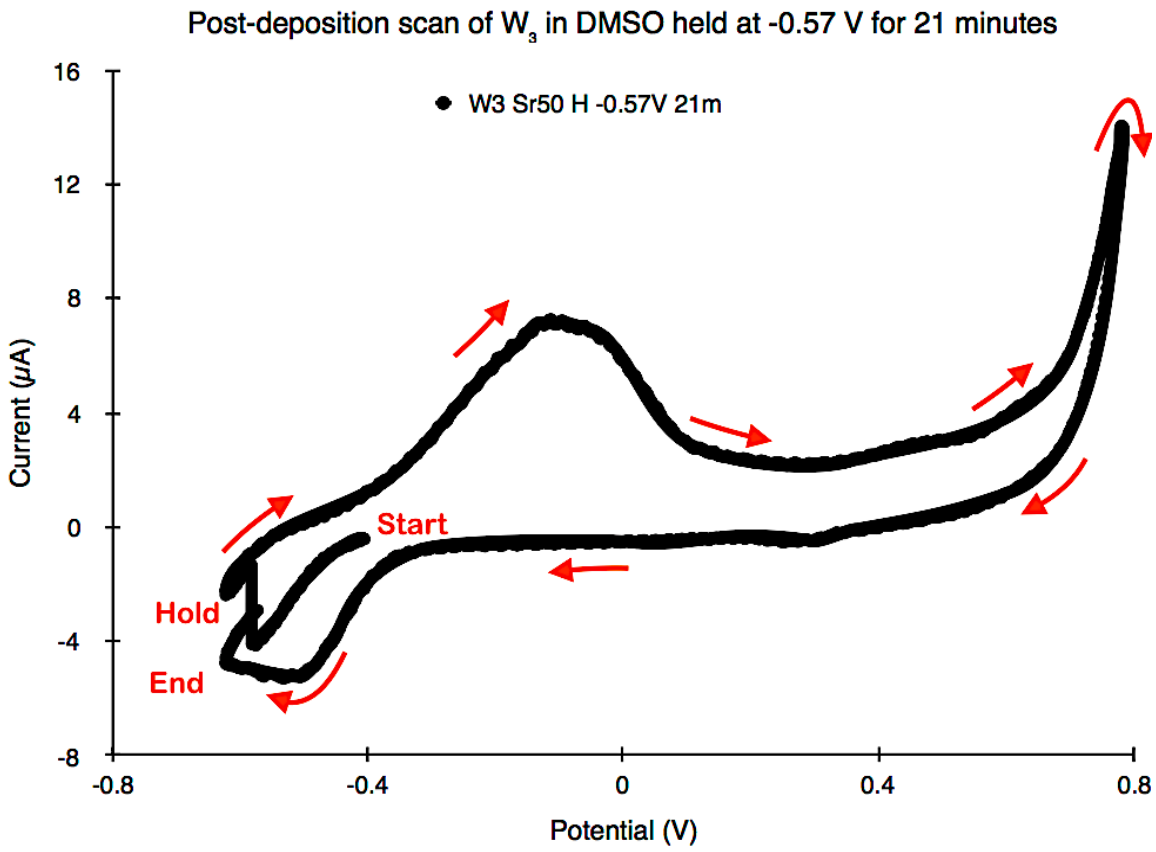

Figure 3.23. CV of the W_3 tri-nuclear cluster scanned at 50 mV/s, held at -0.57 V for 20 minutes at 21.1ºC. As with all previous trimers, no sharp peaks were observed at any scan rate.

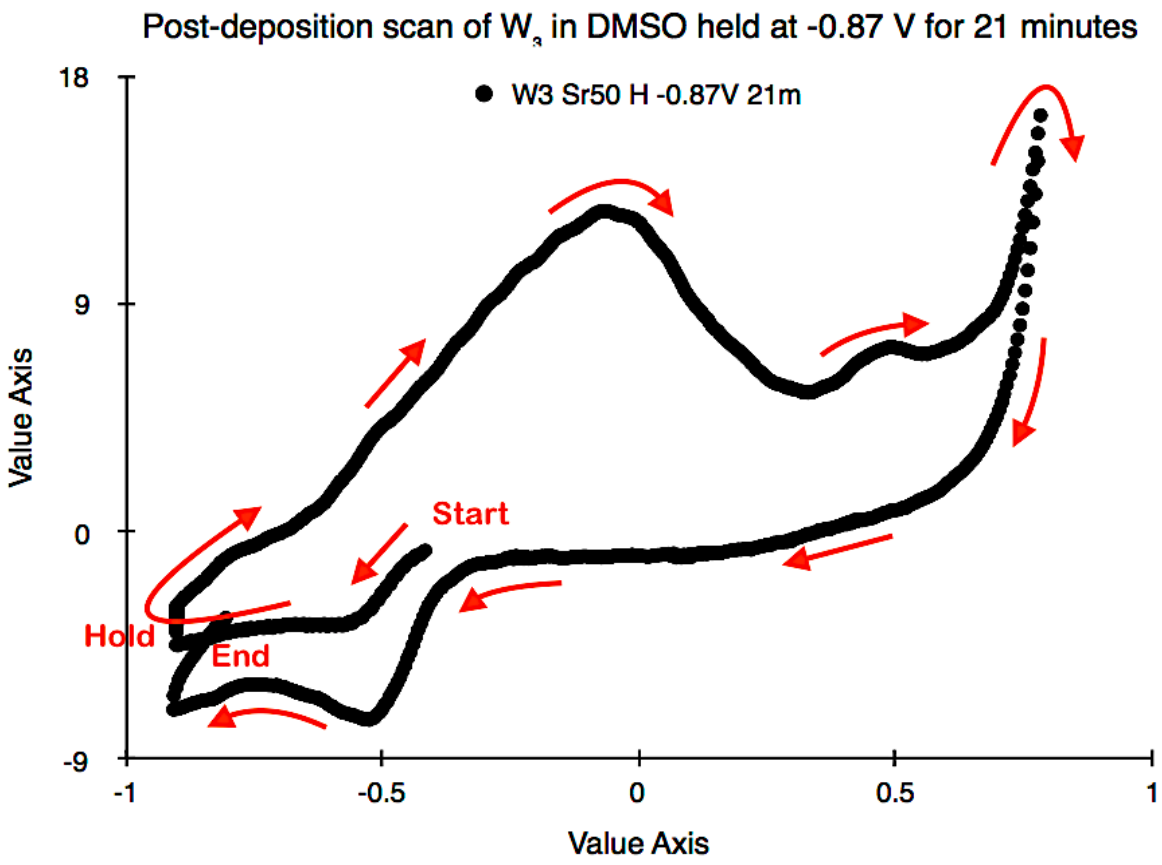

Figure 3.24. CV of the W_3 tri-nuclear cluster scanned at 50 mV/s, held at -0.87 V for 21 minutes at 21.1ºC. As with all previous trimers, no sharp peaks were observed using scan rates of 50, 100, and 200 mV/s.

3.3.2.5 Analysis

Analysis of the electrodeposition attempts in the alternate solvent system, DMSO, revealed that the tri-nuclear clusters failed to deposit onto the Pt electrode system. The plan to test for the catalysis of the carbon-carbon bond of ethanol depended on the successful electrodeposition of the metal clusters onto the Pt electrode. Therefore, a revised plan was implemented to study the tri-nuclear clusters electrochemically and report findings not previously published in the literature. The remainder of the dissertation deals with these new findings.

3.4 Electrochemistry

3.4.1 Electrochemical analysis of the tri-nuclear clusters using cyclic voltammetry

To characterize electrochemical processes, the most useful tool is the technique known as cyclic voltammetry. It offers a direct and powerful, yet relatively simple technique to characterize how easily a compound is able to lose (oxidation) or accept (reduction) an electron (Evans et al., 1983). It is also likely the most versatile of electroanalytical techniques, as evidenced by its widespread use in not just electrochemistry, but inorganic, organic, and even biochemistry (Kissinger and Heineman, 1984). Its strength lies in its ability to generate a species during a scan, and then probe its fate on with successive scans (Ibid.).

This is achieved with a 3-electrode arrangement whereby the potential relative to a reference electrode is scanned at a working electrode while the resulting current is monitored. The technique is ideally suited for a quick search of redox couples present in a system. As reported by Heineman (1984) the voltage applied across these electrodes can be thought of as an excitation signal. During the voltage scan, a CV is obtained by measuring the current at the working electrode, which can now be considered the response signal to the potential (voltage) excitation signal. The voltammogram is a display of current along the vertical axis versus potential along the horizontal axis. As Heineman (1984) mentions, since the potential varies linearly with time, the horizontal axis can also be thought of as a time axis.

As noted by Harvey (2000), the voltammogram is the electrochemical equivalent of a spectrum (such as the "fingerprint" IR spectrum commented on earlier) providing quantitative and qualitative information about the species involved in the oxidation or reduction reaction (Harvey, 2000).

If the voltage of the working electrode is made more positive than that of a redox couple present in the solution, an electron may be stripped from the species (oxidation) in the solution, and delivered to the relatively positively charged electrode. This produces a current (literally the flow of electrons). The current is labeled anodic current when oxidation is occurring. When the voltage at the working electrode is made more negative than the reduction potential of a redox couple, reduction occurs, as the electrons flow from the electrode back to the redox species. This is known as cathodic current (Gosser, 1993).

The graphic result of the CV contains numerous informative parameters, such as the cathodic peak potential Ep,c, the anodic peak potential Ep,a, and the cathodic and anodic peak currents Ip,c and Ip,a, respectively. These are highlighted in Figure 3.25 below.

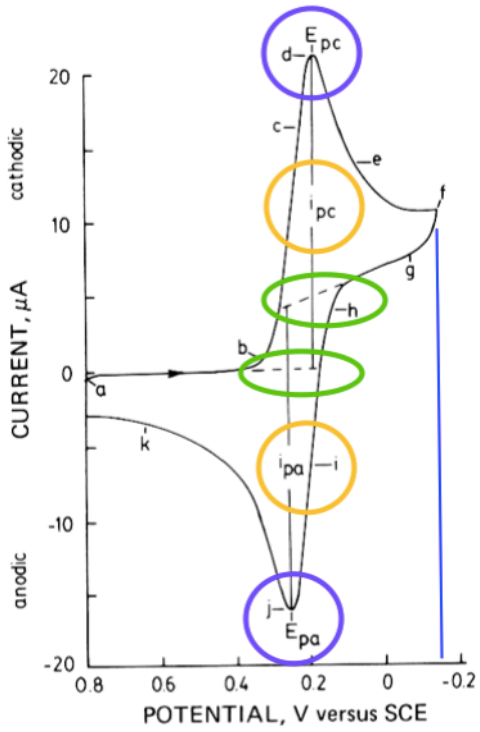

Figure 3.25. A typical CV with the parameters of interest labeled. At point B, the potential is negative enough to reduce the positive oxidation state (+3 in this case) of the redox pair. This cathodic current generated continues to be produced until its peak at point "d". As the current decays due to the consumption of the higher oxidative state to the lower points "d–g", the scan direction is reversed at point "f", towards a positive potential. As the reduced species starts to oxidize, anodic current is generated at points "i"-"k". The current peaks at point "j" as the reduced species is used up. The current then decays "j-k" as the solution surrounding the electrode is depleted of the reduced species (Kissinger & Heineman 1984).

3.4.2 Effect of electron transfer kinetics on the faradaic current

Among the factors which influence current as measured with cyclic voltammetry, is the rate at which mass is transported (mass transport). Another is the rate, or ease, of electron transfer between the electrode and the species reacting at the electrode. A redox reaction is at equilibrium when its electron transfer rates (kinetics) are fast. This is

characteristic of reversible electrochemical reactions. However, if the electron transfer kinetics are slow, the system is then typically electrochemically irreversible. In fact, the current cannot then be predicted by the Nernst Equation (see Equation 3.2 below), whereas it can be with reversible reactions.

Equation 3.2 $$E = E^0 + \frac{0.0592}{n} \log \frac{[Ox]}{[Red]}$$ The Nernst Equation

The Nernst equation gives the relationship between the potential and the concentrations of both the oxidized and the reduced form of the oxidation-reduction (redox) couple at equilibrium. E^0 refers to the potential at standard-state conditions (298K, 1 atm, 1M concentration), and n refers to the number of electrons transferred in the redox process.

3.4.3 Reversible, Irreversible, Quasi-reversible Processes

Another valuable characteristic the CV is capable of revealing, is whether the redox process is reversible or not. It may in fact be reversible, irreversible, or quasi-reversible.

3.4.3.1 Reversible Electron Transfer

The redox couple in which both species (oxidized and reduced form) rapidly exchange electrons with the working electrode is called an electrochemically reversible couple. The formal reduction potential (E°) for a reversible couple is centered between the anodic (Epa) and cathodic (Ep,c) peak potentials (Kissinger and Heineman, 1984) and is shown in Equation 3.3 below.

Equation 3.3 $$E^0 = E_{1/2} = \frac{Ep,a + Ep,c}{2}$$

A similar indicator of reversible electron transfer is called the current function, whose value is given by ($ip / \nu_{1/2}$). The current function should be constant for all scan rates for which the electron transfer is fast enough to maintain the equilibrium ratio between the reduced and the oxidized forms of the redox couple predicted by the Nernst equation, shown in Equation 3.2 (Kelly, 2014).

The number of electrons transferred in the electrode reaction (*n*) for a reversible couple can be determined from the separation between the peak potentials. The value of *n*, as defined in the various CV criteria for reversibility, is usually 1, occasionally 2, and rarely 3 (Evans et al., 1983). For a one-electron oxidation-reduction process, ΔEp, will equal 0.059 V. The values of Ip,a and Ip,c should be identical if it is a reversible process. In other words, Ip,a/Ip,c will equal 1 (Kissinger & Heineman 1984). Equation 3.4 shows the calculation of ΔEp, taken from the difference between the anodic and cathodic peak potentials. The right-most term gives the expected value of ΔEp as a function the number of electrons transferred.

Equation 3.4 $$\Delta E_p = E_{p,a} - E_{p,c} \cong \frac{0.059}{n}$$

3.4.3.2 Irreversible

According to Heineman (1984), electrochemical irreversibility is caused by slow electron exchange of the redox species with the working electrode. This slow electron transfer at

the electrode surface - termed "irreversibility" - causes the peak separation to increase. The peaks will be not only more widely separated, but smaller in size as well (Kissinger and Heineman, 1984). Quantitatively, electrochemical irreversibility is characterized by a separation of peak potentials greater than indicated by Equation 3.4 (Kissinger and Heineman, 1984).

3.4.3.3 Quasi-reversible

A reaction is quasi-reversible if k_f (rate constant in forward direction) and k_b (rate constant in backward direction) are of the same order of magnitude over most of the potential range. It is irreversible if $k_f >> k_b$ for the cathodic peak and $k_b >> k_f$ for the anodic peak. Unlike irreversible reactions, $\Delta Ep > 57/n$ mV.

Overall, the voltammograms of a quasi-reversible system are more drawn out and exhibit a larger separation in peak potentials compared to a reversible system. (Lunsford et al., 1994) provided voltammograms demonstrating the electrochemical reversibility behavior of catechols in ascorbic, and uric acid. In Figure 3.26, the reversibility of catechol is depicted in voltammogram A, while voltammogram B depicts the irreversible nature of ascorbic acid. Figure 3.27 shows how the voltammogram changes with different states of reversibility.

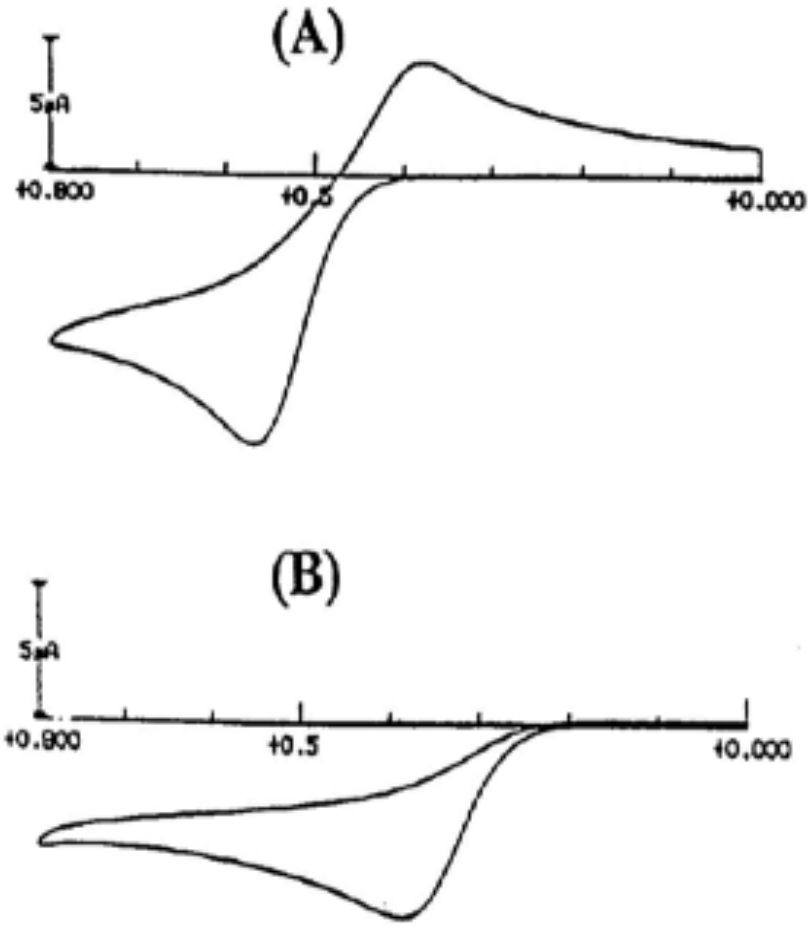

Figure 3.26. Reversible (A) and irreversible (B) voltammograms from Figure 3.7 of Lunsford et al., 1(994) "Electrochemistry and Detection of Catechol at a Conducting Poly(3- methylthiophene) Electrode in the Presence of a Common Interferent, Ascorbic Acid." ECS Transactions 3(10) (Ibid.).

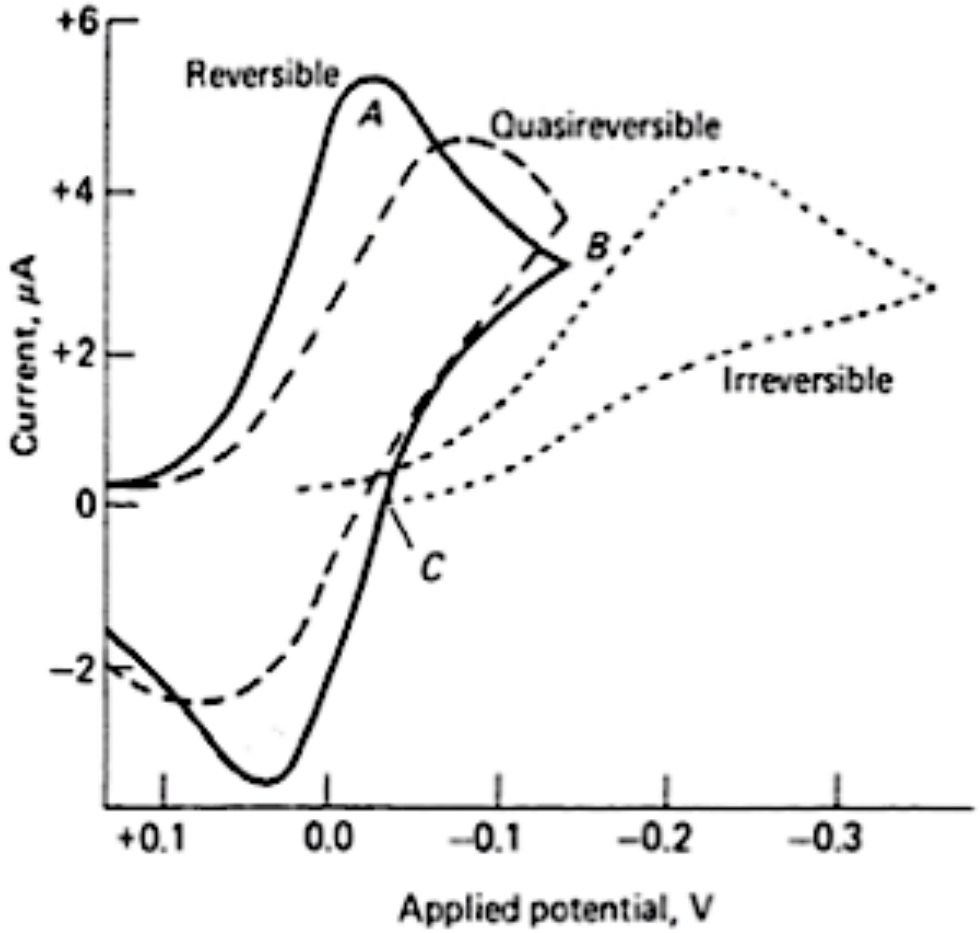

Figure 3.27. An overlay of the three types of reactions, where A represents a Reversible reaction, B a Quasi-irreversible reaction, and C an irreversible reaction, from Figure 3.4B of Lunsford et al., 1(994) Electrochemistry and Detection of Catechol at a Conducting Poly(3- methylthiophene) Electrode in the Presence of a Common Interferent, Ascorbic Acid. ECS Transactions 3(10) (Ibid.).

3.4.4 The Scan Rate

CV allows for a degree of control over the speed at which a scan is run. This is known as the scan rate. The scan rate is useful for a number of reasons.

1. The scan rate can be used to determine is the "system" is reversible. In such a system, the mean peak potential is not affected by the scan rate (Harvey, 2000).
2. If a reaction *is* reversible, the Randles–Sevcik expression can be used to explore the relationship between the concentration and peak current (at 25 °C). The Randles–Sevcik equation can be seen in Equation 3.5.

Equation 3.5 $$ip = 2.69 \times 10^5 n^{3/2} A D^{1/2} C v^{1/2}$$

Where ip = peak current in amps, A = the electrode area (cm^2), D = the diffusion coefficient ($cm^2\ s^{-1}$), C = concentration in mol cm^{-3}, and ν = the scan rate in V s^{-1} (Ibid.).

3. When the square root of the scan rate is plotted with the peak anodic current, the diffusion coefficient can be determined.
4. There can be both electrochemical and purely chemical steps involved in the process being monitored by CV. Scanning at one scan rate may reveal information not revealed at another. For example, a slow scan rate may not pick up a peak because products from the reduction of the analyte may have enough time to engage in a *chemical* reaction whose products are *not* electroactive (Ibid.). Conversely, the electroactive species may require more time to and negative

potential to become the electroactive species. In that case, it is the slower scan rate that reveals the information (Van Benschoten et al., 1983).

In the following section, CVs with multiple scan rates overlaid are displayed.

3.4.5 The molybdenum tri-nuclear cluster (Mo_3)

The behavior of the Mo_3 tri-nuclear cluster $[Mo_3O_2(O_2CCH_3)_6(H_2O)_3](CF_3SO_3)_2$, in the new solvent system when scanned at 200mV/s is shown below in Figure 3.28. The first peak encountered was during the cathodic sweep, at -0.419 V, producing 0.365 μA of current. We believe that this peak represents the *reversible* one-electron reduction of the Mo_3 trimer. A second reduction peak occurred at -0.740 V producing 0.533 μA of current, but showed no concurrent oxidation peak. This peak is believed to represent a further reduction of the trimer by a second electron, but was *ir*reversible. The return anodic sweep displayed an anodic peak potential of -0.444 V, producing 4.222 μA of current. This peak is believed to represent the loss of one electron corresponding to the first redox peak at observed at -0.419 V.

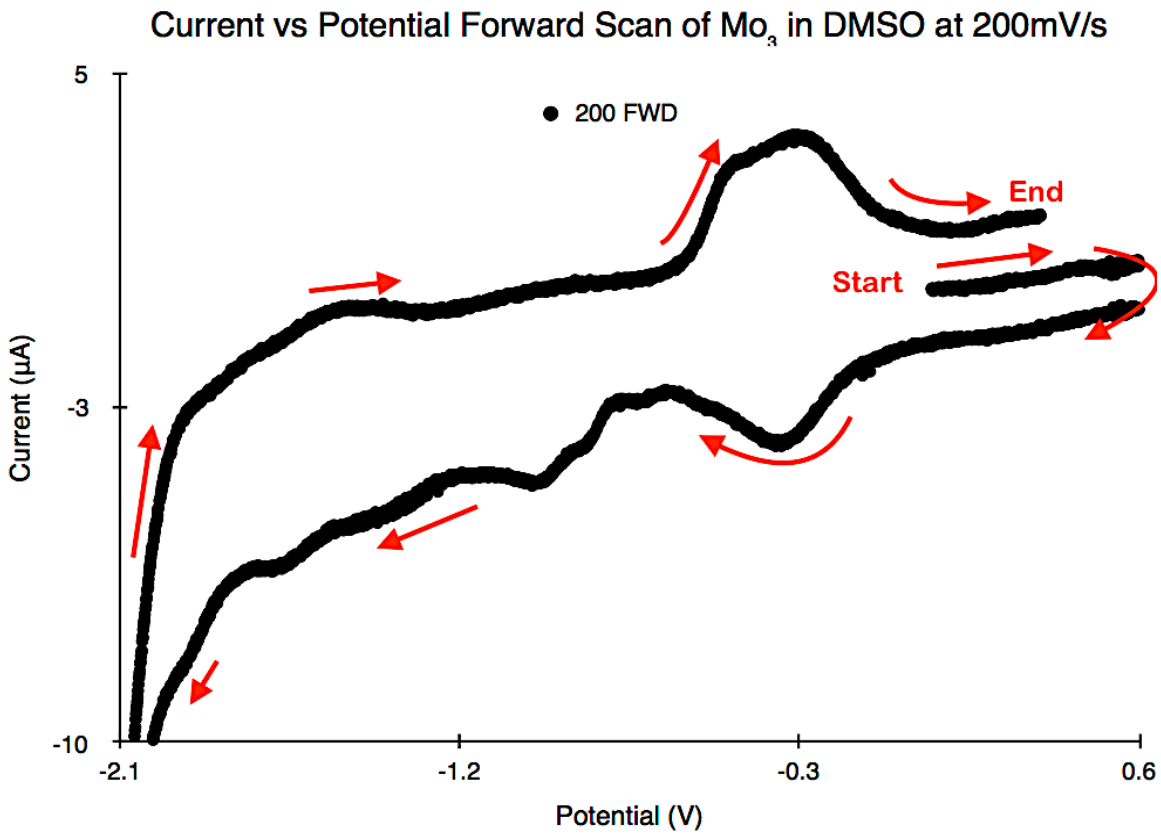

Figure 3.28. CV of the Mo_3 tri-nuclear cluster in the DMSO solvent system. The scan was initiated in the forward/positive direction at a scan rate of 200 mV/s.

CVs at scan rates of 1, 10, 20, 50, 100, 200, 500, and 1000 mV/s were overlaid into one plot, with the scan rates indicated in the plot's legend. Such scans allowed for calculation of the diffusion coefficient by plotting the peak anodic currents against the square-root of the scan rate. Figure 3.29 shows the behavior of the Mo_3 trimer with the scan initiated in the anodic direction. Figure 3.30 shows the same system with the scan initiated in the cathodic direction.

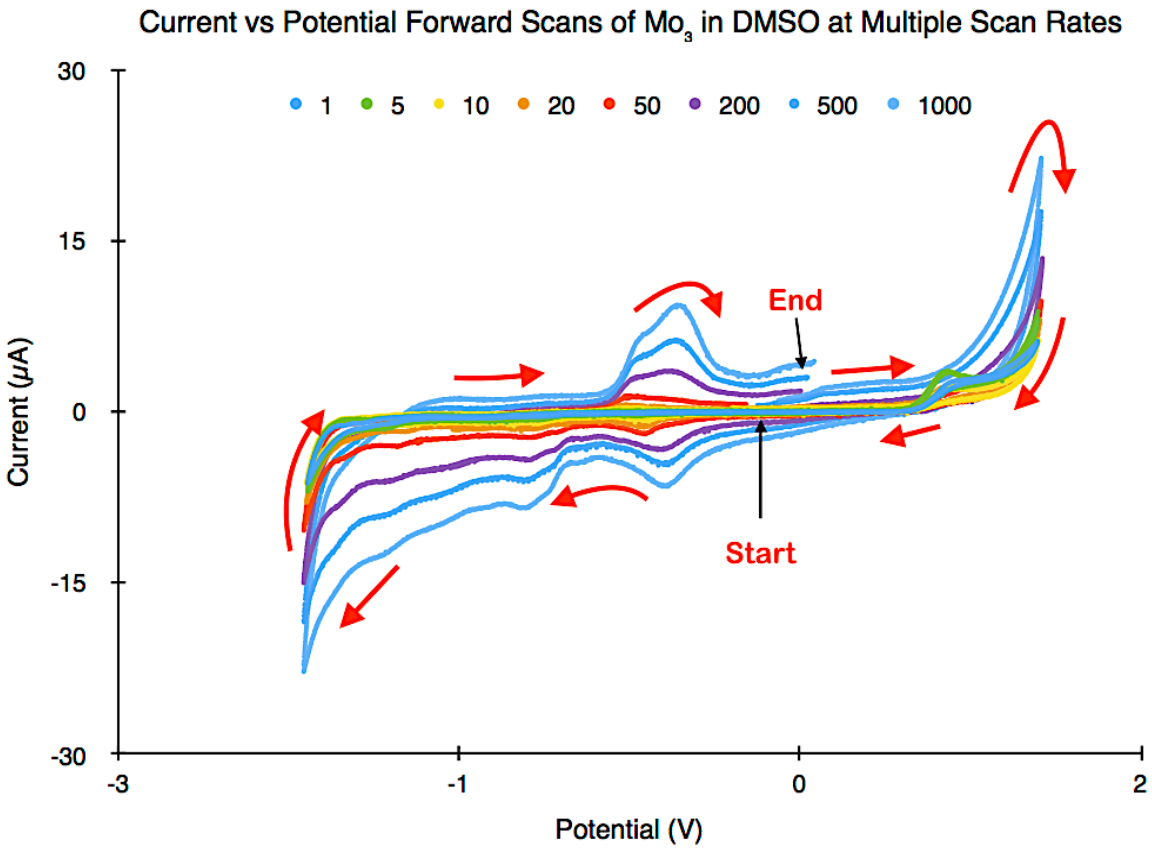

Figure 3.29. CVs of the Mo_3 tri-nuclear cluster in the DMSO solvent system. These scans were initiated in the forward/positive direction at multiple scan rates. This plot contains CVs from nine scan rates (1, 5, 10, 20, 50, 100, 200, 500, and 1000 mV/s) of the Mo_3 trimer.

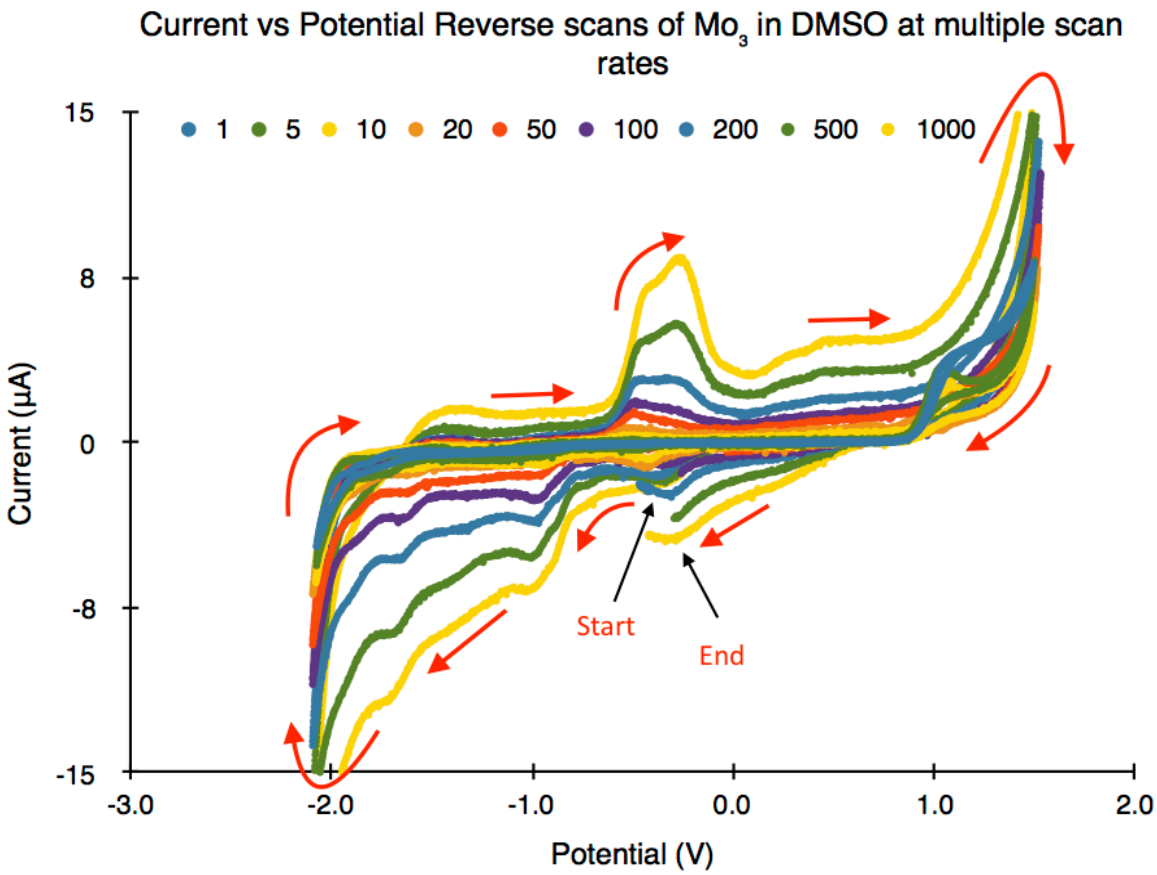

Figure 3.30. CVs of the Mo_3 tri-nuclear cluster in the DMSO solvent system. These scans were initiated in the reverse/negative direction at multiple scan rates. This plot contains CVs from nine scan rates (1, 5, 10, 20, 50, 100, 200, 500, and 1000 mV/s) of the Mo_3 trimer.

3.4.6 The dimolybdenum-tungsten tri-nuclear cluster (Mo_2W)

The CV of the dimolybdenum-tungsten tri-nuclear cluster is shown in Figure 3.31. The CV was obtained by scanning the Mo_2W trimer in the new solvent system at 200mV/s, in the anodic direction. The first peak observed was during the cathodic sweep at -0.432 V producing 2.523 μA of current. It is believed that this peak represents a reversible one-electron reduction of the Mo_2W trimer. A second reduction peak occurred at -1.145 V producing 2.574 μA of current, but showed no concurrent oxidation peak. This peak is believed to represent an *ir*reversible reduction of the trimer by a second electron.

The return anodic sweep displayed an anodic peak potential of -0.320 V, producing 3.332 μA of current. This peak is believed to represent the loss of one electron corresponding to the first redox peak at observed at -0.432 V.

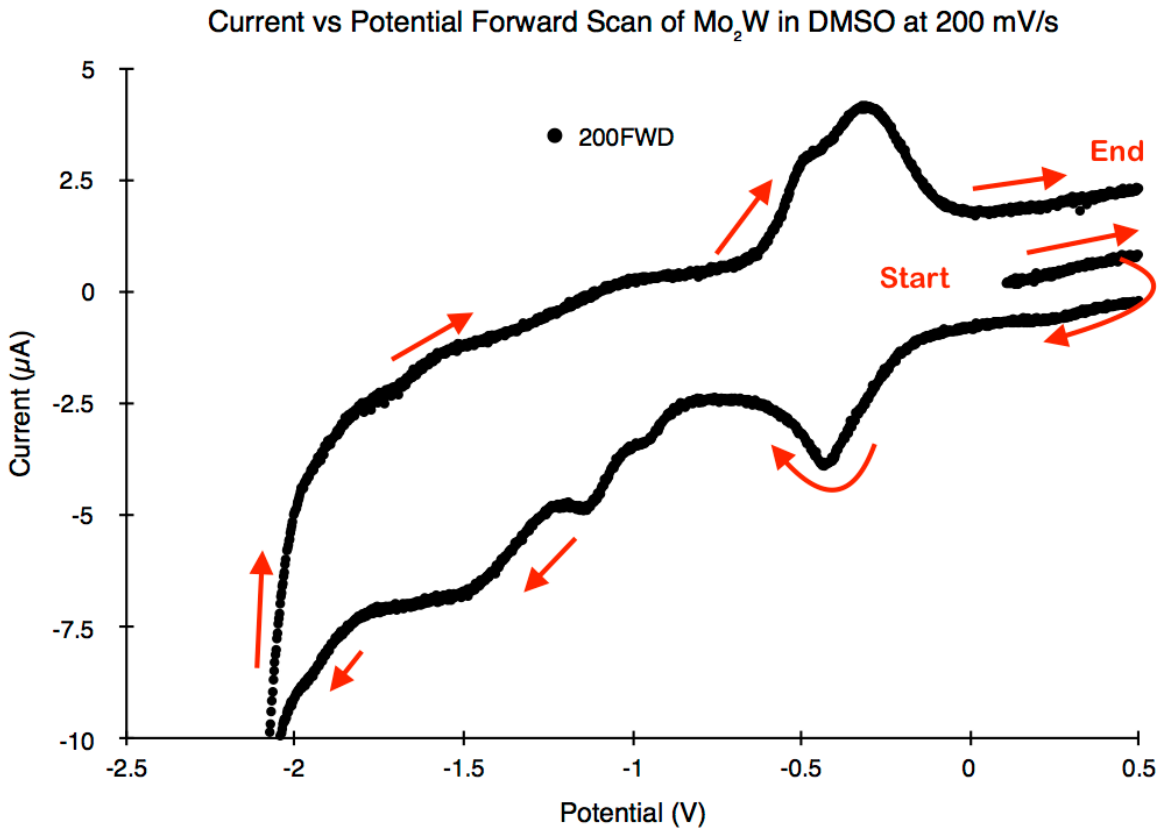

Figure 3.31. CV of the Mo_2W tri-nuclear cluster in the DMSO solvent system. The scan was initiated in the forward/positive direction at a scan rate of 200 mV/s.

Figure 3.32 and Figure 3.33 show the combined scan rates for the Mo_2W tri-nuclear cluster. Figure 3.32 shows the behavior of the Mo_2W trimer with the scan initiated in the anodic direction. Figure 3.33 shows the same system with the scan initiated in the cathodic direction.

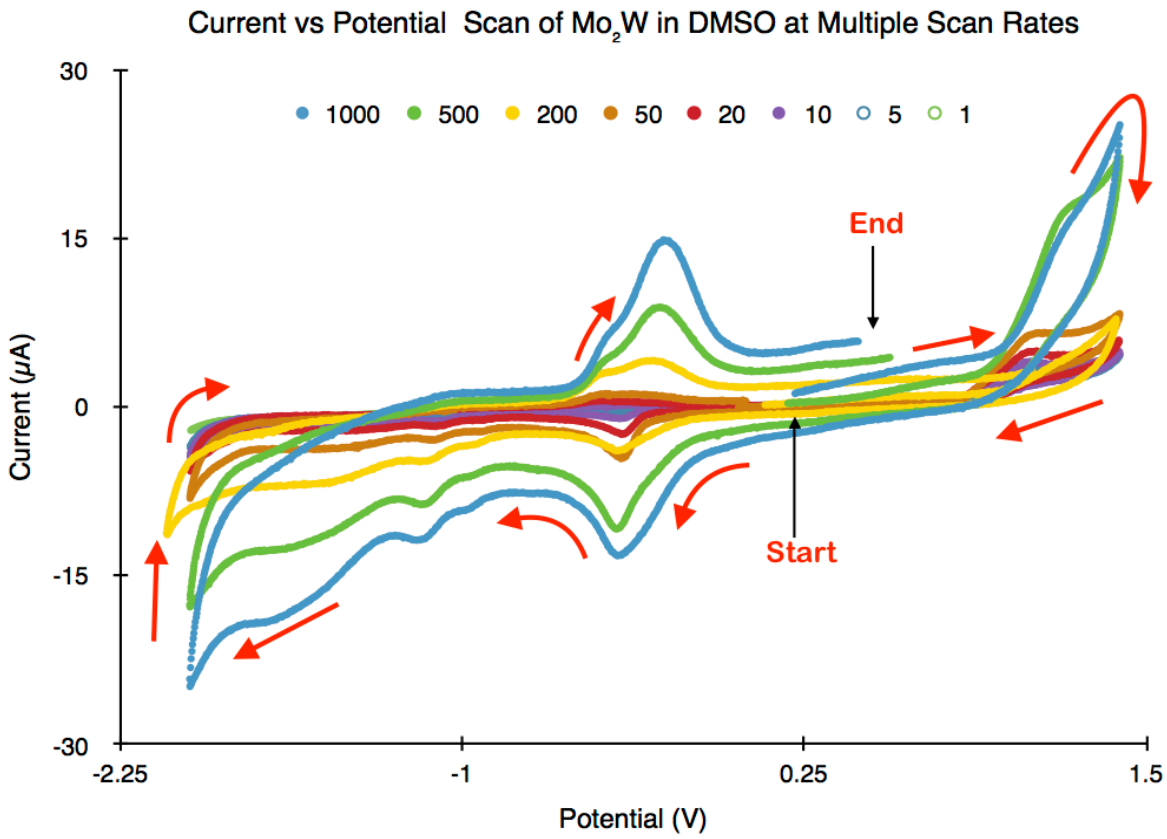

Figure 3.32. CVs of the Mo_2W tri-nuclear cluster in the DMSO solvent system. These scans were initiated in the forward/positive direction at multiple scan rates. This plot contains CVs from nine scan rates (1, 5, 10, 20, 50, 100, 200, 500, and 1000 mV/s) of the Mo_2W trimer.

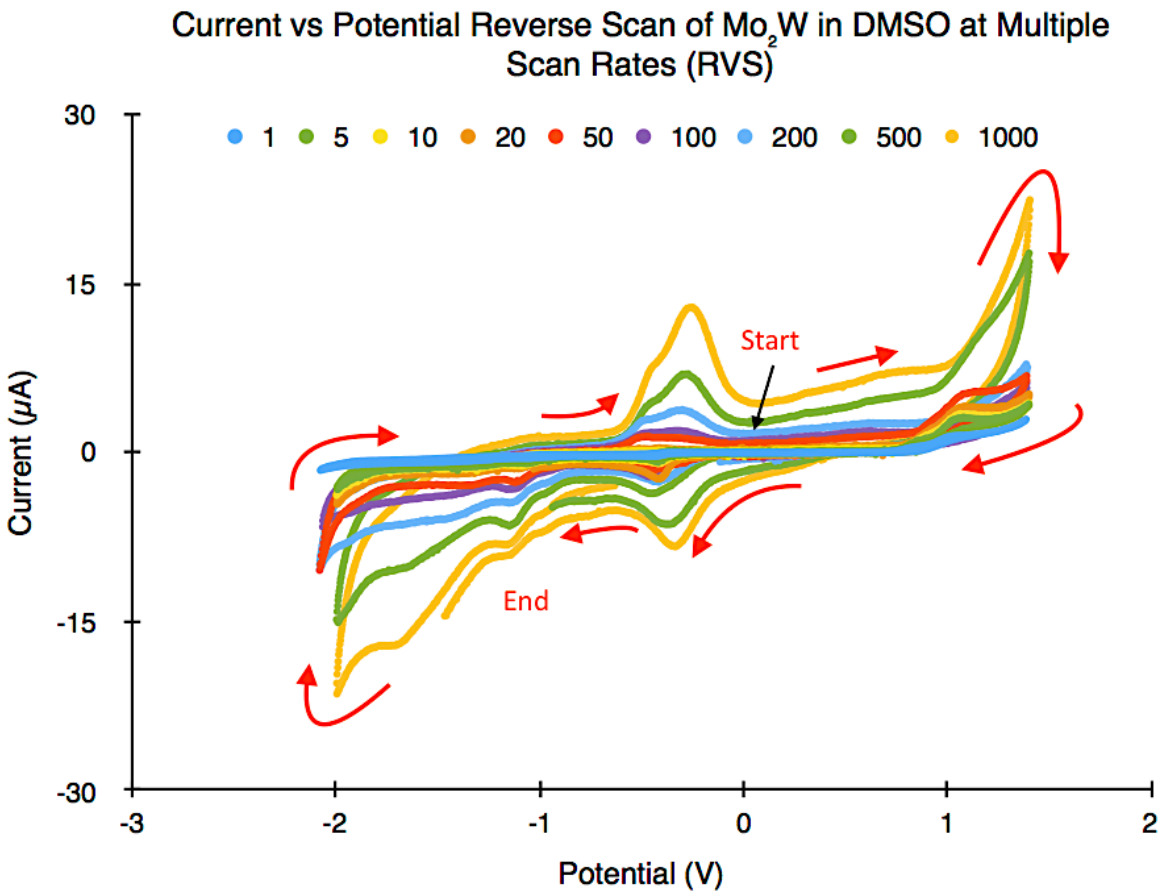

Figure 3.33. CVs of the Mo_2W tri-nuclear cluster in the DMSO solvent system. These scans were initiated in the reverse/negative direction at multiple scan rates. This plot contains CVs from nine scan rates (1, 5, 10, 20, 50, 100, 200, 500, and 1000 mV/s) of the Mo_2W trimer.

3.4.7 The molybdenum-ditungsten tri-nuclear cluster (MoW_2)

Figure 3.34 shows the MoW_2 trimer behavior in the new solvent system when scanned at 200mV/s in the anodic direction. Figure 3.35 shows the same system scanned in the cathodic direction. Scans initiated in the cathodic direction more clearly show both the reversible redox event, as well as two irreversible reduction events. During the cathodic sweep, the first peak was seen at -0.436 V, producing 9.676 μA of current. It appears to us that this peak represents the reversible one-electron reduction of the MoW_2 trimer. The second reduction peak occurred at -1.143 V producing 1.599 μA of current, but showed no concurrent oxidation peak. This peak is believed to represent an irreversible reduction of the trimer by a second electron.

The anodic sweep displayed an anodic peak potential of -0.306 V, producing 6.768 μA of current. This peak is believed to represent the loss of one electron corresponding to the first redox peak at observed at -0.436 V.

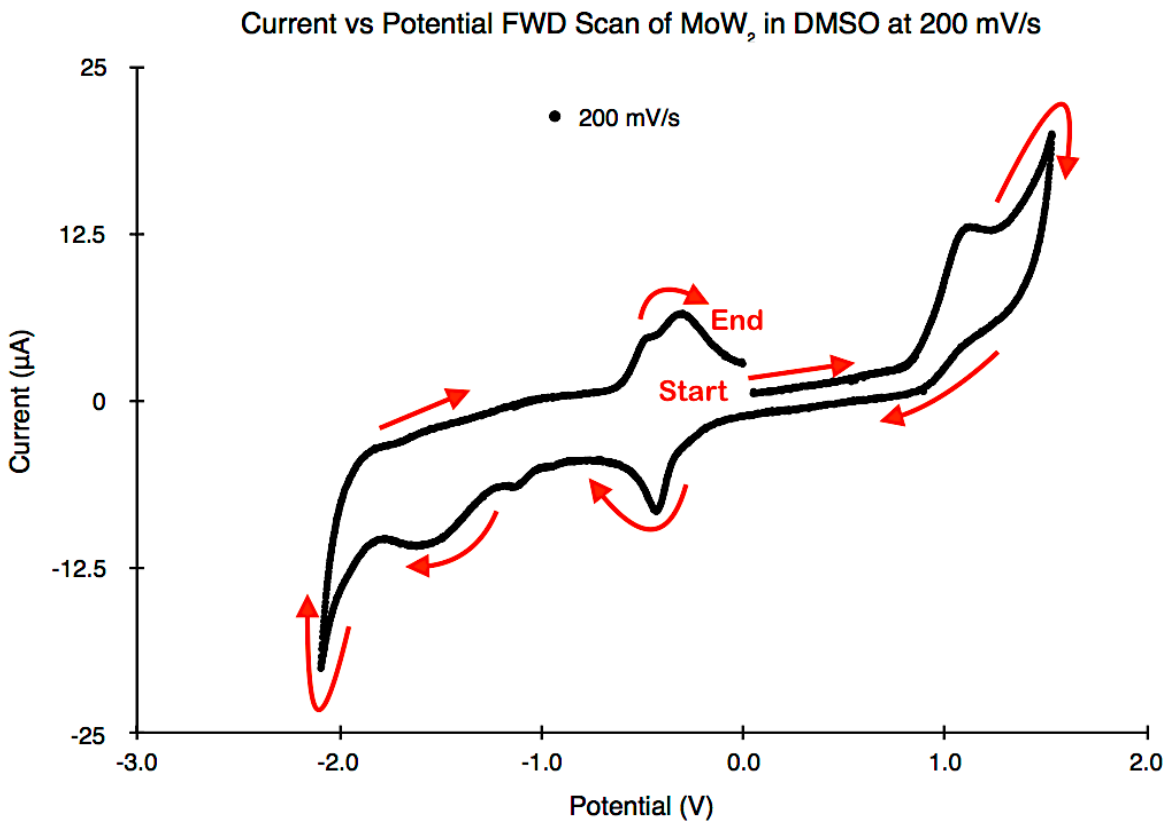

Figure 3.34. CV of the MoW_2 tri-nuclear cluster in the DMSO solvent system. The scan was initiated in the forward/positive direction at a scan rate of 200 mV/s.

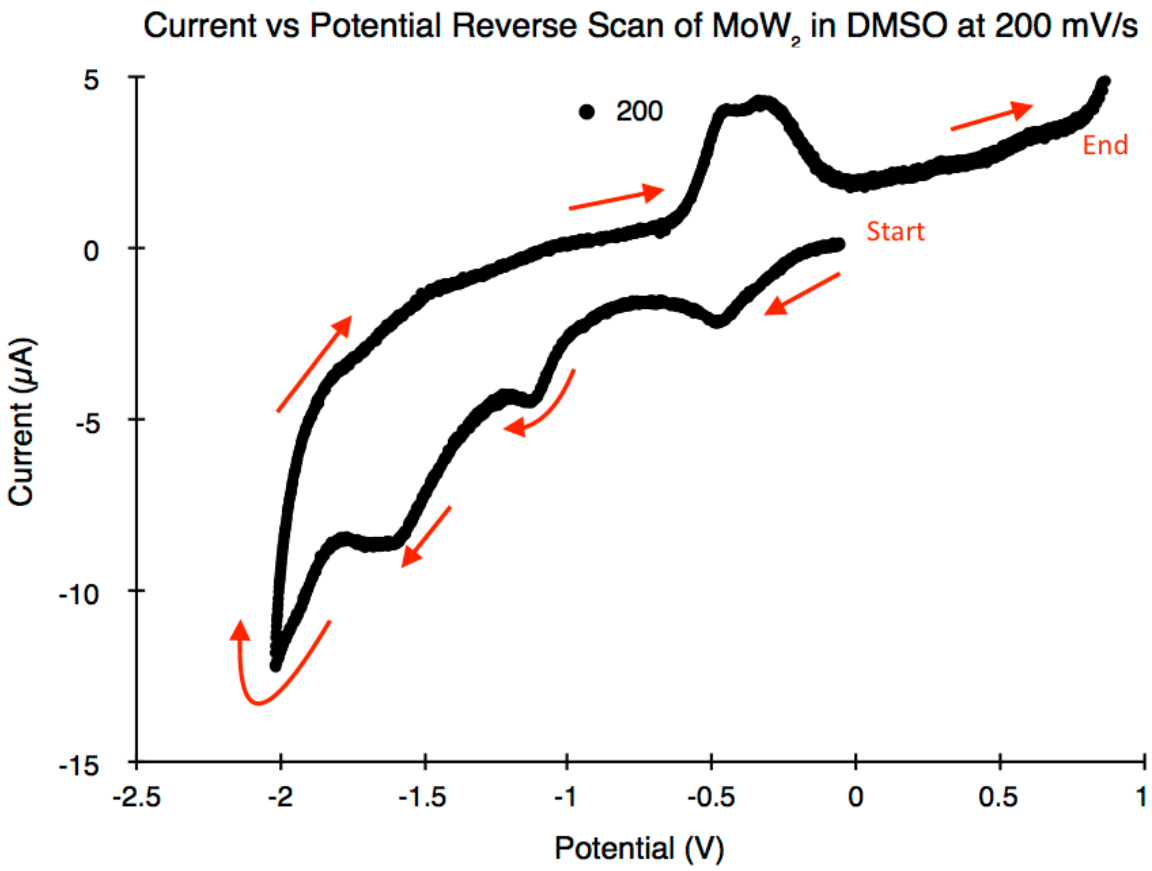

Figure 3.35. CVs of the MoW_2 tri-nuclear cluster in the DMSO/TBAHFP solvent system scanned in the cathodic direction, where three cathodic peaks resolve more clearly.

Figure 3.36 and Figure 3.37 show the combined scan rates for the MoW_2 tri-nuclear cluster. Figure 3.36 shows the behavior of the MoW_2 trimer with the scan initiated in the anodic direction. Figure 3.37 shows the same system with the scan initiated in the cathodic direction.

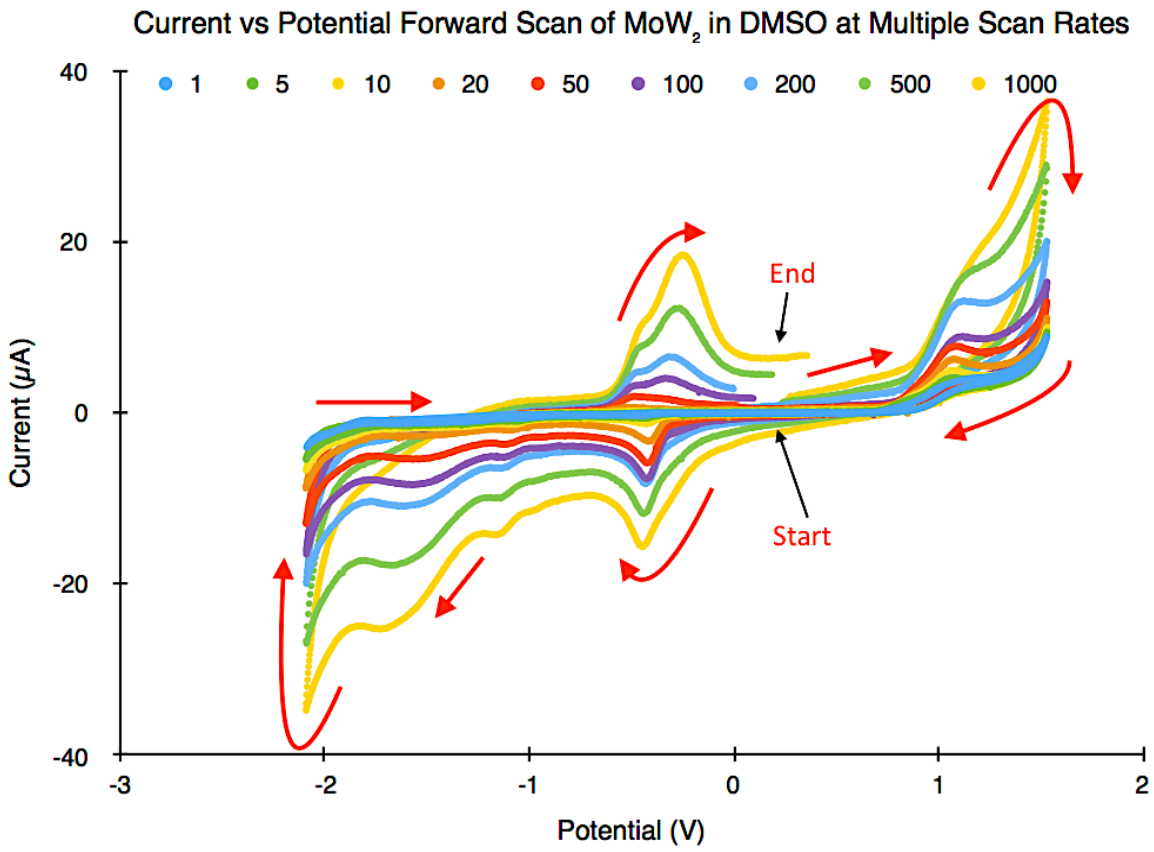

Figure 3.36. CVs of the MoW_2 tri-nuclear cluster in the DMSO solvent system. These scans were initiated in the forward/positive direction at multiple scan rates. This plot contains CVs from nine scan rates (1, 5, 10, 20, 50, 100, 200, 500, and 1000 mV/s) of the MoW_2 trimer.

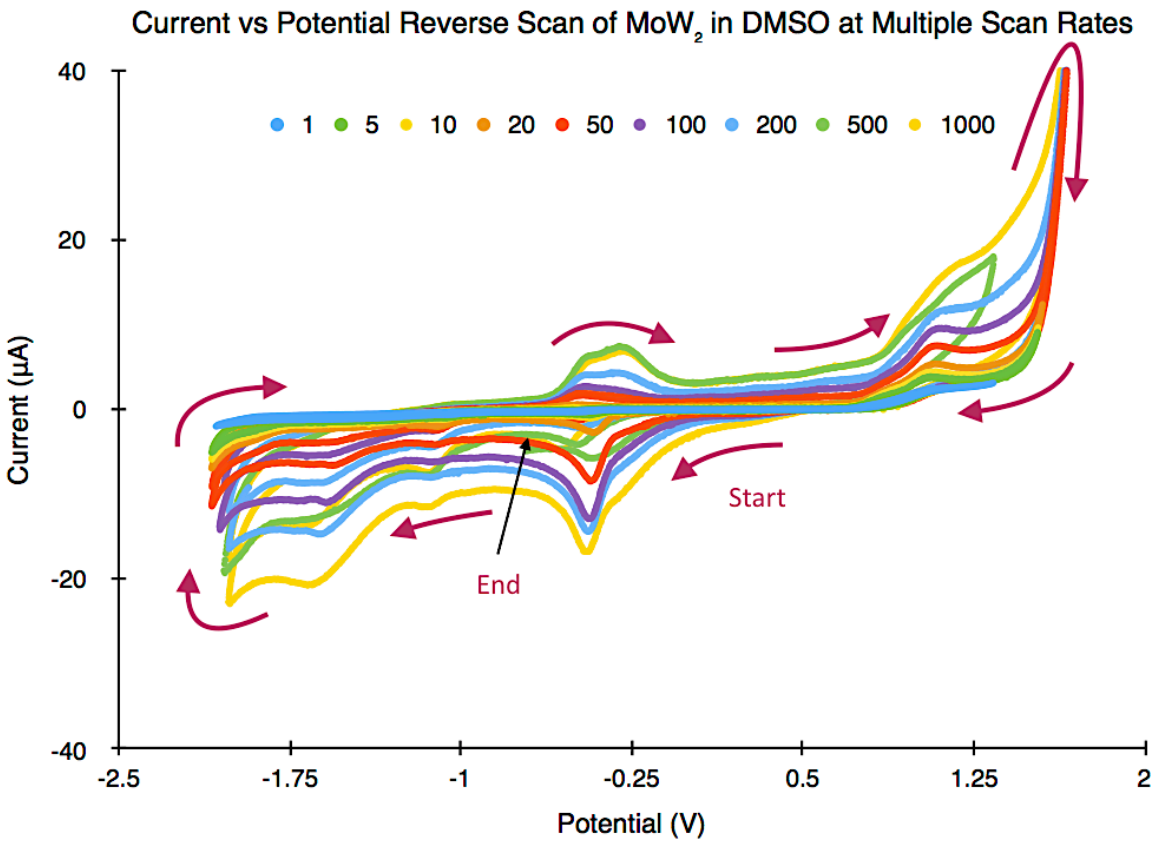

Figure 3.37. CVs of the MoW_2 tri-nuclear cluster in the DMSO solvent system. These scans were initiated in the reverse/negative direction at multiple scan rates. This plot contains CVs from nine scan rates (1, 5, 10, 20, 50, 100, 200, 500, and 1000 mV/s) of the MoW_2 trimer.

3.4.8 The tritungsten tri-nuclear cluster (W_3)

Figure 3.38 shows the behavior of the W_3 tri-nuclear cluster $[W_3O_2(O_2CCH_3)_6(H_2O)_3](CF_3SO_3)_2$, in the new solvent system when scanned at 200 mV/s in the forward (anodic) initial direction. Figure 3.39 shows the W_3 trimer when the scan is initiated in the reverse (cathodic) direction at 20 mV/s, and Figure 3.39 shows a scan in the same direction at 100 mV/s.

The first peak observed during the cathodic sweep was recorded at -0.461 V, producing 1.585 μA of current. We believe that this peak represents a reversible one-electron reduction of the W_3 trimer. A second reduction peak occurred at -0.844 V, producing 0.450 μA of current, with no concurrent oxidation peak. This peak is believed to be an irreversible reduction by a second electron. The return anodic sweep displayed an anodic peak potential of -0.422 V, producing 8.006 μA of current. This peak is believed to represent the loss of one electron corresponding to the first redox peak at observed at -0.461 V. The combined scans for the W_3 trimer in the forward direction are shown in Figure 3.40 and the reverse scans are shown in Figure 3.41.

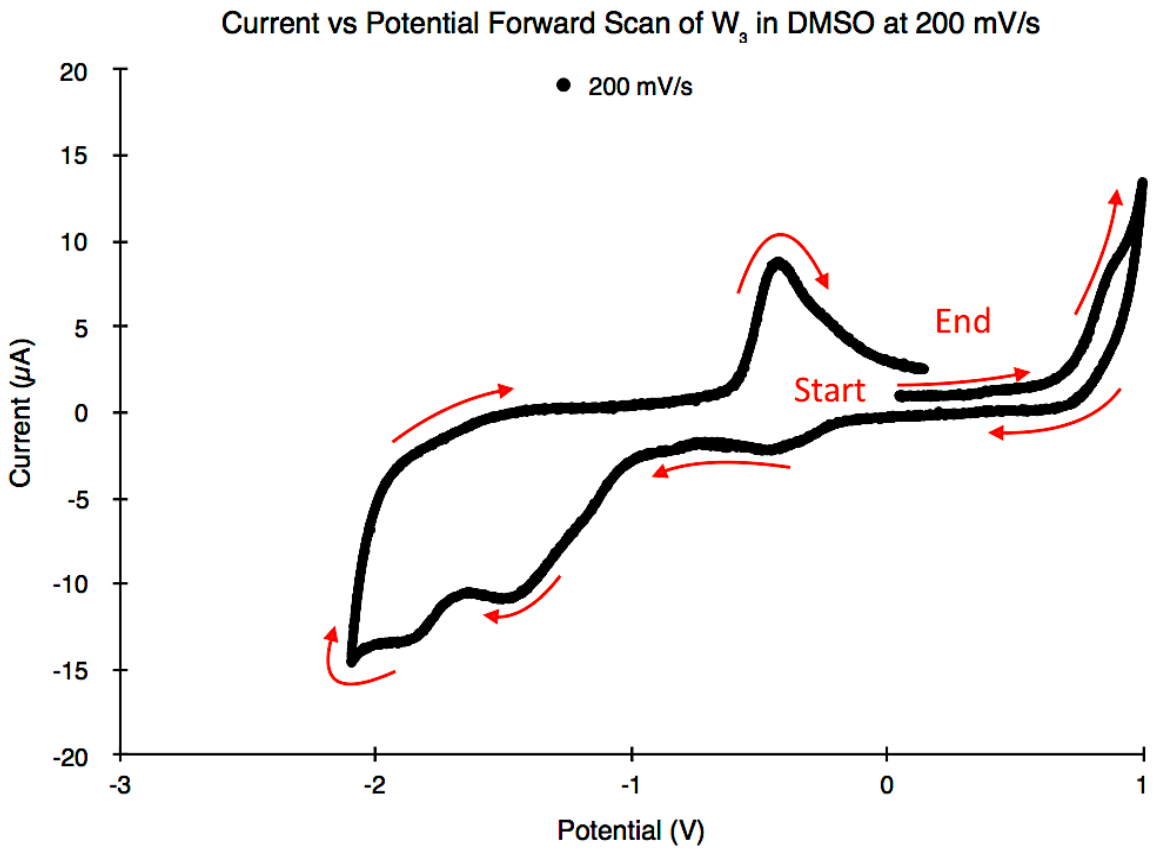

Figure 3.38. CV of the W_3 tri-nuclear cluster in the DMSO solvent system. The scan was initiated in the forward/positive direction at a scan rate of 200 mV/s.

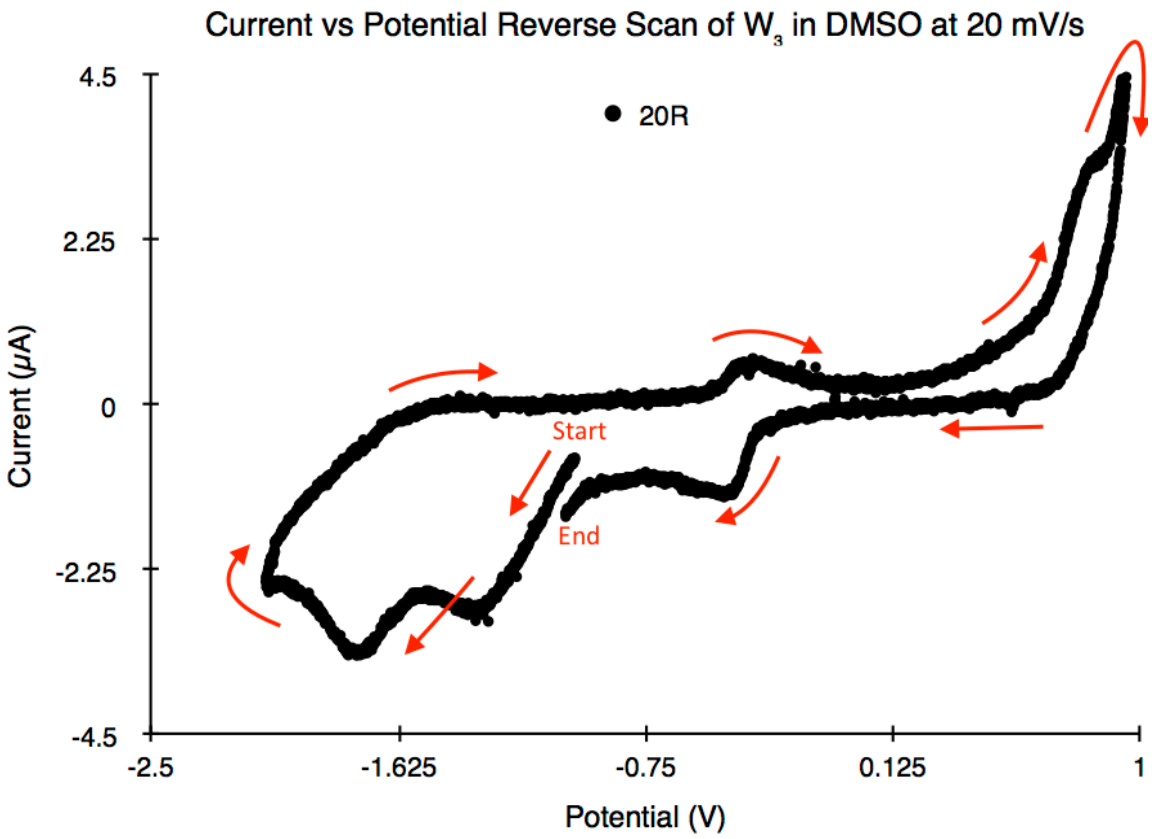

Figure 3.39. CV of the W_3 tri-nuclear cluster in the DMSO solvent system. The scan was initiated in the reverse/negative direction at a scan rate of 20 mV/s.

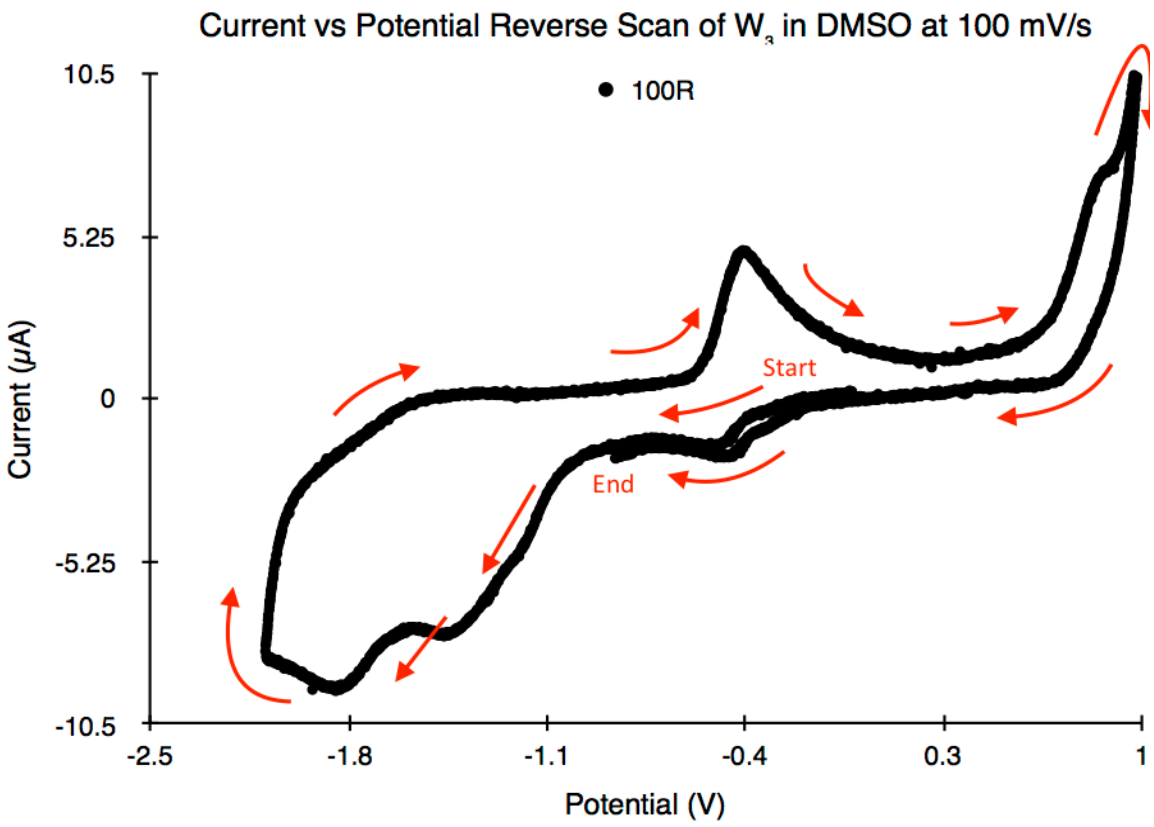

Figure 3.40. CV of the W_3 tri-nuclear cluster in the DMSO solvent system scanned in the reverse/negative direction at a scan rate of 100 mV/s.

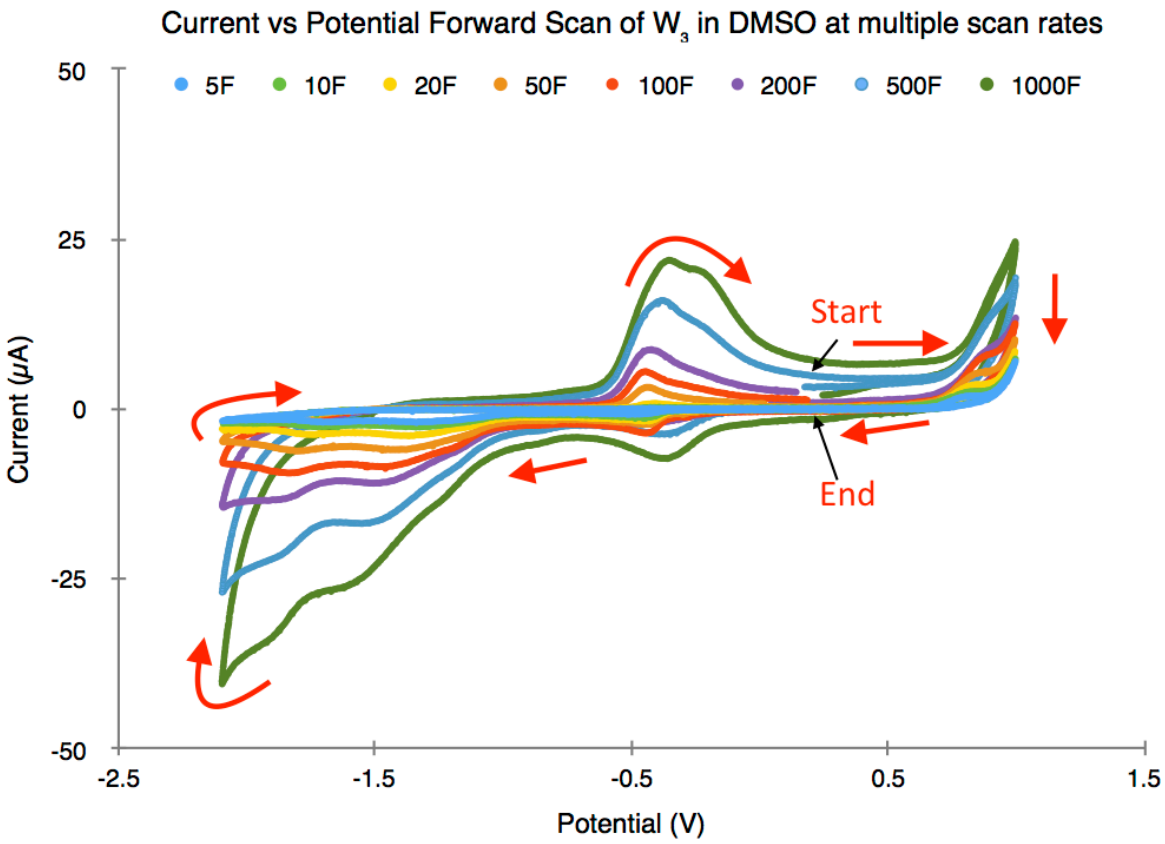

Figure 3.41. CVs of the W_3 tri-nuclear cluster in the DMSO solvent system. These scans were initiated in the forward/positive direction at multiple scan rates. This plot contains CVs from eight scan rates (5, 10, 20, 50, 100, 200, 500, and 1000 mV/s) of the W_3 trimer.

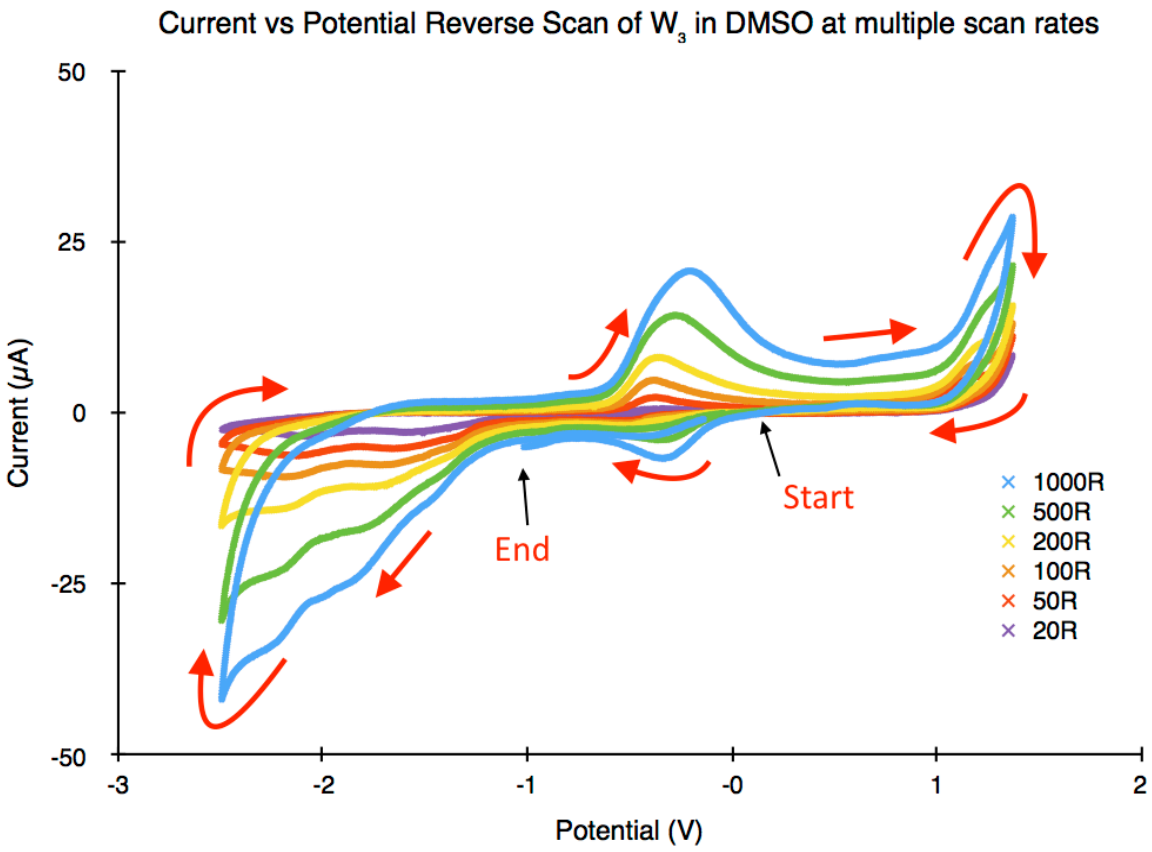

Figure 3.42. CVs of theW_3 tri-nuclear cluster in the DMSO solvent system. These scans were initiated in the reverse/negative direction at multiple scan rates. This plot contains CVs from six scan rates (20, 50, 100, 200, 500, and 1000 mV/s) of the W_3 trimer.

3.5 Acquiring baselines with eL-Chemviewer

The following plots show the interface of the eL-ChemViewer application. The data came from the the CVs acquired with the EG&G 173 potentiostat, and stored as text files. The files are read by eL-ChemViewer and a native CV is created within the program. By moving the cursor along the slope preceding a peak, the program determines the baseline and displays a line from the baseline to the peak, whether positive or negative. The coordinates belonging to these points represent Ep,a and Ip,a, and Ep,c and Ip,c.

These values can then be sent to Microsoft Excel with the click of a button. Once these values were acquired, it was possible to calculate the remaining desired parameters, and finally to determine the diffusion coefficient.

3.5.1 Acquiring baselines for the Mo_3 tri-nuclear cluster

Anodic and cathodic peak potentials (Ep,a, Ep,c) and corresponding current values (Ip,a, Ip,c) for the Mo_3 tri-nuclear cluster were obtained from CVs taken at scan rates of 100, 200, 500, and 1000 mV/s. Values for lower scan rates could not be reliably acquired. Values were also obtained for the second and third irreversible cathodic peaks at 200 mV/s. Figure 3.43 shows the baseline acquisition and determination of the anodic peak current and anodic peak potential for the Mo_3 trimer taken from a CV at 200 mV/s. Figure 3.44 displays the peak cathodic current and peak cathodic potential.

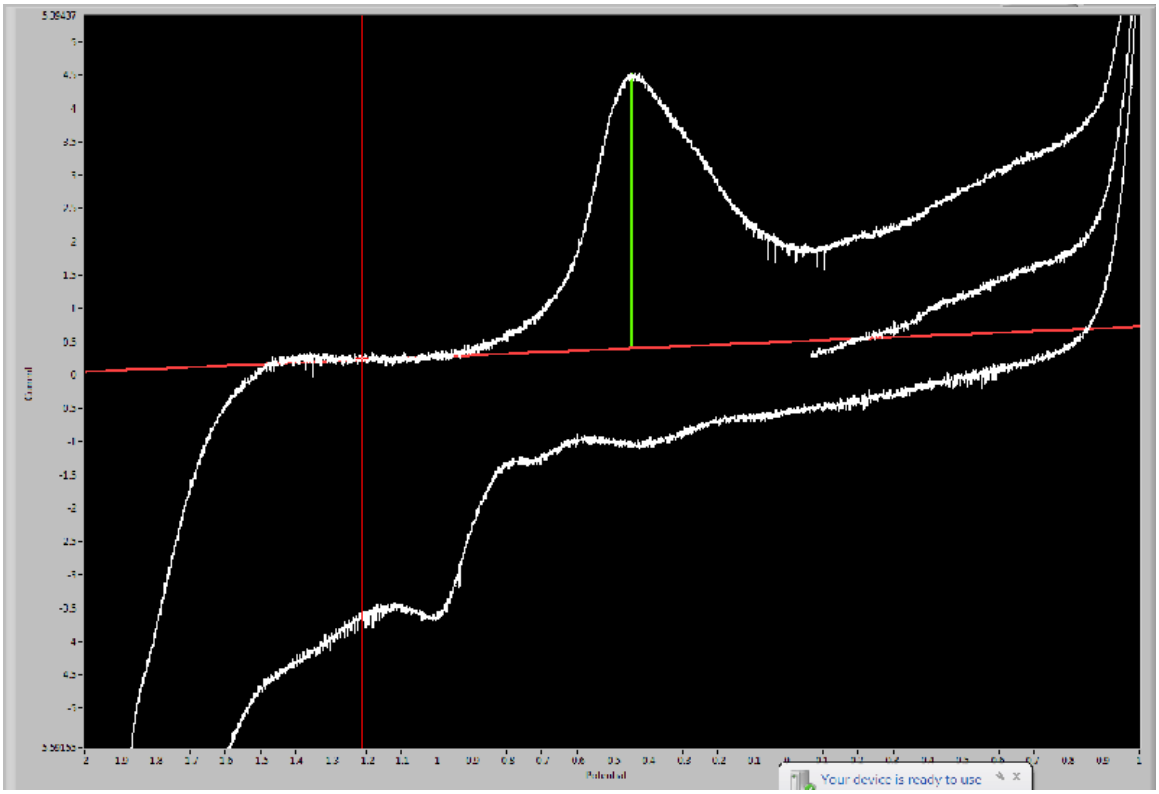

Figure 3.43. This image represents the acquisition of peak anodic potential (Ep,a) and peak anodic current (Ip,a) of the Mo_3 tri-nuclear cluster at 200 mV/s using eL-ChemViewer. The program acquired an Ep,a value of -0.44 V, and an Ip,a of 4.22 µA.

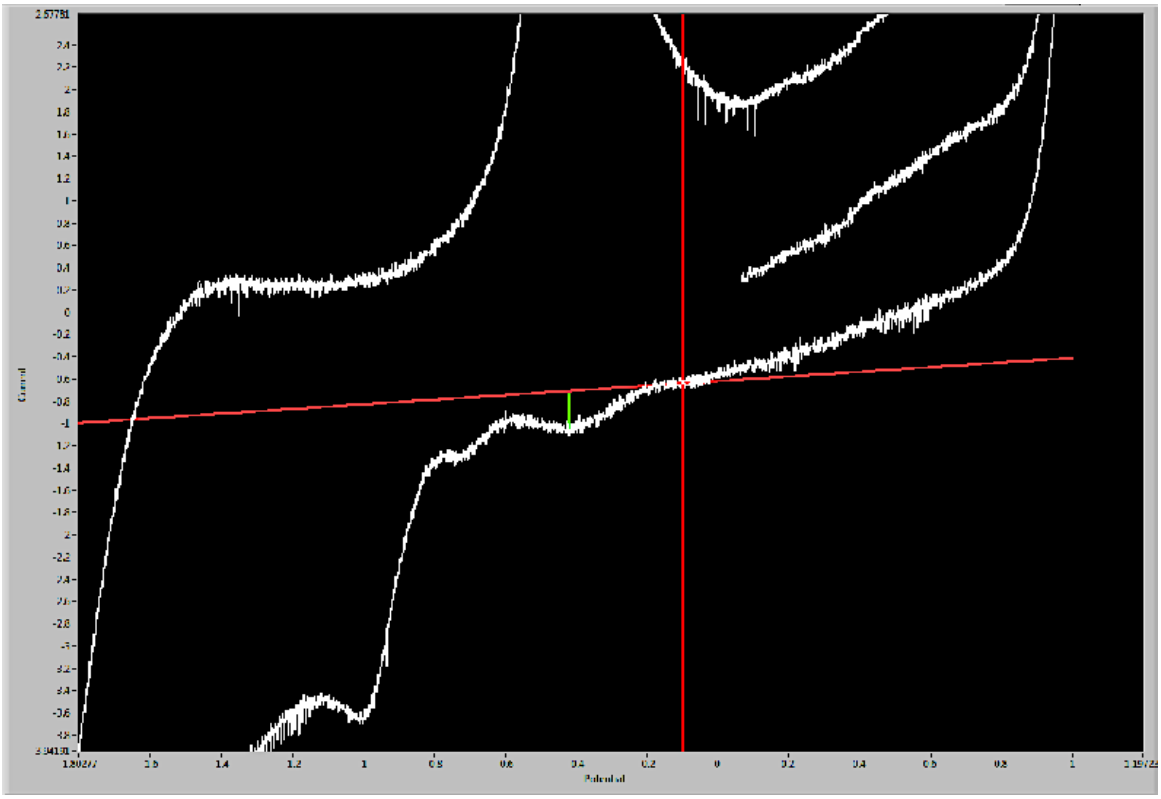

Figure 3.44. This image represents the acquisition of peak cathodic potential (Ep,c) and peak cathodic current (Ip,c) of the Mo_3 tri-nuclear cluster at 200 mV/s using eL-ChemViewer. The program acquired an Ep,c value of -0.42 V, and an Ip,c of -0.37 µA.

3.5.2 Acquiring Baselines for the Mo_2W tri-nuclear cluster

The parameters of Ep,a, Ep,c, Ip,a, Ip,c were obtained at scan rates of 200, 500, and 1000 mV/s. Values for lower scan rates could not be reliably acquired. Values were also obtained for the second reduction peak at 200 mV/s, as well as second and third reduction peaks at 500 and 1000 mV/s. Figure 3.45 below depicts the Ep,a and Ip,a of the Mo_2W tri-nuclear clusters at a scan rate of 200 mV/s. Figure 3.46 shows eL-ChemViewer acquiring Ep,c and Ip,c.

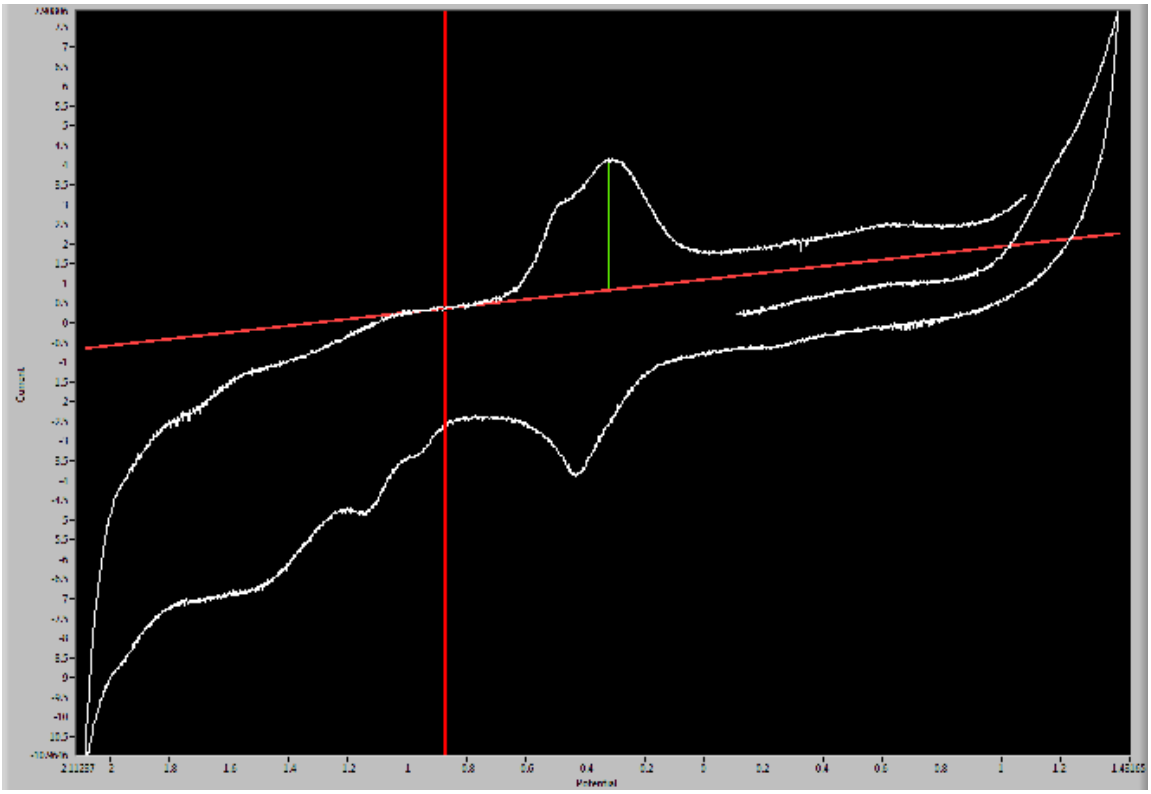

Figure 3.45. This image represents the acquisition of peak anodic potential (Ep,a) and peak anodic current (Ip,a) of the Mo_2W tri-nuclear cluster acquired from a 200 mV/s scan rate using eL-ChemViewer. The program acquired an Ep,a value of -0.32 V, and an Ip,a of 3.33 µA.

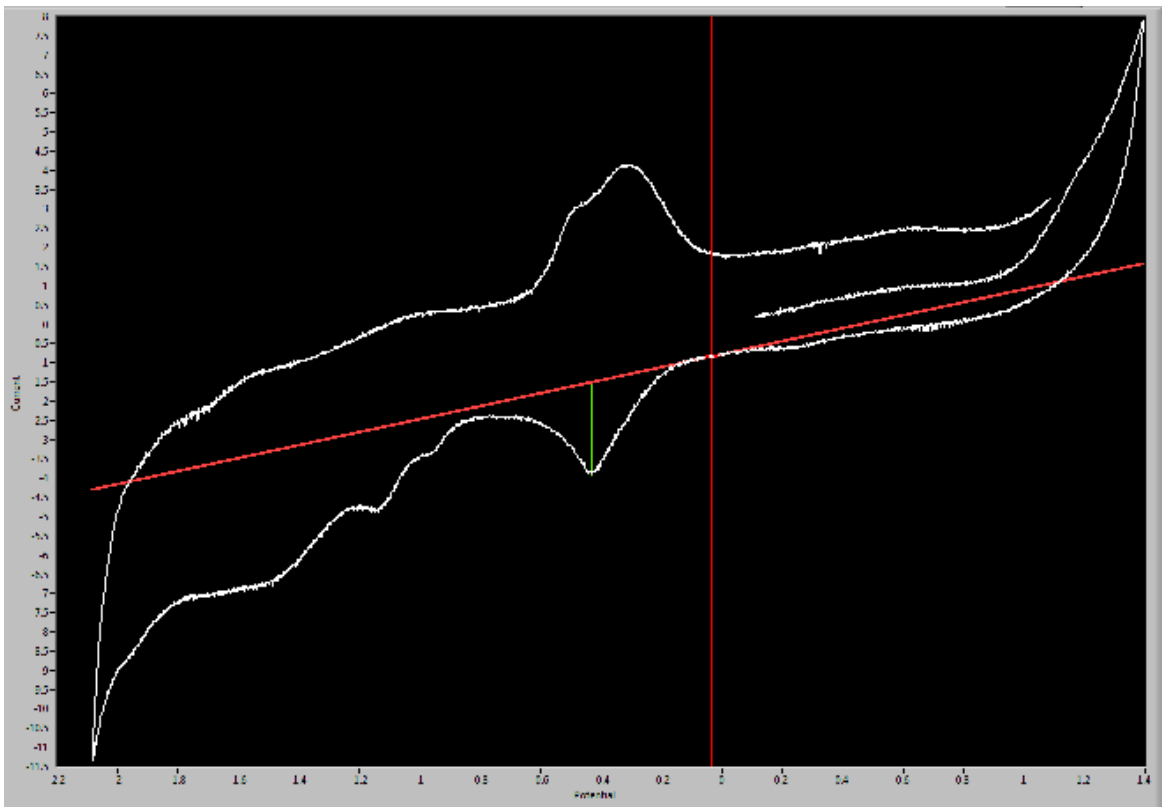

Figure 3.46. This image represents the acquisition of peak cathodic potential (Ep,c) and peak cathodic current (Ip,c) of the Mo_2W tri-nuclear cluster acquired from a 200 mV/s scan rate using eL-ChemViewer. The program acquired an Ep,c value of -0.43 V, and an Ip,c of -2.52 µA.

3.5.3 Acquiring Baselines for the MoW_2 tri-nuclear cluster

The parameters of Ep,a, Ep,c, Ip,a, Ip,c were obtained from CVs obtained at scan rates of 100, 200, 500, and 1000 mV/s. Values were also obtained for the second and third reduction peaks second reduction peaks at 100 and 200 mV/s. The CVs obtained from scan rates of 100 mV/s are displayed below in Figure 3.47, which shows the acquisition of Ep,a and Ip,a, and Figure 3.48 shows the acquisition Ep,c and Ip,c .

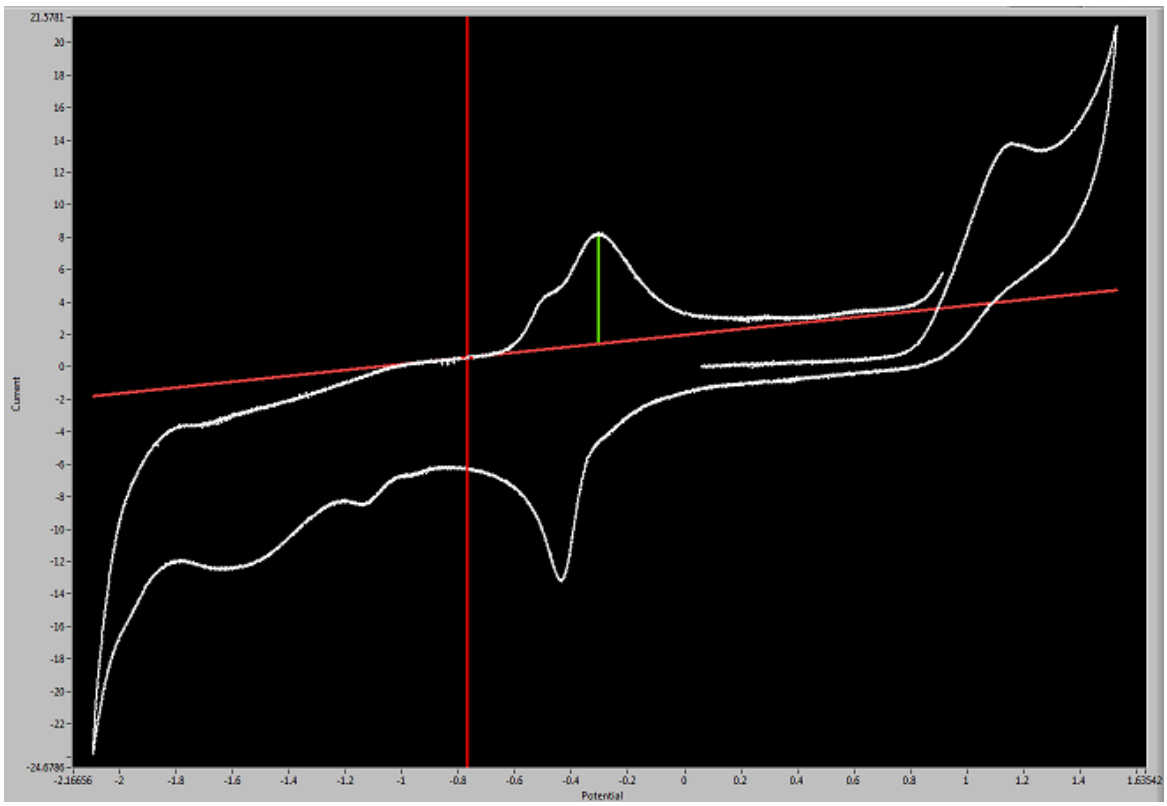

Figure 3.47. This image represents the acquisition of peak anodic potential (Ep,a) and peak anodic current (Ip,a) of the MoW_2 tri-nuclear cluster acquired from a 100 mV/s scan rate using eL-ChemViewer. The program acquired an Ep,a value of -0.33 V, and an Ip,a of 3.33 µA.

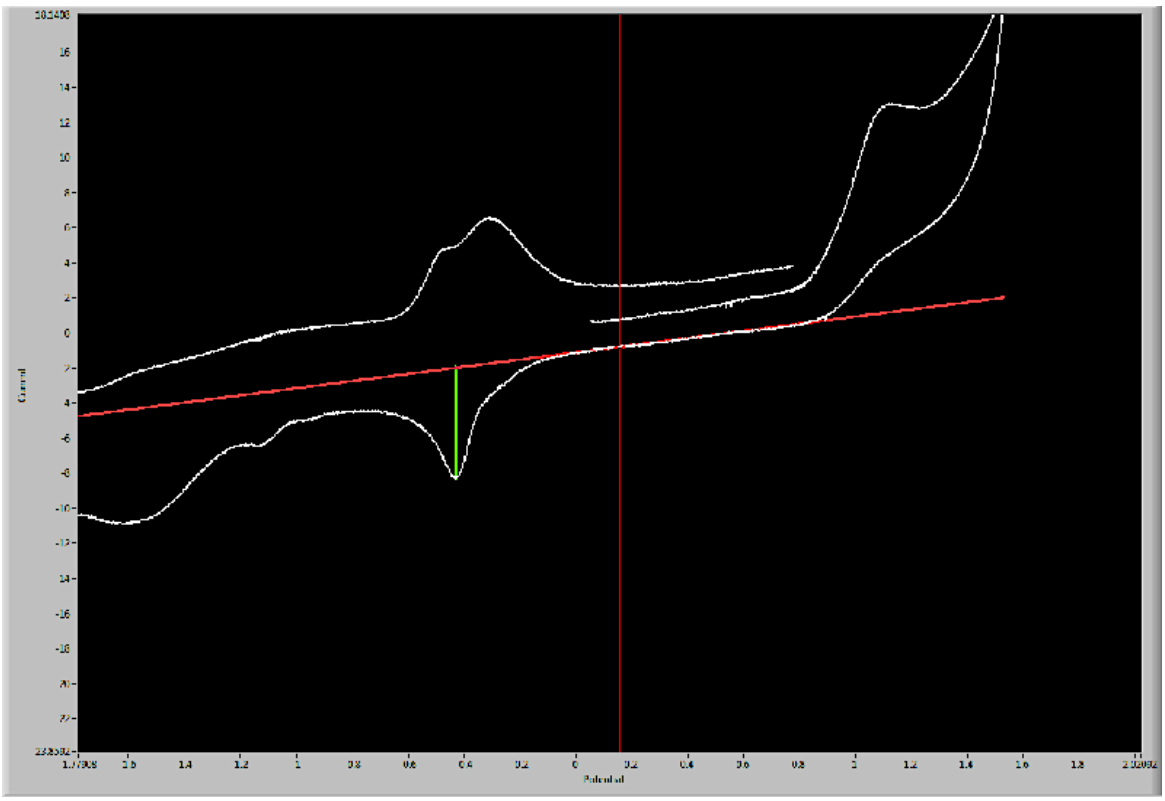

Figure 3.48. This image represents the acquisition of peak cathodic potential (Ep,c) and peak cathodic current (Ip,c) of the MoW_2 tri-nuclear cluster acquired from a 100 mV/s scan rate using eL-ChemViewer. The program acquired an Ep,c value of -0.42 V, and an Ip,c of -6.46 µA.

3.5.4 Acquiring Baselines for the W_3 tri-nuclear cluster

The parameters of Ep,a, Ep,c, Ip,a, Ip,c were obtained at scan rates of 10, 20, 50, 100, 200, 500, and 1000 mV/s. Values were also obtained for the second reduction peak at 200 mV/s and the third reduction peak second reduction peaks at 10, 20, 100, 200, and 500 mV/s. The CVs obtained from scan rates of 100 mV/s are displayed below in Figures 3.49 and Figure 3.50.

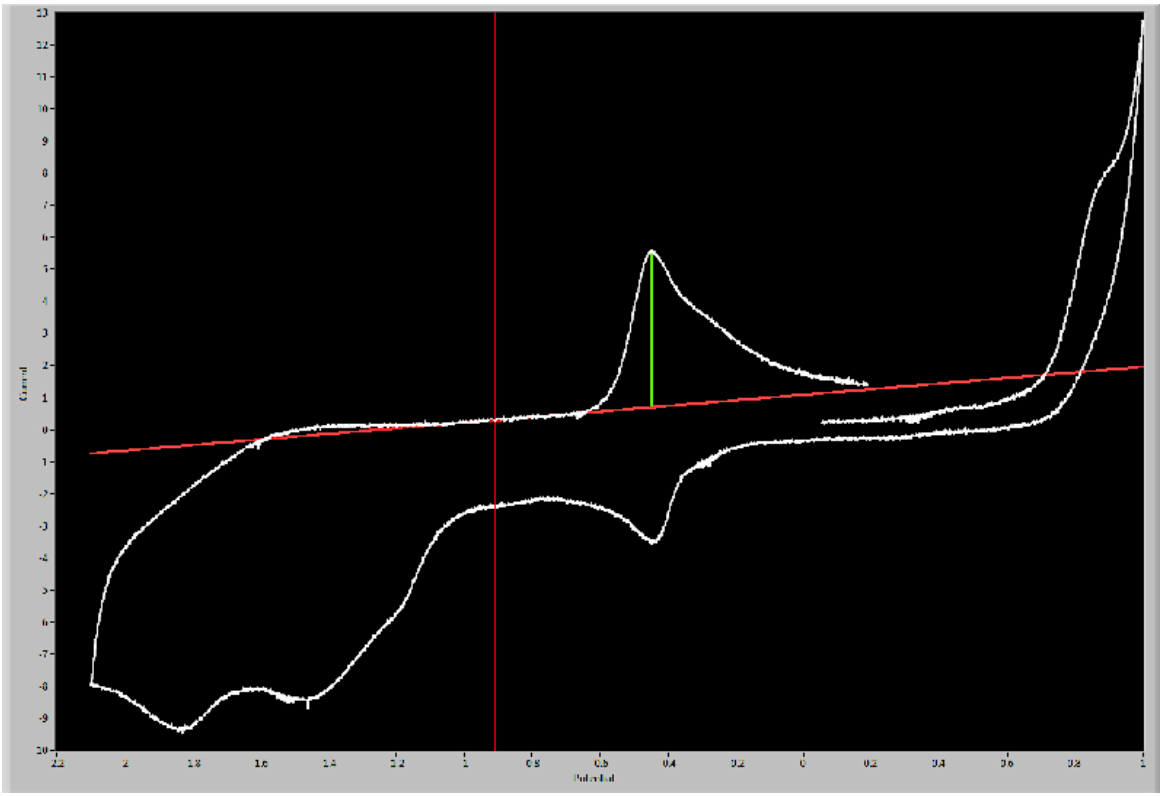

Figure 3.49. This image represents the acquisition of peak anodic potential (Ep,a) and peak anodic current (Ip,a) of the W_3 tri-nuclear cluster acquired from a 100 mV/s scan rate using eL-ChemViewer. The program acquired an Ep,a value of -0.45 V, and an Ip,a of 4.89 µA.

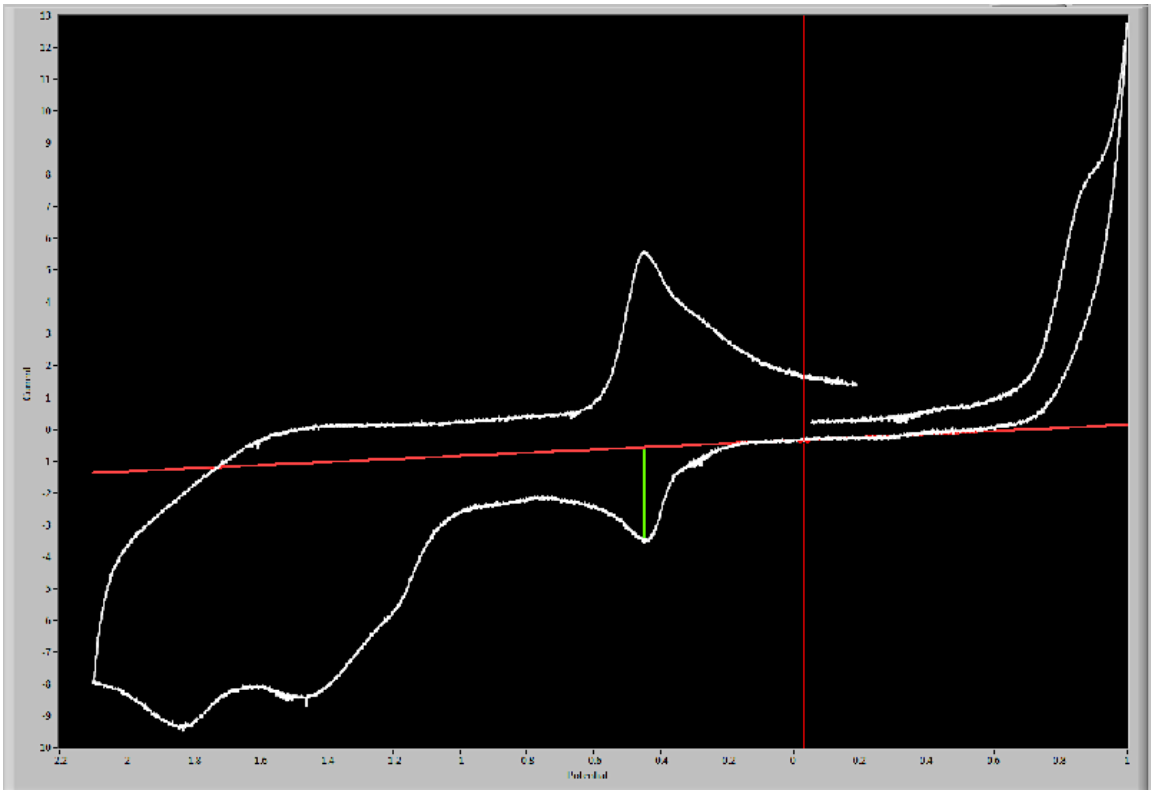

Figure 3.50. This image represents the acquisition of peak cathodic potential (Ep,c) and peak cathodic current (Ip,c) of the W_3 tri-nuclear cluster acquired from a 100 mV/s scan rate using eL-ChemViewer. The program acquired an Ep,c value of -0.45 V, and an Ip,c of -3.02 µA.

The values were tabulated and are shown in the following section.

3.6 Diffusion-limited processes

Electrochemistry, like other chemical processes is not exempt from processes that are rate-limiting. The overall rate of reduction/oxidation at the electrode is limited by the slowest of all the sub-processes involved. These typically include transport of the solvated ion to the electrode surface, the desolvation of the ion, then the redox reaction, etc. But if our redox process(es) are not limited by diffusion as the slowest of these factors, then we could not obtain reliable quantitative data, because any of the slower experimental conditions that are not related to catalyst concentration may control the rate. For a given reaction, there may be electron-transfer steps (E), purely chemical steps (C), and any combination of these (EC, CE, ECE, etc.). They may result from such processes as reaction with solvent, dimerization, radical substrate reactions to name a few. If however, a process is limited by the diffusion of the catalyst species only however, then the current will be conveniently proportional to the analyte concentration according to Fick's law as seen in Equation 3.6:

Equation 3.6 $$dN = -D \times dc/dt\ dx$$

It is therefore useful to learn if a system is diffusion-limited.

3.7 Diffusion coefficients from cyclic voltammetry data

The following tables and plots show the data gathered through CV and processed with eL-ChemViewer software. The values were tabulated and used to determine the diffusion coefficient. The CVs in the previous section were collected for each of the four

trimers in both negative (cathodic) and positive (anodic) initial directions at scan rates of 1, 5, 10, 20, 50, 100, 200, 500, and 1000 mV/s. From this data, the following parameters were measured: Ep,c, Ep,a, $E_{1/2}$ = ½(Ep,c + Ep,a), ΔE = Ep,a - Ep,c (absolute value), Ip,a, Ip,c, and Ip,c/Ip,a. The results are discussed in the Conclusions section.

3.7.1 Electrochemical data for the Mo_3 tri-nuclear cluster

The data for the determination of the characterization of the Mo_3 trimer in DMSO/TBAHFP are collected in Table 3.4 and Table 3.5 below. By determining the peak anodic current heights and plotting them against the square root of the scan rate, the diffusion coefficient can be obtained from the resulting slope. The plot is shown in Figure 3.51.

Table 3.4. The anodic and cathodic peaks for Mo_3 at their respective scan rates.

Scan Rate	Anodic		Cathodic	
Mo_3	Ep,a	Ip,a	Ep,c	Ip,c
100	-0.475	2.919	-0.478	-0.359
200	-0.444	4.222	-0.419	-0.365
500	-0.410	6.505	-0.385	-0.328
1000	-0.380	9.187	-0.326	-0.294

Table 3.5. Mo_3 data calculations

Scan Rate (mV/s)	Scan Rate (V/s)	$(V/s)^{1/2}$	$E_{p,a}$	$I_{p,a}$ (μA)	$E_{p,c}$	$I_{p,c}$	$I_{p,a}$ (A)	ΔE	$E_{1/2}$	$i_{p,c} / i_{p,a}$
100	0.1	0.32	-0.48	2.92	-0.48	-0.36	2.92E-06	-0.95	-0.48	-0.12
200	0.2	0.45	-0.44	4.22	-0.42	-0.37	4.22E-06	-0.86	-0.43	-0.09
500	0.5	0.71	-0.41	6.50	-0.39	-0.33	6.50E-06	-0.80	-0.40	-0.05
1000	1	1.00	-0.38	9.19	-0.33	-0.29	9.19E-06	-0.71	-0.35	-0.03

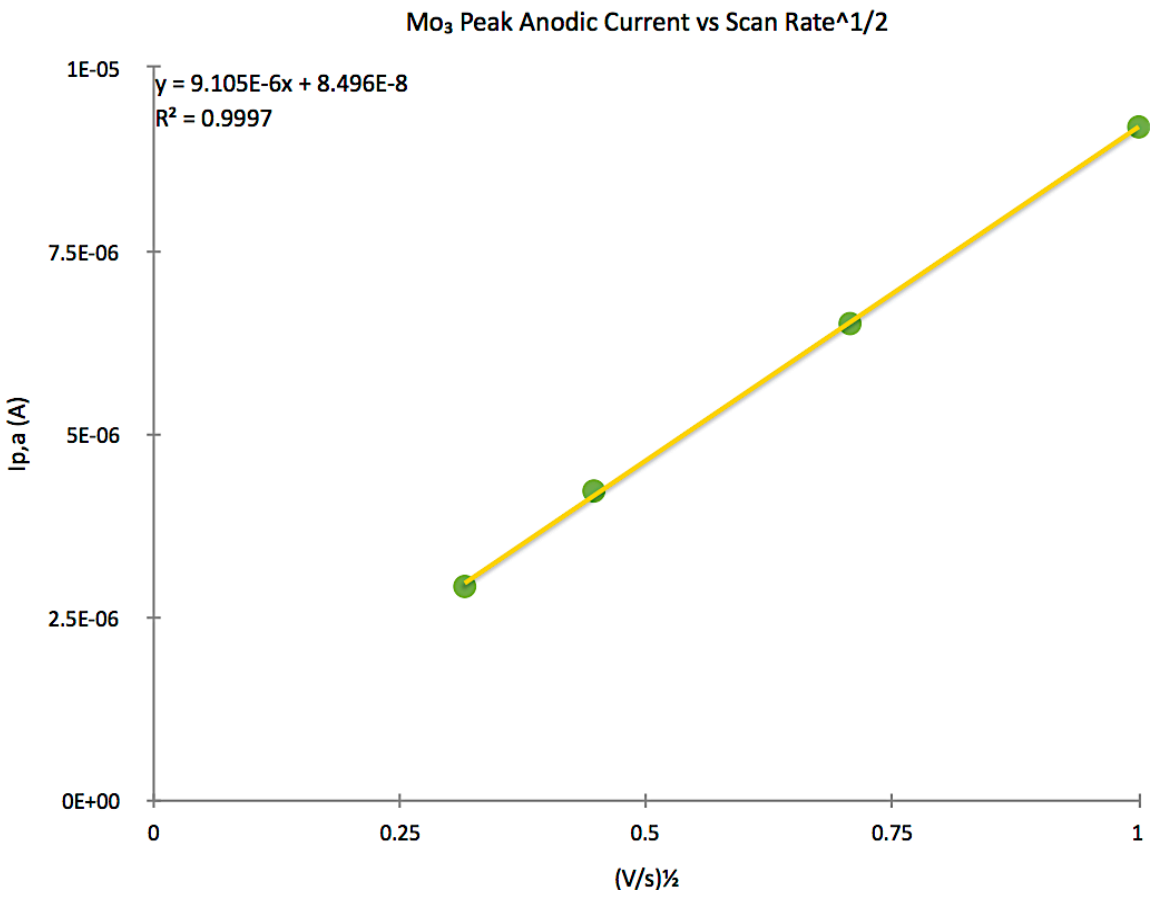

Figure 3.51. Peak anodic current of the Mo_3 tri-nuclear cluster plotted as a function of square root of the scan rate.

3.7.2 Electrochemical data for the Mo_2W tri-nuclear cluster

The data used to determine the coefficient of the Mo_2W trimer in this solvent system is collected in Table 3.6 and Table 3.7 below. The plot of the data is shown in Figure 3.52.

Table 3.6. The anodic and cathodic peaks for the Mo_2W trimer at their respective scan rates.

Scan Rate	Anodic		Cathodic	
Mo_2W	Ep,a	Ip,a	Ep,c	Ip,c
200	-0.320	3.332	-0.432	-2.523
500	-0.276	7.570	-0.433	-7.855
1000	-0.265	12.956	-0.433	-8.139

Table 3.7. Mo_2W data calculations

Scan Rate (mV/s)	Scan Rate (V/s)	$(V/s)^{½}$	$E_{p,a}$	$I_{p,a}$ (μA)	$E_{p,c}$	$I_{p,c}$	$I_{p,a}$ (A)	ΔE	$E_{½}$	$i_{p,c} / i_{p,a}$
200	0.2	0.45	-0.32	3.33	-0.43	-2.52	3.33E-06	-0.75	-0.38	-0.76
500	0.5	0.71	-0.28	7.57	-0.43	-7.85	7.57E-06	-0.71	-0.35	-1.04
1000	1	1.00	-0.27	12.96	-0.43	-8.14	1.30E-05	-0.70	-0.35	-0.63

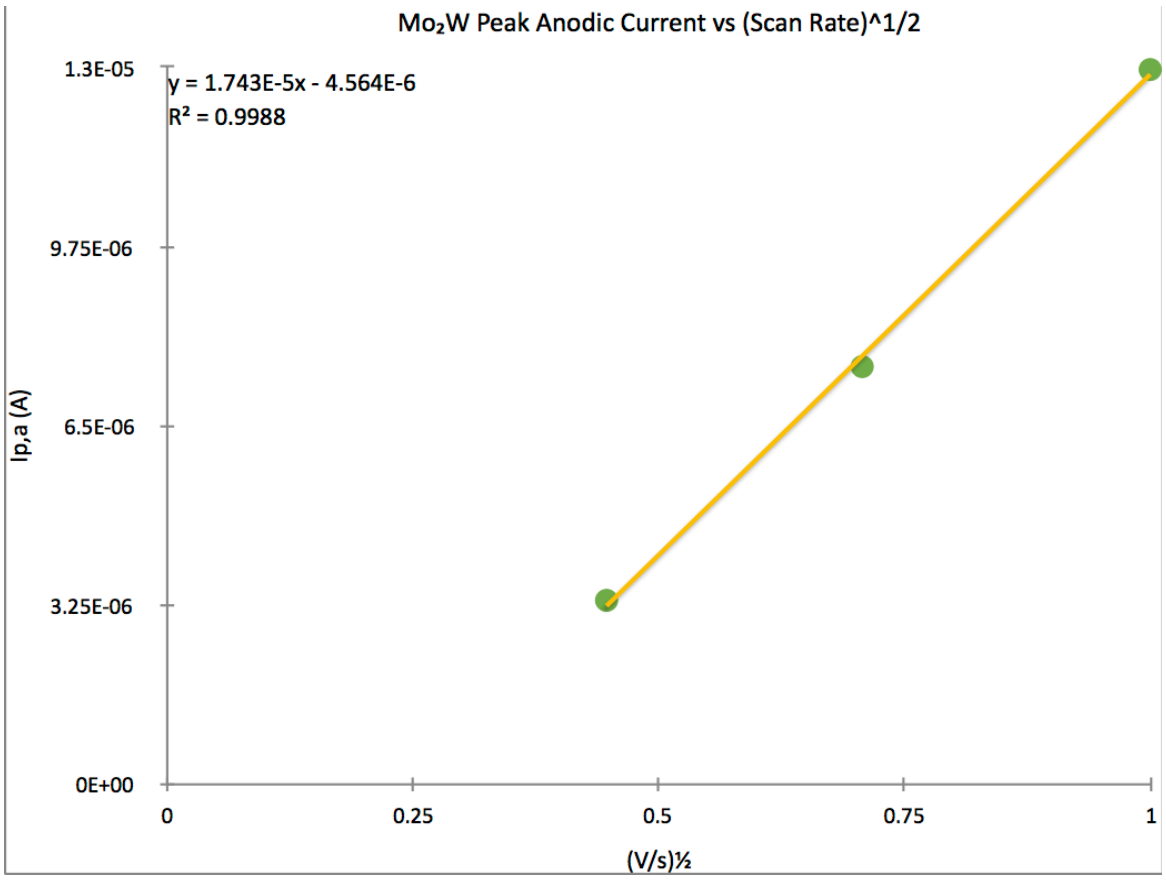

Figure 3.52. Peak anodic current of the Mo_2W tri-nuclear cluster plotted as a function of square root of the scan rate.

3.7.3 Electrochemical data for the MoW_2 tri-nuclear cluster

The data used to determine the coefficient of the MoW_2 trimer is shown in Table 3.8 and Table 3.9 below. The plot is shown in Figure 3.53.

Table 3.8. The anodic and cathodic peaks for the MoW_2 trimer at their respective scan rates.

Scan Rate	Anodic		Cathodic	
MoW_2	Ep,a	Ip,a	Ep,c	Ip,c
100	-0.332	3.325	-0.421	-6.457
200	-0.306	6.768	-0.436	-9.676
500	-0.262	10.251	-0.446	-8.418
1000	-0.247	15.887	-0.447	-10.347

Table 3.9. MoW_2 data calculations

Scan Rate (mV/s)	Scan Rate (V/s)	$(V/s)^{1/2}$	$E_{p,a}$	$I_{p,a}$ (μA)	$E_{p,c}$	$I_{p,c}$	$I_{p,a}$ (A)	ΔE	$E_{1/2}$	$i_{p,c}/i_{p,a}$
100	0.1	0.32	-0.33	3.33	-0.42	-6.46	3.33E-06	-0.75	-0.38	-1.94
200	0.2	0.45	-0.31	6.77	-0.44	-9.68	6.77E-06	-0.74	-0.37	-1.43
500	0.5	0.71	-0.26	10.25	-0.45	-8.42	1.03E-05	-0.71	-0.35	-0.82
1000	1	1.00	-0.25	15.89	-0.45	-10.35	1.59E-05	-0.69	-0.35	-0.65

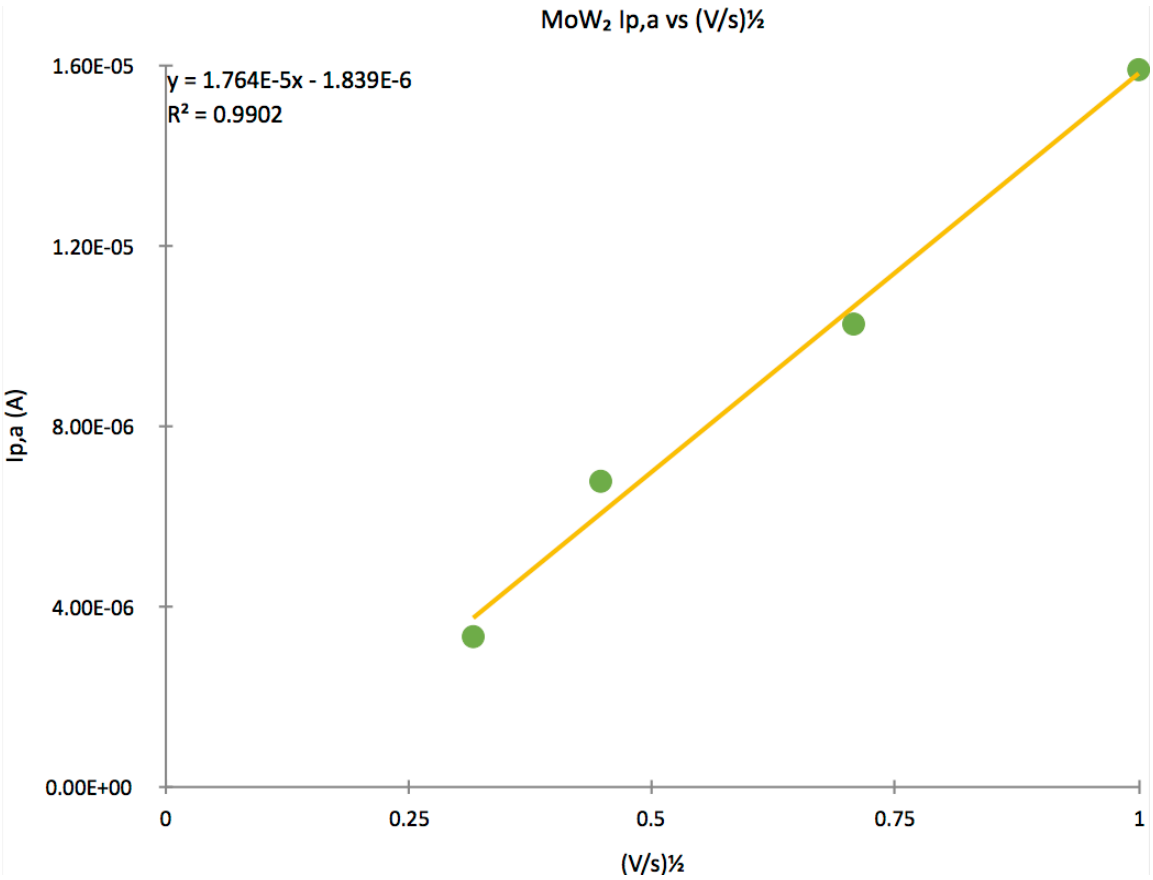

Figure 3.53. Peak anodic current of the MoW_2 tri-nuclear cluster plotted as a function of square root of the scan rate to obtain the slope.

3.7.4 Electrochemical data for the W_3 tri-nuclear cluster

Finally, the data used to determine the coefficient of the W_3 trimer is shown below in Table 3.10 and Table 3.11 below. The plot is shown in Figure 3.54.

Table 3.10. The anodic and cathodic peaks for the W_3 trimer at their respective scan rates.

Scan Rate	Anodic		Cathodic	
W_3	Ep,a	Ip,a	Ep,c	Ip,c
10	-0.427	0.291	-0.445	-1.221
20	-0.430	0.786	-0.435	-1.641
50	-0.437	2.971	-0.446	-2.109
100	-0.447	4.894	-0.448	-3.023
200	-0.422	8.006	-0.461	-1.585
500	-0.380	13.880	-0.373	-2.796
1000	-0.348	17.395	-0.359	-3.844

Table 3.11. W_3 data calculations

Scan Rate (mV/s)	Scan Rate (V/s)	$(V/s)^{1/2}$	$E_{p,a}$	$I_{p,a}$ (μA)	$E_{p,c}$	$I_{p,c}$	$I_{p,a}$ (A)	ΔE	$E_{1/2}$	$i_{p,c} / i_{p,a}$
10	0.01	0.10	-0.43	0.29	-0.45	-1.22	2.91E-07	-0.87	-0.44	-4.20
20	0.02	0.14	-0.43	0.79	-0.44	-1.64	7.86E-07	-0.87	-0.43	-2.09
50	0.05	0.22	-0.44	2.97	-0.45	-2.11	2.97E-06	-0.88	-0.44	-0.71
100	0.1	0.32	-0.45	4.89	-0.45	-3.02	4.89E-06	-0.90	-0.45	-0.62
200	0.2	0.45	-0.42	8.01	-0.46	-1.59	8.01E-06	-0.88	-0.44	-0.20
500	0.5	0.71	-0.38	13.88	-0.37	-2.80	1.39E-05	-0.75	-0.38	-0.20
1000	1	1.00	-0.35	17.40	-0.36	-3.84	1.74E-05	-0.71	-0.35	-0.22

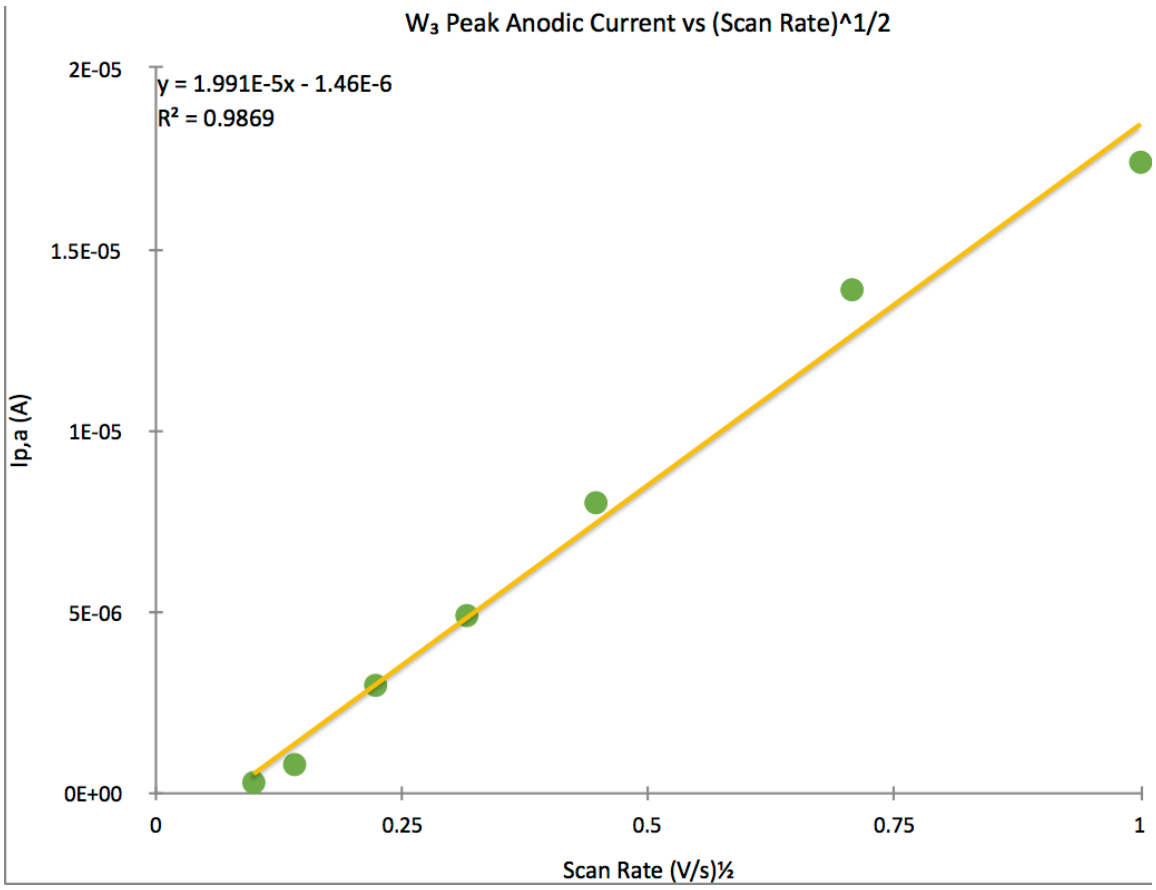

Figure 3.54. Peak anodic current of the W_3 tri-nuclear cluster plotted as a function of square root of the scan rate.

The calculated diffusion coefficients for the four tri-nuclear clusters are below in Table 3.12.

Table 3.12. Diffusion coefficients of the four tri-nuclear clusters with r^2 values.

Trimer	D (cm^2s^{-1})	r^2
Mo_3	9.105E-06	0.9997
Mo_2W	1.743E-05	0.9988
MoW_2	1.764E-05	0.9902
W_3	1.991E-05	0.9869

4. CONCLUSIONS

4. Conclusions

Electrochemical data for the four tri-nuclear clusters in the DMSO/TBAHFP solvent system was measured and collected through CV, and the electrochemical properties reported here for the first time. The diffusion coefficients were experimentally determined from the electrochemical data with the aid of eL-ChemViewer and also reported.

If an analyte displays diffusion-limited behavior, the data will adhere to a linear fit resulting from the plot of the square root of the scan rate against the resulting peak anodic current. Based upon the linear fit of the diffusion data for the four trimers, we conclude that the Mo_3 and Mo_2W tri-nuclear clusters display diffusion-limited behavior in this solvent system, exhibiting correlation coefficient (r^2) values of 0.9997 and 0.9988 respectively. In other words, the data fit tightly to a linear slope. The MoW_2 tri-nuclear cluster also fit fairly well with a correlation coefficient of 0.9902, and it was therefore concluded that this trimer is probably diffusion-limited as well. However, the W_3 tri-nuclear cluster appears less likely to be diffusion-limited as it did not adhere to a linear slope as well as did the other three trimers, with a correlation coefficient of 0.9869.

Curiously, as the percentage of W in the catalysts rose, the behavior was less likely to be diffusion-limited. However, there was no direct relationship found between W content and diffusion-limited behavior.

5. FUTURE STUDIES

Future Studies

Investigators in future studies may wish to explore electrodeposition with these compounds by varying parameters such as temperature, current density, solution concentration, substrate preparation, and type of electrodeposition methods, such as pulse/reverse pulse plating (Gunasekara, 2015, Kim et al., 2004, Suryanto et al., 2012). To date, only a few precious metals such as iridium (Sahin, 2015) and rhodium (Available at: https://www.bnl.gov/newsroom/news.php?a=110898) have been used as catalysts to successfully oxidize the carbon-carbon bond of ethanol.

If these metal clusters can be used to augment the Pt electrode, they may prove to be valuable catalysts for small alcohol molecules such as ethanol and would not require the use of precious metals.

REFERENCES

References

Antolini, E.; Perez, J. *Lecture Notes in Energy* **2013**, 89-127.

Gyenge, E. **2008**, *PEM Fuel Cell Electrocatalysts and Catalyst Layers*, 165-287.

Idriss, H. *Platinum Metals Review* **2004**, *48*, 105-115.

Li, M.; Adzic, R. R. *Lecture Notes in Energy* **2013**, 1-25.

Masa, J.; Ozoemena, K. I.; Schuhmann, W.; Zagal, J. H. *Lecture Notes in Energy* **2013**, 157-212.

Ota, K.-i.; Ishihara, A. *Lecture Notes in Energy* **2013**, 391-416.

Schwarzacher, W. The Electrochemical Society ***Interface*** **2006**, 32-35.

Kissinger, P. T.; Heineman, W. R. *J. Chem. Educ.* **1983**, *60*, 702.

Cotton, F. A. *Chem. Soc. Rev.* **1975**, *4*, 27-53.

Katovic, V.; McCarley, R. E. *J. Am. Chem. Soc.* **1978**, *100*, 5586-5587.

Bursten, B. E.; Green, M. R.; Katovic, V.; Kirk, J. R.; Lightner Jr, D. *Inorg. Chem.* **1986**, *25*, 831-834.

Woods, C. J. Wright State University Thesis **2010**, 1-66.

Telser, J. *University of Florida* **1984**, *PhD*, 1-308.

Cotton, F. A. *Multiple bonds between metal atoms*; Springer Science & Business Media: 2005; pp 818.

Xu, Z. A. Y. W. *ACS Symp. Ser.* **2013**, *Applications of Molecular Modeling to Challenges in Clean Energy*, 135-151.

Katovic, D. *Journal of the Less Common Metals* **1970**, *21*, 325-332.

Tseung, A. C. C.; Chen, K. Y. *Catal. Today* **1997**, *38*, 439-443.

Jiang, Z.; Huang, W.; Zhao, H.; Zhang, Z.; Tan, D.; Bao, X. *Journal of Molecular Catalysis A: Chemical* **2007**, *268*, 213-220.

Li, Z.; Fang, Z.; Kelley, M. S.; Kay…, B. D. *The J. Phys. Chem. C.* **2014**.

Cotton, F. A.; Bratton, W. K. *J. Am. Chem. Soc.* **1965**, *87*, 921-921.

Kennedy, E. N. Wright State University Thesis **2009**, 96.

Endres, F.; MacFarlane, D.; Abbott, A. *Electrodeposition from ionic liquids*; John Wiley & Sons: **2008**.

Seddon, K. R. *Nature materials* **2003**, *2*, 363-365.

Wilkes, J. S.; Zaworotko, M. J. *J. Chem. Soc., Chem. Commun.* **1992**, 965-967.

Ohno, H. *Electrochemical aspects of ionic liquids*; Wiley Online Library: 2005; pp 410.

Nishida, T., Y. Tashiro, M. Yamamoto. **2003**, *120*, 135.

Nakagawa, H., S. Izuchi, K. Kuwana, T. Nukuda, Y. Aihara. *J. Electrochem. Soc.* **2003**, *150*, A695.

Katayama, Y., S. Dan, T. Miura, T. Kishi. *J. Electrochem. Soc.* **2001**, *148*, C102.

Fuller, J., R. T. Carlin, R. A. Osteryoung. *J. Electrochem. Soc.* **1997**, *144*, 3881.

Seddon, K. R.; Stark, A.; Torres, M.-J. *Pure Appl. Chem.* **2000**, *72*, 2275-2287.

Eike, D. M.; Brennecke, J. F.; Maginn, E. J. *Green Chemistry* **2003**, *5*, 323-328.

Zhang, S.; Sun, N.; He, X.; Lu, X.; Zhang, X. *J. Phys. Chem. Ref. Data* **2006**, *35*, 1475.

Tsierkezos, N. G.; Philippopoulos, A. I. *Fluid Phase Equilib.* **2009**, *277*, 20-28.

Wakai, C.; Oleinikova, A.; Ott, M.; Weingärtner, H. *J Phys Chem B* **2005**, *109*, 17028-17030.

Laoire, C. O.; Mukerjee, S.; Abraham, K. M.; Plichta, E. J.; Hendrickson, M. A. *J. Phys.*

Chem. C **2010**, *114*, 9178-9186.

Dancevic, A. Wright State University Thesis **2003**.

Freire, M. G.; Santos, L. M. N. B. F.; Fernandes, A. M.; Coutinho, J. A. P.; Marrucho, I. M. *Fluid Phase Equilib.* **2007**, *261*, 449-454.

Schröder, U.; Wadhawan, J. D.; Compton, R. G.; Marken, F.; Suarez, P. A. Z.; Consorti, C. S.; de Souza, R. F.; Dupont, J. *New J. Chem.* **2000**, *24*, 1009-1015.

Welton, T.; Wasserscheid, P. *Ionic liquids in synthesis, VCH*; Wiley, Weinheim: 2002;

Dyar, H. Wright State University Thesis **1999**.

Xu, D.; Wang, Z.-l.; Xu, J.-j.; Zhang, L.-l.; Zhang, X.-b. *Chemical Communications* **2012**, *48*, 6948-6950.

Lai, S. C. S.; Kleijn, S. E. F.; ztrk, F. T. Z.; van Rees Vellinga, V. C.; Koning, J.; Rodriguez, P.; Koper, M. T. M. *Catal. Today* **2010**, *154*, 92-104.

Asiri, H. A.; Anderson, A. B. *J. Electrochem. Soc.* **2015**, *162*, F115-F122.

Courtois, J. Worcester Polytechnic Institute Theses **2013**.

Kim, Y. K.; Dohnalek, Z.; Kay, B. D.; Rousseau, R. *The Journal of Physical Chemistry C* **2009**, *113*, 9721-9730.

Nakata, K.; Nagasawa, A.; Soyama, N.; Sasaki, Y.; Ito, T. *Inorg. Chem.* **1991**, *30*, 1575-1579.

Bino, A.; Cotton, F. A.; Dori, Z.; Kolthammer, B. W. S. *J. Am. Chem. Soc.* **1981**, *103*, 5779-5784.

Cotton, F. A.; Kühn, F. E. *Inorg. Chim. Acta* **1996**, *252*, 257-264.

Bursten, B. E. C., Albert Hall, Michael B., and Robert C. Najjar. *Inorg. Chem.* **1982**, *21*, 302-307.

Cotton, F. A.; Feng, X. *Inorg. Chem.* **1991**.

Hibble, S. J.; Fawcett, I. D. *Journal of the Chemical Society, Dalton Transactions* **1995**, 2555-2559.

Lawton, D., and R. Mason. *Journal American Chemical Society* **1964**, *87:4*, 921-922.

Santure, D. J., J. C. Huffman, And A. P. Sattelberger. *Inorg. Chem.* **1985**, *24*, 371-378.

Huang, L.; Li, X.; Huang, J.-S.; Yan, D.-C.; Qian-Er, Z. *Jiegou Huaxue* **1994**, *13, No. 2*, 87-90.

D. W. Breck, W. G. E., R. M. Milton, T. B. Reed, and T. L. Thomas. *J. Am. Chem. Soc.* **1956**, 5963-5972.

Shriver, D. F. A. D., Mark A. *The manipulation of air-sensitive compounds*; Wiley. com: **1986**.

Cotton, F. A. *Acc. Chem. Res.* **1969**, *2*, 240-247.

Paul, E. A.; Batten, T. H.; May, M. A.; Sayers, W. R.; Shelton, P. E.; Kojima, T.; Katovic, V. *Inorg. Chem.* **1994**, *33*, 630-631.

Suzuki, T. Wright State University Thesis **1994**.

Wanamaker, M. D. Wright State University Thesis **1998**.

Dyar, H. A. Wright State University Thesis **2001**.

Kissinger, P.; Heineman, W. R. *Laboratory Techniques in Electroanalytical Chemistry*, CRC Press: **1996**; pp 1008.

Liu, C.-Z.; Wang, F.; Stiles, A. R.; Guo, C. *Applied Energy* **2012**, *92*, 406-414.

Olivier-Bourbigou, H.; Magna, L.; Morvan, D. *Applied Catalysis A: General* **2010**, *373*, 1-56.

Adams, R. N. Electrochemistry at solid electrodes; Marcel Dekker Inc: **1969**, 416.

Hrbac, J.; Halouzka, V.; Trnkova, L.; Vacek, J. *Sensors* **2014**, *14*, 13943-13954.

Ardon, M.; Bino, A.; Cotton, F. A.; Dori, Z.; Kaftory, M.; Reisner, G. *Inorg. Chem.* **1982**, *21*, 1912-1917.

Bino, A.; Gibson, D. *J. Am. Chem. Soc.* **1980**, *102*, 4277-4278.

Chisholm, M. A. C., F. A. *Acc. Chem. Res.* **1977**, 356-362.

Cotton, F. A.; Dori, Z.; Kapon, M.; Marler, D. O.; Reisner, G. M.; Schwotzer, W.; Shaia, M. *Inorg. Chem.* **1985**, *24*, 4381-4384.

Cotton, F. A.; Dori, Z.; Marler, D. O.; Schwotzer, W. *Inorg. Chem.* **1983**, *22*, 3104-3106.

Cotton, F. A.; Llusar, R.; Eagle, C. T. *J. Am. Chem. Soc.* **1989**, *111*, 4332-4338.

Davis, J. A. Wright State University Thesis **2012**.

Frock, L. R. Wright State University Thesis **2012**.

Harris, T. L. Wright State University Thesis **2008**.

Katovic, T., Hoxmeier, McCarley. *Journal American Chemical Society* **1975**, *97*.

Katovic, V.; McCarley, R. E. *Inorg. Chem.* **1978**, *17*, 1268-1270.

Martinez, M.; Ooi, B. L.; Sykes, A. G. *J. Am. Chem. Soc.* **1987**, *109*, 4615-4619.

Ryan, T. R. A. R. E. M. *Inorg. Chem.* **1982**, *21*, 2072-2079.

Stephenson, T. A.; Bannister, E.; Wilkinson, G. *Journal of the Chemical Society (Resumed)* **1964**, 2538-2541.

Ubadigbo, L. N. **2009**,

Zaitsev, A. A.; Korotkov, N. A.; Lazarev, M. *Metal Science and Heat Treatment* **1976**, *18*, 873-876.

Zhuang, B.; Yu, P.; He, L.; Huang, L.; Pan, G. *Polyhedron* **1998**, *17*, 4393-4402.

Wang, B.; Sasaki, Y.; Nagasawa, A.; Ito, T. *J. Am. Chem. Soc.* **1986**, *108*, 6059-6060.

Cotton, F. A.; Dori, Z.; Marler, D. O.; Schwotzer, W. *Inorg. Chem.* **1984**, *23*, 4738-4742.

Patel, A., and David Richens. *Journal American Chemical Society Commun.* **1990**, 274-276.

Earle, M. J.; Gordon, C. M.; Plechkova, N. V.; Seddon, K. R.; Welton, T. *Anal. Chem.* **2007**, *79*, 758-764.

Yang, P.; Zhao, Y.; Su, C.; Yang, K.; Yan, B.; An, M. *Electrochim. Acta* **2013**, *88*, 203-207.

Oskam, G. *J. Electrochem. Soc.* **1999**, *146*, 1436.

Siek, M.; Kaminska, A.; Kelm, A.; Rolinski, T.; Holyst, R.; Opallo, M.; Niedziolka-Jonsson, J. *Electrochim. Acta* **2013**, *89*, 284-291.

Giridhar, P.; Weidenfeller, B.; El Abedin, S. Z.; Endres, F. *Phys Chem Chem Phys* **2014**, *16*, 9317-9326.

Abdel Aal, A.; Voigts, F.; Chakarov, D.; Endres, F. *J Solid State Electrochem* **2012**, *16*, 3027-3036.

Le Vot, S.; Roué, L.; Bélanger, D. *Electrochim. Acta* **2012**, *59*, 49-56.

Abdel Aal, A.; Gobran, H. A.; Muecklich, F. *J. Alloys Compd.* **2009**, *473*, 250-254.

Nakouzi, E.; Sultan, R. *Chaos* **2011**, *21*, 043133.

Chen, P.-Y.; Chang, Y.-T. *Electrochim. Acta* **2012**, *75*, 339-346.

Abbott, A. P.; McKenzie, K. J. *Phys Chem Chem Phys* **2006**, *8*, 4265-4279.

Ghaziof, S.; Raeissi, K.; Golozar, M. A. *Surface and Coatings Technology* **2010**, *205*, 2174-2183.

Kalska-Szostko. Recent Trend in Electrochemical Science and Technology **2012**, 261-280.

Kim, Y.; Jung, J.; Kim, S.; Chae, W.-S. *Mater. Trans.* **2013**, *54*, 1467-1472.

Endres, F. *Phys. Chem. Chem. Phys.* **2001**, *3*, 3165-3174.

Garcia, E. M.; Lins, V. F. C.; Matencio, T. *Metallic and Oxide ElectrodepositionModern Surface Engineering Treatments* **2013**.

Raeissi, K.; Saatchi, A.; Golozar…, M. A. *Surface and Coatings ...* **2005**,

Caballero-Calero, O.; Díaz-Chao, P.; Abad, B.; Manzano, C. V.; Ynsa, M. D.; Romero, J. J.; Rojo, M. M.; Martín-González, M. S. *Electrochim. Acta* **2014**, *123*, 117-126.

Gagne, R. R., Carl A. Koval, and George C. Lisensky. *Inorg. Chem.* **1980**, *19*, 2854-2855.

Abdel Aal, A.; Hassan, H. B. *J. Alloys Compd.* **2009**, *477*, 652-656.

Liu, Z.; Abedin, S. Z. E.; Endres, F. *Electrochim. Acta* **2013**, *89*, 635-643.

Roquero, P.; Ordonez, L. C.; Herrera, O.; Ugalde, O.; Ramírez, J. *International Journal of Chemical Reactor Engineering* **2007**, *5*.

Kawamura, G.; Okamoto, H.; Ishikawa, A.; Kudo, T. *J. Electrochem. Soc.* **1987**, *134*, 1653-1658.

Gosser, D. K. J. *Voltammetry: Simulation and Analysis of Reaction Mechanisms*; VCH Publishers: **1993.**

Kelly, R. S. The Analytical Sciences Digital Library. A Peer Reviewed Collection of Web Resources. http://collection.asdlib.org/?p=428, **2014**.

Evans, D. H.; O'Connell, K. M.; Petersen, R. A.; Kelly, M. J. *J. Chem. Educ.* **1983**, *60*, 290.

Kissinger, P. T.; Heineman, W. R. *J. Chem. Educ.* **1984**, *60*, 702.

Lunsford, S. K.; Galal, A.; Akmal 2, N.; Ma 3, Y. L.; Zimmer, H.; Mark Jr, H. B. *Anal. Lett.* **1994**, *27*, 2141-2151.

Harvey, D. *Modern analytical chemistry*; McGraw-Hill New York: **2000**.

Van Benschoten, J. J.; Lewis, J. Y.; Heineman, W. R.; Roston, D. A.; Kissinger, P. T. *J. Chem. Educ.* **1983**, *60*, 772.

Gunasekara, R. A. Electro Chemical Deposition: Principles, Methods and Applications **2015.**

Suryanto, B. H. R.; Gunawan, C. A.; Lu, X.; Zhao, C. *Electrochim. Acta* **2012**, *81*, 98-105.

Kim, H.; Subramanian, N. P.; Popov, B. N. *J. Power Sources* **2004**, *138*, 14-24.

Sahin, O., Hilal Kivrak, Mustafa Karaman1, Dilan Atbas. *American Journal of Materials Science and Engineering* **2015**, *3*, 15-20.